DISSERTATION

CONDITIONS LEADING TO EXTRINSIC AND INTRINSIC ECOSYSTEM CHANGE ACROSS LARGE ENSEMBLES OF CLIMATE FUTURES

Submitted by

Daniel M. Hueholt

Department of Atmospheric Science

In partial fulfillment of the requirements

For the Degree of Doctor of Philosophy

Colorado State University

Fort Collins, Colorado

Summer 2025

Doctoral Committee:

Advisor: James W. Hurrell
Co-Advisor: Elizabeth A. Barnes

Jeffrey R. Pierce
Danica Lombardozzi

ABSTRACT

CONDITIONS LEADING TO EXTRINSIC AND INTRINSIC ECOSYSTEM CHANGE ACROSS LARGE ENSEMBLES OF CLIMATE FUTURES

Natural climate variability and forced change influence ecosystems through the direct impacts of changing environmental conditions ("extrinsic change"), and by altering internal ecosystem dynamics ("intrinsic change"). While simulating complex ecosystems and species-level change remains challenging, Earth system models are often capable of capturing patterns of the regional-scale climate conditions which lead to ecological change. Investigating these climate conditions allows models to be leveraged in studying ecosystem change without requiring direct simulation of ecological processes. In this dissertation, we explore conditions driving extrinsic and intrinsic ecosystem change in large ensembles of climate futures with external forcings from anthropogenic warming and stratospheric aerosol injection, a hypothetical method of climate intervention.

In the first project, we use the Community Earth System Model 2 Large Ensemble to describe how climate variability and change affect Arctic growing season warmth. Using a novel statistical metric, we find that many simulated Arctic ecoregions have already entered a state in which the warming trend dominates over internal variability. Storylines of cases where this "crossover" occurs earlier or later connect these events to coupled climate variability. The second study uses climate speeds–a metric of the rate of movement of thermal niches–to explore possible ecosystem impacts from design choices in stratospheric aerosol injection scenarios. We find highly distinct profiles of ecological risk in two simulations with similar global temperature targets but a 10-year delay in deployment. In the final study, we explore intrinsic change by using an ecological niche model to project future changes to habitat suitability for the Gyrfalcon (*Falco rusticolus*), a large predatory bird which is a top consumer in the tundra. Climate warming leads to a poleward contraction in suitability over the 21st century; a climate intervention scenario with global temperature

reduction rapidly reverses overall trends but yields distinct regional patterns. Storyline methods reveal a substantial role for internal variability even under very strong external forcings. This dissertation provides new methods to use climate models to probe extrinsic and intrinsic ecosystem change, and reveals insights into potential ecological impacts from climate intervention methods.

ACKNOWLEDGEMENTS

I am grateful to my advisors, Jim Hurrell and Elizabeth Barnes, for their consistent mentorship, guidance, insight, and collaboration throughout my time at Colorado State University. I thank Jeff Pierce and Danica Lombardozzi for their thoughtful feedback while serving on my PhD committee. Ariel Morrison contributed valuable scientific insight on each of the projects in this work, not to mention a sounding board during many data wrangling adventures. Discussions with Megan Franke on studying environmental parameters to make inferences about unresolved processes inspired the fundamental concept of this dissertation.

My work in this dissertation was supported by the National Science Foundation (NSF) Graduate Research Fellowship Program (Grant 006784). GRFP funding provided me the independence to pursue the interdisciplinary topics in this dissertation.

The Department of Atmospheric Science staff are all crucial to the positive working environment of our program. I had the privilege to work most closely with Sarah Tisdale, Nate Gronlund, Dinara Khakimova, Samantha Reynolds, and Noel Bryan; I extend thanks to each of them. For the record, I have yet to make a problem so large that Sarah can't fix it.

It took a village (or several villages!) to get to this point. I am so grateful for the community I've been part of in Fort Collins, including the Barnes Group, the Hurrell Group, my cohort and friends at CSU, the CIRA/ATS Mentoring Program Team, and St. Luke's Episcopal Church (especially the Creation Care Team); not to mention all of my friends and family in North Carolina and around the globe. I want to call out my ATS304 crew–Megan Franke, Lee Brent, Anindita Chakraborty, Bali Summers, and Sabrina Cohen–the strangest part of graduating might be no longer sharing an office with you! The unconditional support of my parents David and Therese Hueholt, my brother William Hueholt, and my aunt Claire Trout played an immeasurable role in this time–and throughout my life.

Finally, in the last five years, Charlotte Connolly and I have spent more hours together sharing science, graduate school, and life than I could label with an order of magnitude. Here's to the next project we tackle–or at least the next Minecraft world we make!

DEDICATION

I dedicate this dissertation to the mentors who worked with, encouraged, challenged, and helped me to grow–as a scholar and a human–in my journey to graduate school, including:

Sandra Yuter, Barbara Furr, and Kate Cardamone.

TABLE OF CONTENTS

LIST OF TABLES

LIST OF FIGURES

Chapter 1

Introduction

Impacts from anthropogenic climate change are well-documented in ecosystems around the globe, ranging from the Arctic to the Antarctic and from alpine environments to coastal communities [2–7]. Climate change affects ecosystems through the direct impacts of changing environmental conditions ("extrinsic change" [8], e.g., species shifting poleward to follow their thermal niches [9–11]) and by altering internal ecosystem dynamics ("intrinsic change" [8], e.g., disruption to specific species that produce nonlinear impacts on the whole ecosystem [12, 13]). Ecological risks are expected to worsen in all future scenarios–even those with ambitious mitigation targets–and are projected to lead to the widespread redistribution and extinction of species [14–19].

The worsening of climate risks and slow pace of international efforts to reduce emissions have led many scientific organizations to call for research into climate intervention methods to reduce greenhouse gas concentrations or directly cool the planet [20–23]. Stratospheric aerosol injection (SAI) is a hypothetical intervention method to emit particles into the upper atmosphere and reflect away a small portion of incoming sunlight, thereby cooling the planet [20]. SAI is analogous to natural processes that occur after extreme wildfires and volcanic eruptions [24–26]. Recent scholarship on climate intervention has contributed to knowledge around topics such as societal impacts, changes to Earth system dynamics, and scenario design (e.g., [27–36]. However, potential ecological impacts from climate intervention remain a key knowledge gap [21, 37]. In particular, there have been no studies of intrinsic ecosystem change or species-level impacts under SAI [37]

In addition to the influence of external forcings such as climate change or climate intervention, ecosystems are affected by fluctuations from natural climate variability arising from sources including the El Niño-Southern Oscillation or Arctic Oscillation [38–40]. Most research projecting future ecological change attempts to remove climate variability to focus on the forced response, or neglects the influence of natural variability (e.g., [9, 41–44]. Since contributions from climate

variability may amplify or oppose the forced response [45–47], better characterizing the range of outcomes possible with this variability is crucial to projecting future ecosystem impacts.

Earth system models can sample many climate states when run with perturbed initial conditions to generate an ensemble of simulations [46,47]. Large ensembles allow the estimation of the forced response to external change and sampling of the range of climate variability [47–49]. Individual ensemble members can be used to explore plausible cases of future events, a method known as a "storyline" approach [50–52]. Storylines have proven to be a powerful tool in studying phenomena where contributions from both the forced response and internal variability are important, such as anticipating extreme events or social surprises [51, 53, 54]. To our knowledge, however, these storyline methods have not yet been applied to study ecological impacts.

While prognostic simulation of complex ecosystems and species-level processes remains challenging, present-generation Earth system models can capture regional patterns of many climate parameters [55–58]. Existing fieldwork and theoretical studies have linked various environmental parameters to changes in ecosystems (e.g., [9, 10, 59, 60]). These environmental parameters facilitate model analysis into potential ecosystem change without requiring simulation of the ecosystem itself. This approach is analogous to model-based studies of environmental thermodynamic and kinematic parameters to explore changes to severe weather without requiring the explicit simulation of convection [61].

In this dissertation, we use output from existing large ensemble climate model simulations to study conditions leading to extrinsic and intrinsic ecosystem change in future scenarios of climate change and intervention. We apply storyline methods to explore contributions from internal variability along with the forced response.

Chapter 2, in concert with Appendix A as supplementary material, is currently in review as:

- Hueholt, D.M., E.A. Barnes, J.W. Hurrell, D. Lombardozzi, & A.L. Morrison. Exploring the Influence of Internal Climate Variability and Forced Change on Arctic Greening. In review at *One Earth*, 2025.

Chapter 3, together with Appendix B as supplementary material, is published as:

- Hueholt, D.M., E.A. Barnes, J.W. Hurrell, & A.L. Morrison (2024). Speed of environmental change frames relative ecological risk in climate change and climate intervention scenarios. *Nature Communications*, 15(1), 3332.

Chapter 4, with Appendix C as supplementary material, is currently in preparation for submission:

- Hueholt, D.M., E.A. Barnes, J.W. Hurrell, & A.L. Morrison. Potential distribution of a top Arctic predator under multiple climate futures. To be submitted.

Finally, Chapter 5 summarizes this work and looks ahead to future research directions.

Chapter 2

Exploring the influence of internal climate variability and forced change on Arctic greening

See footnote for publication information.[1]

2.1 Introduction

Warming Arctic temperatures drive both increased productivity in temperature-limited ecosystems and changes in species composition as woody plants advance into ice- and snow- dominated landscapes [62, 63]. This “Arctic greening" has been a prominent feature of Arctic environmental change since the late 20th century [62–67], especially because temperatures have risen faster in the Arctic than the rest of the globe [68, 69]. Extensive evidence spanning field studies [59, 60, 62, 64, 70–78], satellite measurements [3, 63, 65–68, 76, 77, 79–83], airborne remote sensing [71, 82, 84, 85], dendrochronology [59, 60, 65, 73–75, 78, 80, 86–90], proxy data [91–93], experimental tracts [88, 94, 95], and Indigenous knowledge [65, 96] has linked Arctic greening to temperature anomalies, particularly on timescales of a decade or longer. Growing degree days, the annual sum of daily temperatures above 5 °C, provide an important metric of growing season warmth and serve to tightly connect observed Arctic ecosystem change to ambient environmental conditions [59, 60, 73, 97].

The climate state at any given location and time consists of the response to external forcings, such as anthropogenic climate change, combined with fluctuations from internal climate variability [46, 47]. Fluctuations from climate variability affect terrestrial ecosystems on interannual to decadal timescales, and may amplify or oppose long-term forced trends [38–40]. When local warming trends exceed internal variability, temperature limitations due to cold no longer restrain

[1]This work is under review for publication as: Hueholt, D.M., E.A. Barnes, J.W. Hurrell, D. Lombardozzi, & A.L. Morrison. Exploring the Influence of Internal Climate Variability and Forced Change on Arctic Greening. In review at *One Earth*, 2025.

plant recruitment and greening may be sustained as long as the trend persists [70]. Most prior work projecting future changes from Arctic greening remove the contribution from internal variability and consider the forced response to climate change alone [41, 42].

Large ensemble climate model simulations sample many plausible climate states, allowing quantification of past and future forced change and internal variability [46–48]. While directly simulating land surface change in Earth system models remains challenging [55, 56], models can often effectively represent regional-scale patterns of climate variables [57, 58]. The well-established connection between growing degree days and Arctic greening [59, 60, 73, 97] enables model analysis of the climate conditions driving the ecosystem response without requiring direct simulation of land surface change. This approach is analogous to studies analyzing large-scale drivers of other climate phenomena that cannot yet be explicitly simulated in models, such as severe weather [61].

We use the Community Earth System Model 2 (CESM2) [57] Large Ensemble (LENS2) [48] to explore the role of internal climate variability and the forced response to climate change in growing degree days over the Arctic. We identify that most terrestrial Arctic ecoregions [1] have already crossed over into a state dominated by the warming trend. We take a storyline approach to connect cases of earlier and later crossover relative to the ensemble mean to specific forms of coupled climate variability. Conditions unprecedented in the Preindustrial baseline ("no-analog climate states") in the same model [57] begin to emerge over the Arctic in the mid-21st century. Finally, we contextualize model findings with historical observations using a new dataset of growing degree days derived from the Global Historical Climatology Network (GHCN) [98].

2.2 Results

2.2.1 The forced warming trend is already dominant in most Arctic ecoregions

Growing season temperature conditions in most Arctic ecoregions [1] have already experienced "forced crossover" (Figure 2.1, see Methods for details), which we define as conditions when the ensemble mean is greater than 80% of samples from the Preindustrial simulation (see Methods).

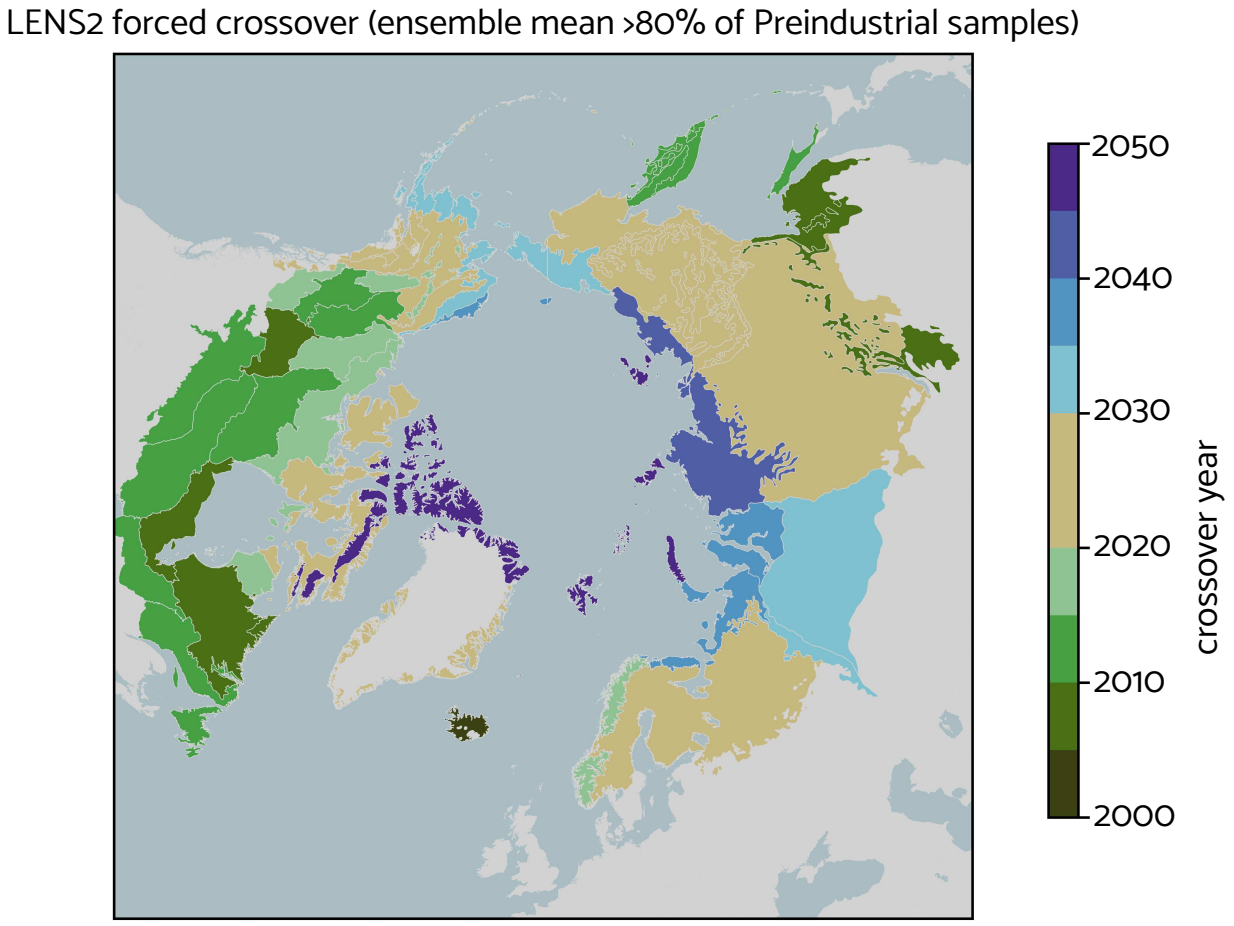

Figure 2.1: Forced crossover (ensemble mean >80% of Preindustrial samples) in growing degree days from the Community Earth System Model 2 Large Ensemble (LENS2) for ecoregions [1] poleward of 50 °N.

This illustrates how the warming trend already dominates over internal variability for much of the Arctic. Similar geographic patterns are seen in the raw data when the output is not aggregated by ecoregion (Figure S1).

The finding that forced crossover has already occurred in almost all ecoregions demonstrates how anthropogenic climate change has greatly impacted the coupled Arctic climate-ecological system in these CESM2 simulations. Central and eastern Canada experience uniform crossover times in the early 21st century (Figure 2.1), likely due to the flat topography in this region which produces a relatively homogeneous climate state. The highest-latitude tundra around the Arctic circle has not yet crossed over as these regions remain too cold (i.e., conditions rarely above 5 °C) for a substantial response in growing degree days.

Due to the role of internal variability in the real-world ecosystem response [38,40], it is difficult to directly connect the timing of forced crossover to observed historical land surface and ecosystem changes. Forced crossover in this model does broadly align with observed state changes in ecosystem composition in regions such as Quebec (early 2000s treeline and shrubline advance [62,74,96]) and the Canadian low Arctic (early 2000s shrubline advance and lichen dieback [82]). Regions where forced crossover has not yet occurred display increased productivity but not yet a change in ecosystem composition (e.g., Alaskan coastal tundra [76], Svalbard [77]).

2.2.2 Storylines of plausible crossover events in individual ensemble members

The climate states within the ensemble provide a distribution of plausible “member crossovers" (Figure 2.2a, thin gray lines) in addition to the estimate of “forced crossover" (Figure 2.2a, thick gray line) for any given location. Member crossover may be earlier or later than forced crossover, reflecting how internal variability may accelerate or delay when the climate state begins to consistently exceed conditions in the preindustrial simulation due to the forced response. Since the variability in individual members is greater than in the ensemble mean, we set the threshold to define member crossover higher (ensemble member exceeding 90% of Preindustrial samples, see Methods for details) than for forced crossover (ensemble mean exceeding 80% of Preindustrial samples).

Here, we show the distribution of member and forced crossover times for a point in the Brooks Range of Alaska (Figure 2.2a, thick gray line). At this location, forced crossover is estimated to occur in 2022. The 10th to 90th percentile of member crossover times ranges from 2011 to 2037. The early end of the range of member crossover times is consistent with field observations showing that the treeline is currently undergoing a rapid expansion which was observed to begin in the early 21st century [75].

From the distribution of member crossovers, we choose storylines corresponding to the 10th and 90th percentile of simulated crossovers (Figure 2.2a, thick pink and blue lines; Figure 2.2b,c)

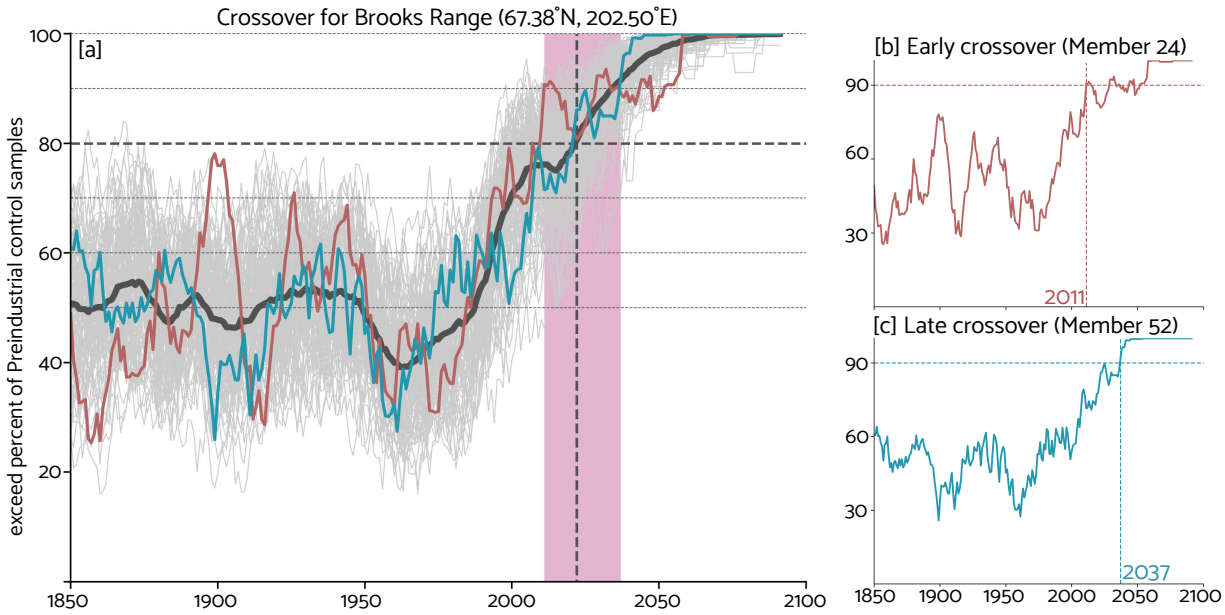

Figure 2.2: Timeseries of exceedance of preindustrial control baseline, showing forced crossover (panel a, ensemble mean >80% of Preindustrial control samples) and storylines of early (10th percentile; pink line panel a, shown alone in panel b) and late (90th percentile; blue line panel a, shown alone in panel c) member crossover (ensemble member >90% of Preindustrial control samples) in growing degree days from the Community Earth System Model 2 Large Ensemble (LENS2) for a point in the Brooks Range (67.38 °N, 202.50 °E). Thick gray line in panel a denotes the ensemble mean, with pink shading showing the 10th to 90th percentile of member crossover. Horizontal dashed line shows exceedance threshold for crossover; vertical solid line shows year when this crossover occurs. Thin horizontal dashed lines visually define other possible exceedance thresholds.

to illustrate how internal variability may amplify or suppress the expression of the forced response at this location in the Brooks Range. In the fully-coupled model, these early and late crossover events can be connected to internal climate variability in other parts of the Earth system. We identify coherent features in the pattern of sea surface temperature (SST) during the decade leading to crossover in these storylines (Figure 2.3).

An anomalously warm North Pacific and Beaufort Sea occur in the storyline of early crossover (Figure 2.3a), with cold anomalies for the same regions in the late crossover case (Figure 2.3b). These patterns appear consistent with those of Pacific Decadal Variability (PDV) [99]. Composites of the decades leading up to the earliest (Figure 2.3c) and latest (Figure 2.3d) 20 crossover events show similar features to those in the individual storylines, indicating that a positive or negative phase of the PDV may amplify or suppress the rate of terrestrial ecosystem change in this location

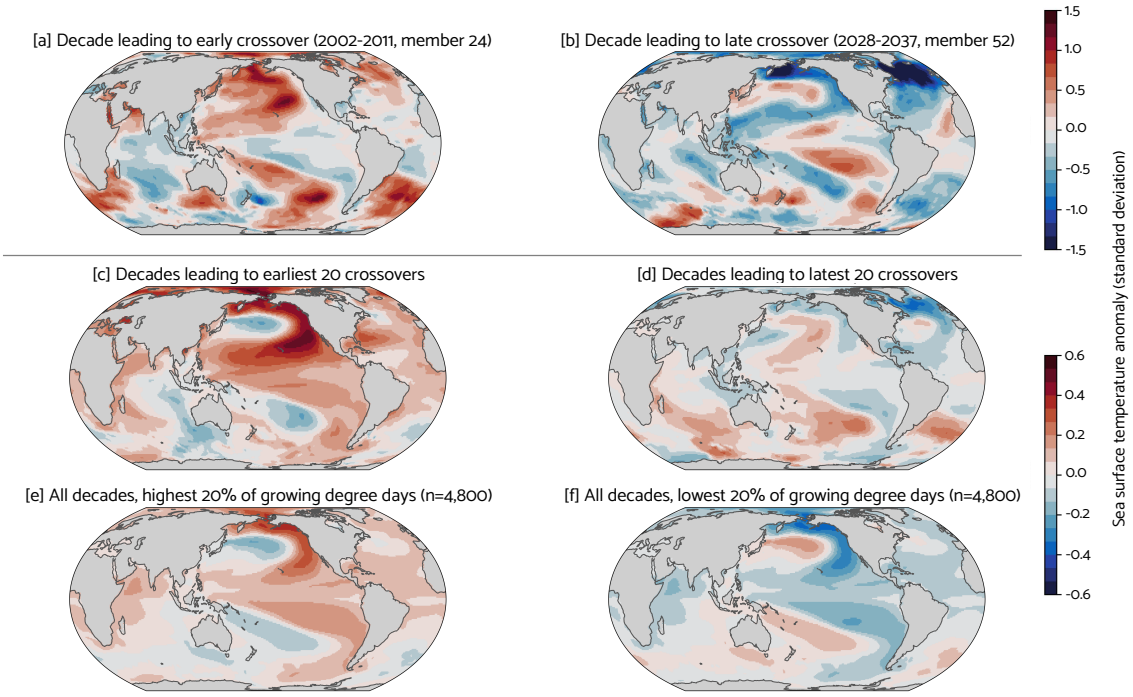

Figure 2.3: Sea surface temperature anomalies in members from the Community Earth System Model 2 Large Ensemble (LENS2) corresponding to a storyline of early (10th percentile, panel a) and late (90th percentile, panel b) member crossover; the average of earliest 10 crossovers (panel c) and latest 10 crossovers (panel d); and the average of the highest (panel c) and lowest (panel d) 20% of growing degree days in each decade 1850-2100 for a point in the Brooks Range of Alaska (gray dot, 67.38 °N, 202.50 °E).

in Alaska. The positive SST pattern is stronger in the composite of early crossovers (Figure 2.3c) than the negative SST anomalies in the composite of late crossovers (Figure 2.3d). This suggests that positive phases of the PDV may contribute more to advancing the time of crossover than negative phases contribute to delaying it.

Composites of all 10-year average SST maps associated with the highest and lowest 20% of growing degree days for this same location show similar PDV-like patterns (Figure 2.3e,f). Positive and negative PDV-like anomaly structures are associated with locally increased (Figure 2.3e) and suppressed growing degree days (Figure 2.3f), respectively. The SST anomaly patterns are stable over time (Video B.1, Video B.2), providing further confidence that these represent a robust association between SST variability and the environmental conditions driving ecosystem change in the Arctic.

Not every geophysical quantity displays consistent patterns associated with enhanced or suppressed growing degree days. For example, similar composites based on sea level pressure associated with the highest and lowest 20% of growing degree days show no clear anomalies (not shown). This is consistent with the larger contribution from the ocean than the atmosphere to Earth system variability on decadal timescales [100].

2.2.3 No-analog crossover begins in the mid-21st century

A location experiences “no-analog crossover" in a given member when it exceeds every sample in the Preindustrial control. On average, no-analog crossover begins to occur in most ecoregions in the mid-21st century (Figure 2.4). No-analog conditions are not required for ecosystem change to occur, since Arctic greening is already widespread [62, 63], but may be associated with the formation of novel communities and species interactions [101–103].

The spatial pattern (Figure 2.4) of no-analog crossover is broadly similar to the pattern of forced crossover (Figure 2.1). The primary feature is the latitudinal gradient, with earlier emergence at lower latitudes and later emergence towards the pole. The earliest emergence of no-analog conditions is projected in the topographically flat regions of central and eastern Canada. Certain ecoregions in Greenland and western Scandinavia experience an early-century forced crossover (Figure 2.1), but a late-century no-analog crossover (Figure 2.4). This may be due to the influence of the North Atlantic warming hole, where a slowdown in the Atlantic Meridional Overturning Circulation slows the rate of change for the regional climate over the 21st century in CESM2 [104].

2.2.4 Contextualization of model results with observed changes in growing degree days

Growing degree days derived from weather stations around the circumpolar region in the Global Historical Climatology Network (GHCN) [98] provide insight into change over the historical period. GHCN stations show variability on interannual and decadal timescales, with a longer-term forced trend clear at most sites beginning in the late 20th century (a selection of which

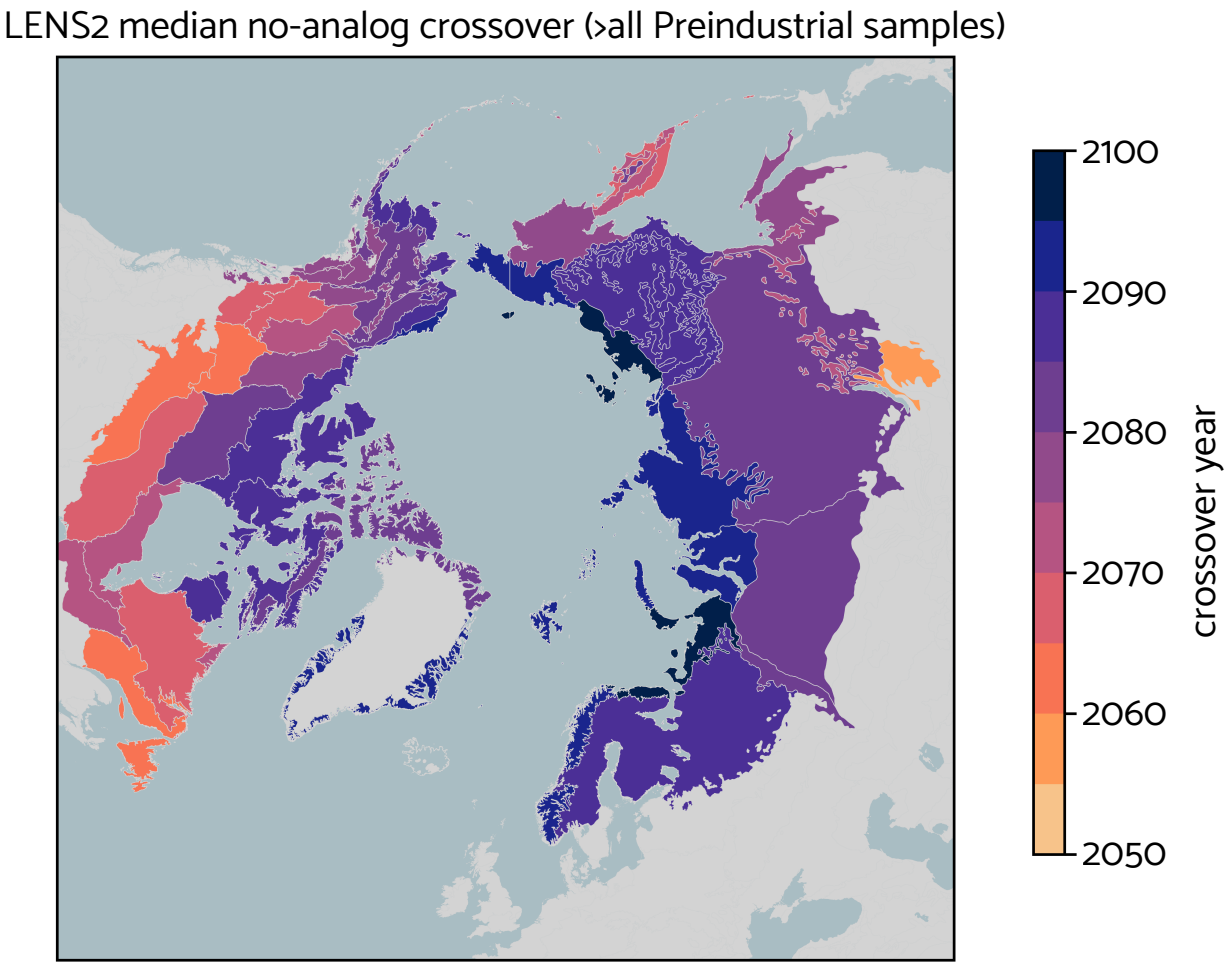

Figure 2.4: Median no-analog crossover (ensemble member >all Preindustrial samples) in growing degree days from the Community Earth System Model 2 Large Ensemble (LENS2) for ecoregions [1] poleward of 50 °N.

is shown in Figure 2.5). Certain very high-latitude sites, such as the Ostrov Vrangelya weather station (Figure 2.5e), exhibit an emergence of growing degree days from a baseline of near-zero occurrence in the early 20th century.

Trends in growing degree days across the circumpolar region show the relative influence of internal variability and forced change on different timescales. On 30-year timescales, trends in growing degree days are broadly positive beginning in the late 20th century, consistent with the forced response to anthropogenic global warming (Figure 2.5). On 10-year timescales, which are crucial for ecosystem responses [3, 60, 72, 78, 89], trends remain much more variable due to the relatively larger contribution of internal variability. The trends in this historical record illustrate

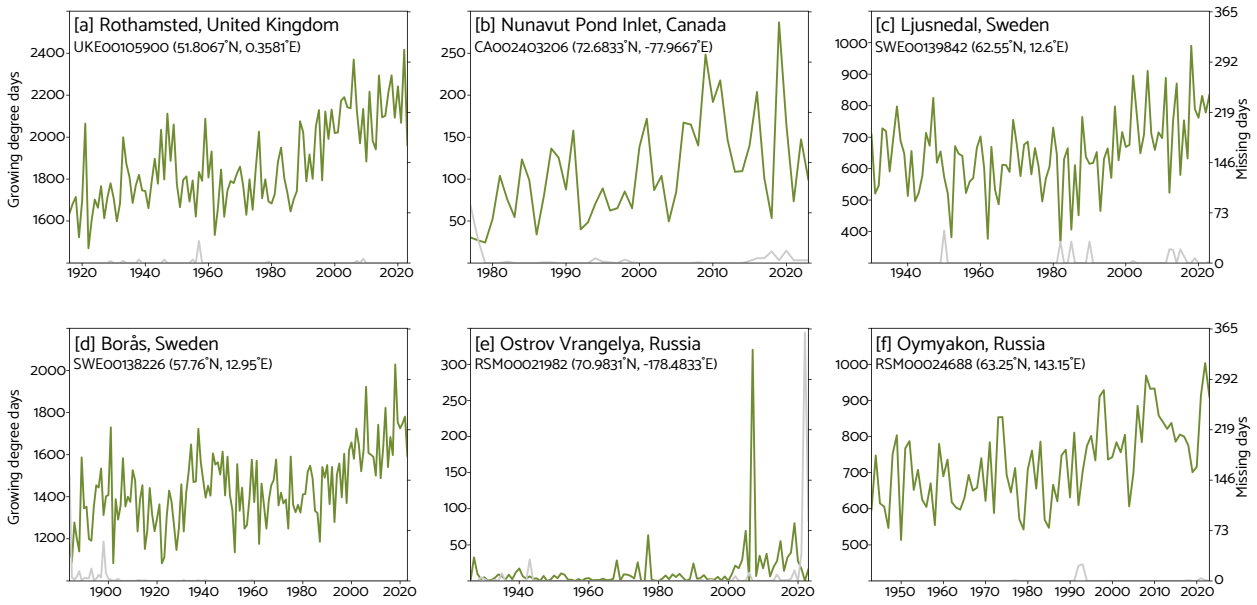

Figure 2.5: Timeseries of annual growing degree days (green, left axis) and missing days per year (gray, right axis) calculated from selected Global Historical Climatology Network weather stations poleward of 50 °N. All stations shown are missing less than 3% of days and have a period of record >30 years. Note that the left y-axis range is different for each panel.

the importance of both internal variability and the forced response on the conditions that drive observed ecosystem change.

The distribution of growing degree day trends in LENS2 captures the vast majority of station observations on both 30-year and 10-year timescales (Videos B.3 and B.4, dots without circles). Formal climate model evaluation against individual station records is challenging due to factors including representativeness error [105–107], data homogenization issues on multidecadal timescales [98], and underconstrained contributions from historical internal variability [108]. Still, this analysis indicates that LENS2 displays grid-box scale distributions of long-term trends and decadal variability in growing degree days that are consistent with reality; failing this test would have been strong evidence against model adequacy for this analysis [109, 110].

2.3 Discussion

We use a large ensemble of climate model simulations [48] to explore the influence of the forced response to climate change and internal variability in growing degree days over the Arctic.

Most Arctic ecoregions have already experienced forced crossover and entered a regime where growing season environmental conditions are dominated by the warming trend. Storyline analysis in an Earth system framework illustrates how coupled internal variability influences the conditions experienced by ecosystems. These storylines reveal that Pacific and Arctic SST variability affect growing degree days in the Brooks Range of Alaska–a region where rapid expansion of the treeline is ongoing [75]. No-analog crossover relative to a preindustrial simulation is projected to occur during the mid- to late-21st century for most locations. Growing degree days in CESM2 are consistent with long-term trends and decadal variability over the observational record.

On a circumpolar scale, the high-latitude ecosystem response to climate change is driven by increasing growing degree days [59,60,73,97]. Local-scale and species-level changes are often determined by other climatic drivers, including changes in soil moisture [66], seasonal precipitation [111], or wildfire activity [79, 112, 113]. Non-climatic factors such as recruitment [70, 86, 89, 91], interspecies interactions [114–116], and life history [60, 70] also affect the timing and scale of the ecosystem response; in particular, grazing by reindeer and caribou can halt greening processes in certain cases [117]. Thus, changing thermal conditions do not always immediately alter ecosystem composition [60, 70, 90, 115]. Once environmental conditions no longer limit plant growth, however, both paleoclimatic evidence and observational data indicate ecosystem change may occur very rapidly (on interannual to decadal timescales) when favorable recruitment conditions subsequently occur [59, 75, 89, 91].

Our analysis of a single model large ensemble under one future emissions scenario (Shared Socioeconomic Pathway 3-7.0 [118]) neglects both structural and scenario uncertainty in favor of studying climate variability. The configuration of CESM2 used in LENS2 exhibits biases in Arctic sea ice due to cloud-aerosol-chemistry interactions [57, 119], and SSP3-7.0 is not consistent with current policy pledges by governments [120] and recent emissions estimates [121]. However, on the near-term time horizons relevant for the phenomena we study, internal variability exerts a greater influence in the Arctic than either structural uncertainty [122] or scenario uncertainty [123]. The choice of scenario may play a role in the late-century timing of no-analog crossover

(Figure 2.4). Higher-emissions scenarios such as SSP3-7.0 remain useful by probing a wider variety of futures which are possible–even if less likely–due to factors such as negative socio-political surprises [54] or an unfavorable realization of the pattern effect [124].

Storylines explore plausible individual future cases from within a distribution of possible climate states, and are increasingly used in analyses where the combination of variability and forced change are crucial to anticipate impacts [50,52]. Examples of storyline applications include assessing climate risk [51,52], exploring surprising futures [54], and anticipating extreme events [50,53]. As ecosystems respond to the combination of forced change and variability [38,40,125], storylines have the potential to prove similarly useful in exploring ecological change when an environmental driver is clearly defined.

2.4 Methods

2.4.1 Growing degree days

Growing degree days describe the annual sum of temperature above a base value (Equation 2.1) [97, 126]. In Equation 2.1, GDD denotes growing degree days, T_{d_i} the daily temperature on a given day i, $n = 365$ the annual sum, and b some base threshold. We choose $b = 5$ °C following the Arctic International Tundra Experiment (ITEX) protocols [97], as well as observational studies and dendrochronological evidence [60, 73] which support the use of this base value for Arctic terrestrial ecosystem change.

$$GDD = \sum_{i=1}^{n} H(T_{d_i}); H(T_{d_i}) \begin{cases} (T_{d_i} - b) & T_{d_i} > b \\ 0 & T_{d_i} \leq b \end{cases} \tag{2.1}$$

We use the term “growing degree days" to match the ITEX protocols [97]. This same quantity may also be called the “thermal sum above base temperature" [71]. Percent changes for growing degree days in Videos B.3 and B.4 are calculated from an ordinary least squares linear regression following U.S. Environmental Protection Agency guidelines [126].

2.4.2 Model simulations

We use output from two sets of climate model simulations performed with the Community Earth System Model version 2 (CESM2) using the Community Atmosphere Model version 6 (CAM6) to explore changes in growing degree days in the Arctic [57]. CESM2(CAM6) is a best-in-class Earth system model which has been used to submit simulations to the United Nations Intergovernmental Panel on Climate Change Coupled Model Intercomparison Project (CMIP) [57, 58]. We further contextualize the performance of CESM2(CAM6) with growing degree day observations in the main body of the paper.

The CESM2 Large Ensemble (LENS2) [48] is an initial condition ensemble with 100 different realizations of the historical period (1850-2014) and 21st century (2015-2100). Between 1850 and 2014, the simulation is forced with boundary conditions derived from observations over the historical record. Ensemble variability is generated through both microperturbations to the atmospheric state and macroperturbations to the ocean state to disperse both atmospheric and oceanic internal variability. 50 members of the ensemble follow CMIP6 forcings over the historical period; another 50 members use a smoothed version of the biomass burning fluxes to dampen spurious variability [127]. From 2015-2100, LENS2 follows the low-mitigation, high-forcing Shared Socioeconomic Pathway 3-7.0 (SSP3-7.0) scenario [48, 118]. For clarity, we note that ensemble members from LENS2 referenced in the text are zero-indexed for consistency with the Python codebase.

The CESM2(CAM6) Preindustrial control is a 2000-year free-running simulation with boundary conditions fixed at 1850 estimates [57]. The Preindustrial simulation does not correspond to conditions experienced by ecosystems in the real-world preindustrial era, which would include natural forcings such as volcanic eruptions (e.g., a “Last Millennium" simulation) [128]. For the purposes of this work, a selection of climate states with internal variability but no long-term changes in external forcing [129] provides the proper baseline to calculate a distribution shift as external forcings become relatively larger. This baseline would not be suited to make claims about the adaptive capacity of specific ecosystems based on conditions experienced in their evolutionary history.

2.4.3 Surface station data

We calculate growing degree days for surface observations from the Global Historical Climatology Network (GHCN) [98] to explore historical climate change and contextualize model performance. GHCN aggregates weather station data from a breadth of sources worldwide into a single dataset with uniform quality assurance. We select stations poleward of 50 °N to include the latitudes conventionally associated with Arctic greening [63]. For our analysis, we include stations only where data is recorded on greater than 97% of days and the record is longer than 30 years (Figure 2.5, Video B.3) or 10 years (Video B.4). We apply no further quality control or homogenization to the data record.

2.4.4 Crossover definitions

We define crossover by comparing samples of 10-year rolling averages from each member and the ensemble mean of LENS2 relative to the Preindustrial simulation. In the absence of additional external forcings, the members and mean of LENS2 would exceed samples from the Preindustrial with 50% frequency, that is, they would be equally likely to be higher or lower than the Preindustrial values. (A special case occurs for points where growing degree days do not occur; in this case, samples from both simulations will be equal to zero.) Given a perfect estimation of the forced response by an infinitely large ensemble, any departure from 50% in the ensemble mean would be indicative of “crossover" into a new regime.

The finite 100-member ensemble of LENS2 introduces uncertainty, necessitating the choice of a stricter threshold to identify crossover. We define forced crossover at a given location when the ensemble mean exceeds 80% of Preindustrial samples. We define member crossover for an ensemble member at a given location when it exceeds 90% of Preindustrial samples. The greater threshold for member crossover accounts for the larger variability in individual realizations as opposed to the ensemble mean. We define no-analog crossover for an ensemble member at a given location when it exceeds all Preindustrial samples.

The choice of threshold involves subjectivity. We design the metric to address the question of when the warming trend emerges from decadal variability. Visually, the choice of 80% is well beyond any variance in the ensemble mean during the 1850-1900 period when human influence on the climate was relatively small compared to present (Figure 2.2a, thick line); the choice of 90% for member crossover prevents false positives during this same period (Figure 2.2a, thin lines). No-analog crossover provides an intuitive metric of the time when climate conditions reach a completely novel state relative to the Preindustrial simulation. Readers can choose their own threshold on Figure 2.2a by examining the other dashed horizontal lines, or by altering the figure in the associated code (see Data and Code Availability statement).

Crossover provides a non-parametric effect size statistic that leverages the large number of simulated climate states in both LENS2 and the long Preindustrial simulation by comparing samples from each. Its unit of "exceed X% of preindustrial samples" intuitively addresses our goal of identifying when the warming trend emerges relative to preindustrial variability. The crossover metric requires no further assumptions about the statistical properties of the data or its trends, such as linearity, homoscedasticity, or normality.

2.4.5 Data and code availability

- LENS2 [48] is available at the National Science Foundation National Center for Atmospheric Research Climate Data Gateway doi.org/10.26024/kgmp-c556
- Output from the CESM2 preindustrial control [57] is available at the World Data Center for Climate doi.org/10.26050/WDCC/AR6.C6CMNRCES2
- The Global Historical Climatology Network [98] record is available at Amazon Web Services registry.opendata.aws/noaa-ghcn/ under resource name arn:aws:s3:::noaa-ghcn-pds
- Analysis code and derived growing degree days datasets used in this work will be permanently archived on the Open Science Framework subsequent to peer review.
- Portions of the work make use of the colormaps in the CMasher package [130].

Chapter 3

Speed of environmental change frames relative ecological risk in climate change and climate intervention scenarios

See footnote for publication information.[2]

3.1 Introduction

The imprint of anthropogenic climate change is clear in ecosystems worldwide, with worsening impacts expected under all future emissions pathways [11, 14, 15, 17, 40, 131, 132]. High-impact risks such as these motivate the study of potential climate intervention methods to reduce climate impacts as efforts to decarbonize continue [20, 21]. Stratospheric aerosol injection (SAI) is a hypothetical method to limit warming or cool the planet by adding reflective particles to the stratosphere [20]. Many different potential SAI deployment scenarios could complement emissions reductions. For example, SAI could be used to maintain global temperatures at or below some critical threshold, or to rapidly reduce temperatures [20, 21, 30, 133, 134]. In contrast to carbon dioxide removal interventions, which operate on slower timescales [135], solar radiation management methods such as SAI currently represent the only known method to quickly alter global mean temperatures with near-future technology [20, 21].

Species habituated to environmental niches must shift their range, adapt, or be extirpated as ambient conditions shift geographically in a changing climate [10, 19]. The climate velocity of 2 meter temperature expresses the movement of thermal conditions, and can be used to address the question: How fast, and in what direction, must an organism move over a period to stay in the

[2]This work is published as: Hueholt, D.M., E.A. Barnes, J.W. Hurrell, & A.L. Morrison (2024). Speed of environmental change frames relative ecological risk in climate change and climate intervention scenarios. *Nature Communications*, 15(1), 3332.

same temperature conditions in which it started? [9, 10]. Species have varying ability to shift their range in response to climate change; on average, marine organisms can move more quickly than terrestrial species, and trees have among the slowest responses of all forms of life [11, 91, 136]. Climate impacts to ecology emerge from many sources beyond temperature, including changes in precipitation [19], biogeochemistry [10, 15], or interactions among species [12, 137]. Species with very short life histories (e.g., bacteria) can adapt to a changing climate through evolution, while more complex organisms may be able to employ behavioral adjustments [19, 40, 138, 139]. Populations unable to adapt or shift their range at sufficient rates may be at risk of extirpation– which often takes place abruptly following subsequent extreme events rather than as a slow, linear process accompanying the climatic change [40, 140]. The climate velocity provides a general metric for perturbations to large-scale ecology by the movement of thermal niches, rather than a tool to describe all types of impacts [9, 10, 137].

Future values of the scalar magnitude of climate velocity (which we refer to as the climate speed) under scenarios consistent with present policy exceed mean dispersal rates of known terrestrial ($\lessapprox$2 km/yr [9, 11]) and marine species ($\approx$7 km/yr [11]), and are expected to redistribute and endanger ecosystems globally [10, 17, 132]. The use of SAI has the potential to contribute an additional dimension of particularly rapid temperature change at the start or end of an intervention. Abrupt warming and cataclysmic climate speeds (“termination shock") are possible if an SAI intervention were to be terminated from masking a higher radiative equilibrium, or potentially dangerous cooling may occur at the start of an intervention intended to rapidly reduce global temperatures [136, 141]. While the specific choices involved in generating a termination shock are clear [136, 141, 142], the strategic design decisions that could result in dangerous cooling rates are currently unknown.

We analyze climate speeds in the 20-year period following SAI deployment in simulations performed in the Community Earth System Model Version 2 with Whole Atmosphere Community Climate Model (CESM2[WACCM6]) under the Assessing Responses and Impacts of Solar climate intervention on the Earth system with stratospheric aerosol injection (ARISE) protocol [57, 134, 143].

ARISE simulations were constructed to allow outcomes to be directly connected to specific strategic design choices in each scenario. The ARISE-1.5 scenario portrays the deployment of SAI in 2035 to maintain the Paris Agreement global temperature target of 1.5°C above preindustrial against moderate-mitigation climate change (Shared Socioeconomic Pathway [SSP] 2-4.5) [134]. ARISE-DelayedStart has a similar target of ≈1.37°C but SAI deployment in 2045, yielding a rapid temperature reduction due to warming over the intervening decade [144]. A 10-year period represents a plausible delay that could come about from global governance and decisionmaking processes [30, 145]. We compare these scenarios against baselines of preindustrial climate variability over the millennium prior to 1850 (Last Millennium, 850-1849) and no-SAI climate change consistent with present policy (SSP2-4.5) [121, 143, 146–148].

3.2 Results

3.2.1 Distinct responses linked to strategic choices

Global maps of climate speeds (Figure 3.1) reveal highly distinct outcomes in the pattern of ecosystem risk in each of the four scenarios, reflecting their individual temperature trends over time (Figure 3.2).

Substantial climate speeds forced by warming occur nearly globally under no-SAI SSP2-4.5 (Figure 3.1ab). The majority of land area (61%) is exposed to potentially dangerous climate speeds beyond 2 km/yr (Figure B.1a). Very large climate speeds are projected to cause extreme ecosystem stress in tropical regions where spatial gradients are weak (Figure 3.1ab) [132, 149]. For example, ensemble mean climate speeds averaged over the Amazon region (as defined by the IPCC Working Group 1 Fifth Assessment Report [150]) are 12 km/yr, suggesting that tropical terrestrial species would need to move poleward or up topography by 240 km in order to remain in their starting conditions over this 20-year period. Sharp topographic gradients buffer climate speeds and allow relict populations to shelter in microclimates, but these communities often have low connectivity [14, 151] and persistent warming may render these niches inaccessible [9, 14, 16, 151]. Poor connectivity can occur elsewhere due to causes including fragmentation by human land use such

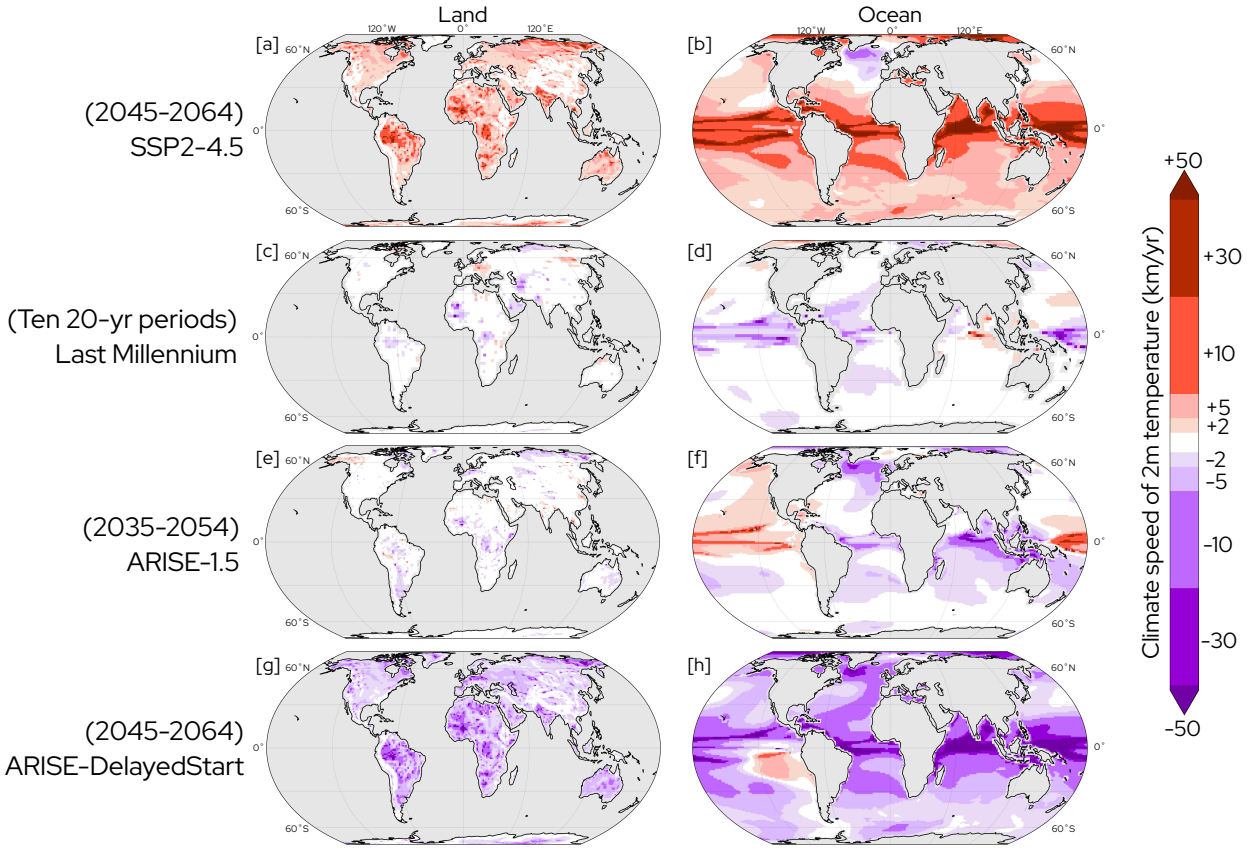

Figure 3.1: 20-year climate speeds of 2-meter (2m) temperature on land (left column) and ocean (right column) in the ensemble mean for Shared Socieconomic Pathway 2-4.5 (SSP2-4.5) [a,b], the mean of ten 20-year periods (to match ensemble size in Assessing Responses and Impacts of Solar climate intervention on the Earth system (ARISE) simulations, see Methods) in the Last Millennium [c,d], and ensemble mean for ARISE-1.5 [e,f], and ARISE-DelayedStart [g,h]. The sign indicates whether the change in temperature associated with the climate speed is positive or negative. Masked area shown in gray (ocean for [a,c,e,g], land for [b,d,f,h]).

as urbanization [152, 153], or natural barriers as in semi-enclosed marine basins like the Mediterranean Sea [154]. This fragmentation impedes the ability of many ecological communities to shift in response to climate changes and may increase population vulnerability [151, 152, 155].

In the ocean, while depth gradients in temperature allow some species to escape climate change, non-thermal constraints prevent many from shifting vertically [10, 149, 156]. Climate speeds are large in the Arctic, where the warming rate is high due to Arctic amplification [157]. Transport barriers imposed by the edge of continents and the North Pole mark poleward limits on terrestrial and marine species [17, 158]. Negative climate speeds occur in the North Atlantic warming hole (Figure 3.1b) where a decreasing temperature trend is driven by the weakening Atlantic Merid-

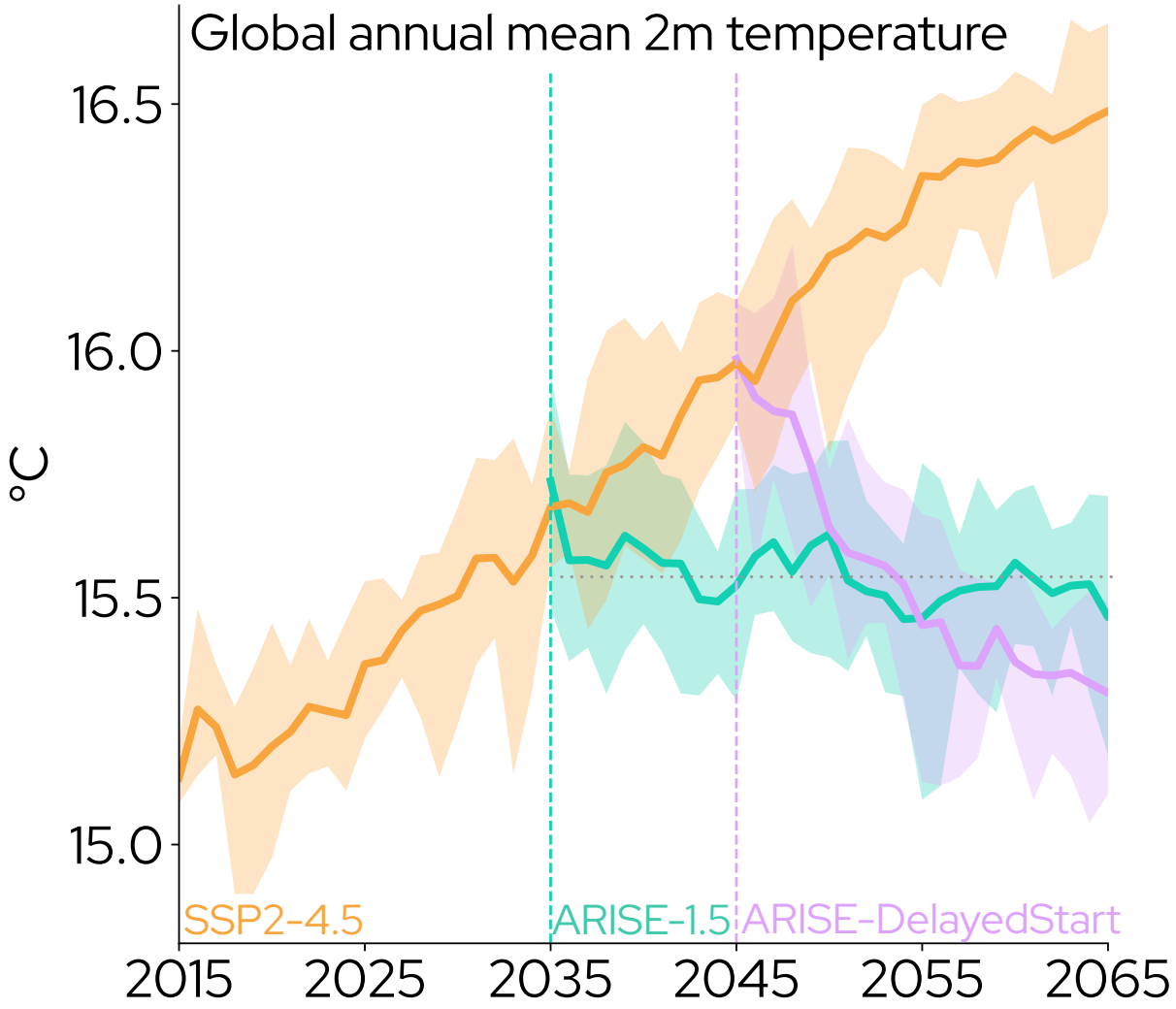

Figure 3.2: Timeseries of global annual mean 2-meter (2m) temperature in the Shared Socioeconomic Pathway 2-4.5 (SSP2-4.5) and Assessing Responses and Impacts of Solar climate intervention on the Earth system (ARISE) 1.5 and DelayedStart simulations. Thick lines portray the ensemble mean; shading shows variability spanning the maximum to minimum ensemble member at each year. Vertical dashed lines denote the deployment of SAI in 2035 (ARISE-1.5) and 2045 (ARISE-DelayedStart), while the horizontal dotted line displays an approximate temperature threshold of 1.5°C above preindustrial. Colors used to distinguish different simulations.

ional Overturning Circulation in these simulations [104, 159]. Analogous to historical ecosystem responses to persistent internally-driven temperature anomalies [38,40], it is possible the North Atlantic may experience competing ecosystem responses between negative climate speeds associated with the warming hole and positive climate speeds elsewhere in the basin.

Climate speeds averaged over ten 20-year periods from the Last Millennium (Figure 3.1cd) are small, reflecting the relatively smaller magnitudes and slower evolution of climate forcings over this epoch. Volcanoes exert the largest external forcing on surface temperatures over the Last Millennium, but their influence is highly nonlinear and only persists for a few years [160, 161]. As the climate velocity does not provide meaningful insight on these timescales [10], we omit periods within 5 years of a large volcanic eruption (defined as 10 teragrams of stratospheric sulfate injection [147]). Internally-driven climate variability [46, 129], natural phenomena such as solar cycles [162], small volcanic eruptions [163], or anthropogenic land use changes [164] can still cause nonzero regional-scale climate speeds (e.g., in Eastern Europe on Figure 3.1c). Climate speeds are larger over the ocean (Figure 3.1d) than land (Figure 3.1c), reflecting the smaller spatial temperature gradients in marine environments [149]. Where temperature gradients are shallowest over the tropical oceans, even small perturbations to temperature can drive nonzero climate speeds [149]. The small magnitude of these climate speeds indicate internal variability and natural forcings over this period could lead to distributional shifts among species, but would not likely exceed their dispersal capabilities. A purely unforced simulation with boundary conditions fixed at 1850 (Figure B.2) produces qualitatively similar results.

The 20-year climate speeds following deployment of ARISE-1.5 in the year 2035 (Figure 3.1ef) to maintain global mean temperature at 1.5°C above preindustrial are relatively small compared to no-SAI SSP2-4.5 (Figure 3.1ab). These climate speeds reflect the nearly flat temperature trends implied by the use of SAI to maintain temperature (Figure 3.2). Over land, climate speeds in ARISE-1.5 (Figure 3.1e) are similar in magnitude to those in the Last Millennium simulation (Figure 3.1c). Climate speeds over the ocean (Figure 3.1f) are largely negative in sign. Since global temperatures are slightly above the 1.5°C target when the intervention is deployed in 2035, ARISE-1.5 forces a small negative trend in temperature (Figure 3.2). On regional scales, internal climate variability can overwhelm the forced response to the SAI intervention (e.g., Figure 3.1f in the eastern Pacific) [33, 165]. Negative climate speeds occur in the North Atlantic warming hole similar to no-SAI SSP2-4.5, as the weakening of the Atlantic Meridional Overturning Circulation

is partially offset–but not halted–by the SAI intervention in ARISE-1.5 [134, 159, 166]. Much more ocean area is exposed to climate speeds of 2 km/yr (48%) and 5 km/yr (17%) in ARISE-1.5 than the Last Millennium (23% and 8%, respectively). These values are within the observed mean dispersal rates of marine species (≈7 km/yr [11, 131]), and little area is exposed to climate speeds that exceed these values in ARISE-1.5 (Figure B.1b).

The SAI strategy in ARISE-DelayedStart produces large 20-year climate speeds (Figure 3.1gh) due to the negative temperature trend necessary to quickly reach the temperature target following deployment in 2045 (Figure 3.2). A greater amount of land and ocean area is exposed to dangerous climate speeds in ARISE-DelayedStart (Figure 3.1gh) as opposed to no-SAI SSP2-4.5 (Figure 3.1ab; Figure B.1). Two-thirds of land area (66%) is exposed to climate speeds beyond 2 km/yr; 13% of total land area (comparable to the size of South America) and more than a third of the world ocean (35%) are exposed to climate speeds greater than 10 km/yr in ARISE-DelayedStart (Figure 3.1). Five percent of the ocean is exposed to climate speeds beyond 50 km/yr (Figure 3.1h, Figure B.1b), which surpasses even the capability for extreme range shifts observed in many invasive species [167]. During the 20-year period following deployment, ARISE-DelayedStart depicts a forcing from climate speeds to global and regional ecosystems (Figure 3.1gh) that exceeds the corresponding time period in no-SAI SSP2-4.5 (Figure 3.1ab), and draws a striking contrast to the small values under ARISE-1.5 (Figure B.3). This phenomenon of large climate speeds forced by rapid global temperature reduction could be viewed as a “deployment shock," similar to the termination shock previously identified if an intervention ceases at a high radiative equilibrium [136, 141].

3.2.2 Internal climate variability modulates conditions

Land and ocean median climate speeds in the Last Millennium simulation (Figure 3.3a) illustrate the range of values experienced in 20-year periods in the preindustrial climate. The small magnitude of these climate speeds are within the range of dispersal rates for terrestrial and marine species [9, 11]. When considering the full distribution of 20-year periods during the Last Millen-

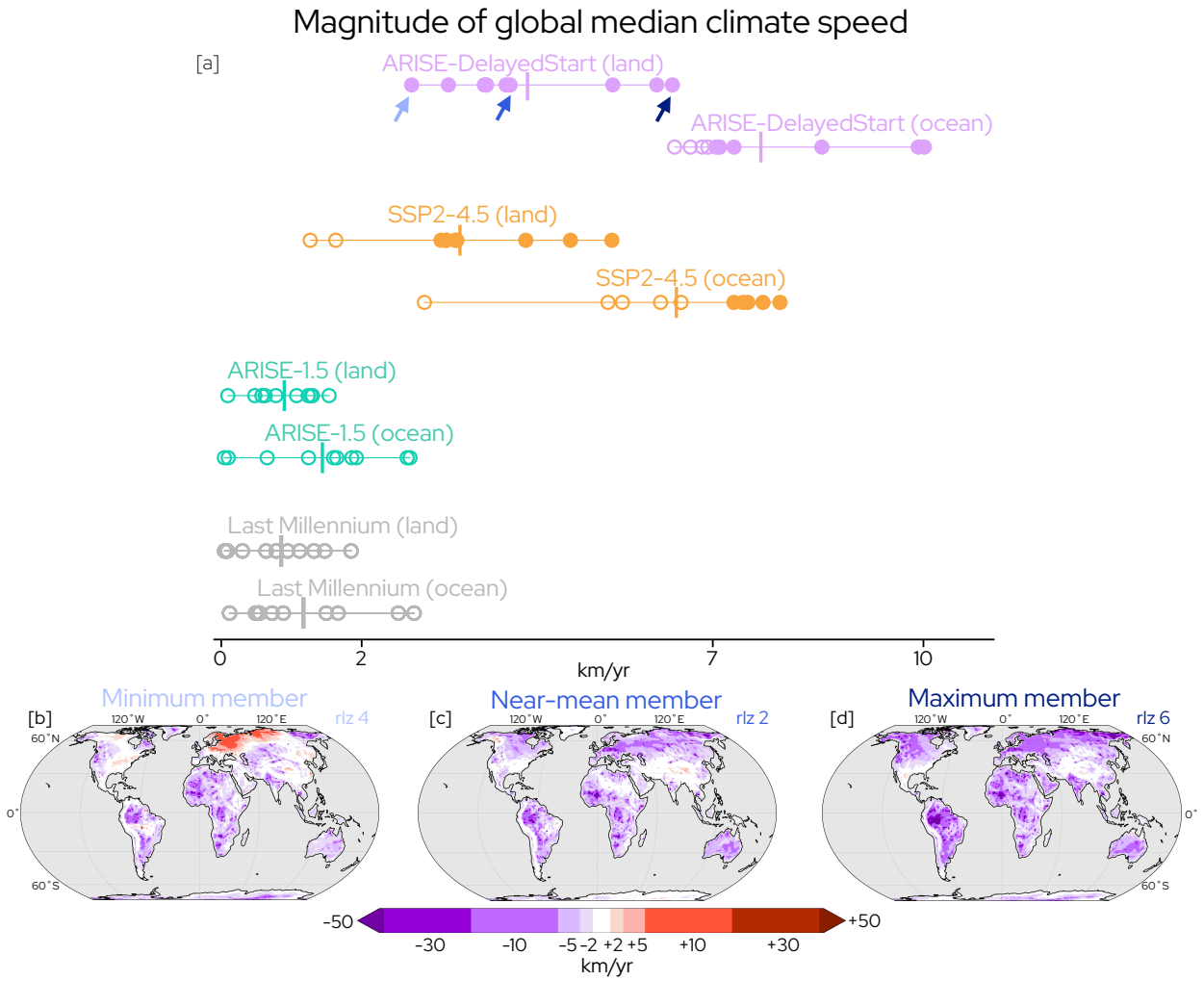

Figure 3.3: Magnitude of global median climate speed of 2-meter temperature over land and ocean [a] in Shared Socioeconomic Pathway 2-4.5 (SSP2-4.5), Last Millennium, and Assessing Responses and Impacts of Solar climate intervention on the Earth system (ARISE) 1.5 and DelayedStart simulations. Maps of ensemble member with minimum [b], near-ensemble mean [c], and maximum [d] median climate speed over land in ARISE-DelayedStart. In [a], open circles denote climate speeds within the mean dispersal speed of terrestrial or ocean species, closed circles signify climate speeds exceeding mean dispersal speeds, and vertical bars show the ensemble mean. Arrows in [a] denote ensemble members [b], [c], and [d]. Climate speeds are calculated over 2035-2054 (ARISE-1.5), 2045-2064 (ARISE-DelayedStart and SSP2-4.5), and ten 20-year periods (Last Millennium). Colors in [a] distinguish different simulations. See Figure B.4-B.7 for individual members in all simulations. Masked ocean area shown in gray [b-d].

nium, climate speeds infrequently exceed mean dispersal rates of terrestrial species ($\approx$ 2 km/yr) and never exceed those of marine species ($\approx$ 7 km/yr) (Figure B.9a). Median climate speeds over both the land and ocean from the ARISE-1.5 scenario where SAI is used to maintain global mean temperature fall within the distribution of Last Millennium variability (Figure 3.3a). The global

land and ocean median climate speeds in ARISE-1.5 are statistically indistinguishable from the Last Millennium simulation under a robustness test [165]. Climate speeds under no-SAI SSP2-4.5 robustly exceed both the Last Millennium and ARISE-1.5 over the land and ocean. In ARISE-DelayedStart, climate speeds surpass all other scenarios: the distribution is entirely separated from ARISE-1.5 or the Last Millennium, and robustly larger in magnitude than no-SAI SSP2-4.5 over land.

Contributions from internal variability are large on decadal to interdecadal timescales, such as the 20-year periods examined here, even in the presence of an external climate forcing such as an SAI intervention [33, 46, 165]. While analyzing the ensemble mean (Figure 3.1) allows for investigation of the response to a climate forcing, each individual ensemble member (Figure 3.3bcd) illustrates a plausible representation of the conditions that could be experienced under a single realization of internal variability. We describe the evolution of members across the ensemble of ARISE-DelayedStart to provide an example of the role of internal variability in the presence of a forced response to an SAI scenario of rapid temperature reduction. Climate speeds are large across the ensemble of ARISE-DelayedStart, exceeding dispersal rates in marine ($\approx$7 km/yr) and terrestrial species ($\lessapprox$2 km/yr) in every ensemble member over land and six members over the ocean (Figure 3.3a). Still, on regional scales in individual members, internal variability from sources such as the El Niño-Southern Oscillation or Pacific Decadal Variability can moderate trends or even flip their sign (Figure 3.3b) [46]. Other members display a spatial pattern more similar to the ensemble mean (Figure 3.3c). When average global trends from internal variability are in phase with the forced response, individual realizations can experience negative climate speeds of greater magnitude everywhere around the globe (Figure 3.3d). In one realization of ARISE-DelayedStart, this amplification from internal variability produces extreme median climate speeds over the global ocean exceeding 10 km/yr.

Previous analysis shows that the noise introduced by internal variability may impede detection of the surface climate response and lead to the perceived failure of an intervention [20, 33, 168]. The planetary-scale cooling in ARISE-DelayedStart is strong enough to entirely separate its dis-

tribution from no-SAI SSP2-4.5 when the sign of the trend is considered (Figure B.9b); even in the member with the smallest global median climate speed, few regions see a sign opposite to the forced response (Figure 3.3b). These results suggest that perceived failure at a regional or planetary scale would be much less likely under scenarios with rapid temperature reduction.

3.2.3 Relative ecological risk from climate speeds

Climate speeds of 10 km/yr provide a threshold of extreme risk by exceeding the dispersal rates of both adaptable families (such as mammals) and terrestrial and marine species on average [9, 11, 136]. We plot the global area exposed to these climate speeds against the annual rate of global temperature change for a wide range of datasets to efficiently summarize ecological risk (Figure 3.4; see Table 3.1 in Methods for detailed data descriptions), and subsequently describe the implications for each product in the context of this figure. The mean of all non-overlapping 20-year Last Millennium time periods is located at the origin, reflecting conditions that ecosystems experienced over the millennium before the Industrial Revolution began. The maximum area exposed (10% of global area) to the threshold climate speed over Last Millennium variability is denoted by the horizontal dotted line (Figure 3.4). Greater distance from the origin beyond this dotted line denotes a relatively higher profile of ecological risk.

The European Reanalysis Version 5 (ERA5) [169] provides an observationally-constrained global estimate of climate speeds during the recent past (1996-2015) [169,170]. Over this same period, a historical simulation (CESM2-Historical [57]) displays a larger area exposed to the threshold climate speed and a higher rate of temperature change than in ERA5. The physical reasons underlying the overly rapid warming rate in CESM2-Historical during this period are an ongoing area of research, and likely include errors in prescribed biomass burning emissions [127]. More generally, discrepancies between ERA5 and historical simulations may partly be due to structural differences between the single realization of real-world climate variability and the ensemble mean forced response [108]. Overall, both ERA5 and CESM2-Historical display climate speeds beyond

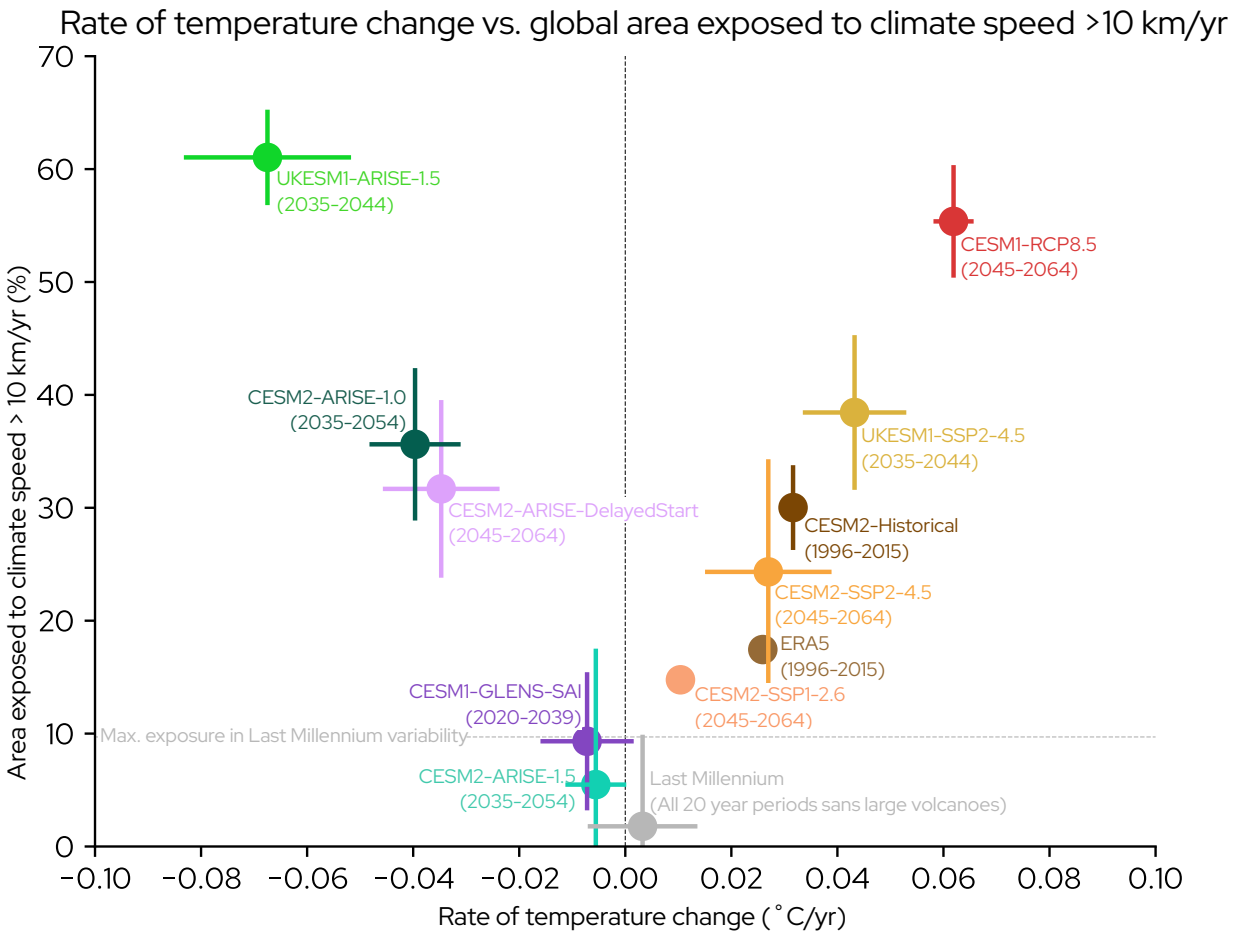

Figure 3.4: 20-year rate of temperature change per year vs. percent of area exposed to a climate speed of 2-meter temperature with magnitude greater than 10 km/yr for various scenarios of climate change, climate intervention, and historical products. Dots denote ensemble mean, and lines display the width of the ensemble variability. The colors of each dot help visually distinguish datasets from each other. Vertical dashed line shows 20-year change in temperature of 0 °C/yr. Horizontal dashed lines represent the maximum 20-year area exposed to threshold climate speed in the Last Millennium variability (10%). See Table 3.1 in Methods for detailed descriptions of each dataset in figure, which are listed here from left to right: United Kingdom Earth System Model 1 (UKESM1)-Assessing Responses and Impacts of Solar climate intervention on the Earth system (ARISE)-1.5, Community Earth System Model 2 (CESM2)-ARISE-1.0, CESM2-ARISE-DelayedStart, Community Earth System Model 1 (CESM1)-Geoengineering Large ENSemble (GLENS)-Stratospheric Aerosol Injection (SAI), CESM2-ARISE-1.5, Last Millennium, CESM2-Shared Socioeconomic Pathway 1-2.6 (SSP1-2.6), European Reanalysis 5 (ERA5), CESM2-SSP2-4.5, CESM2-Historical, UKESM1-SSP2-4.5, and CESM1-Representative Concentration Pathway 8.5 (RCP8.5).

Last Millennium conditions and within the range of mid-century SSP2-4.5, consistent with known historical and expected future ecosystem stress from warming [11, 16, 40, 131, 132, 156].

No-SAI future scenarios expose substantial global area to large climate speeds from warming and cluster on the right half of Figure 3.4. Scenarios with higher mitigation (SSP1-2.6), moderate

mitigation (SSP2-4.5), and no mitigation (RCP8.5) all exceed the Last Millennium baseline, with increased emissions causing greater ecological risk. The relatively higher risk portrayed in the SSP2-4.5 simulation in the United Kingdom Earth System Model version 1 (UKESM1-SSP2-4.5) (see Methods for full description) as opposed to CESM2-SSP2-4.5 primarily stems from the more rapid warming rates due to the higher climate sensitivity in UKESM1 [171]. The above results are in keeping with previous findings of widespread ecosystem stress under all future emissions pathways [11, 14–17, 40, 131, 132, 156], with the most extreme risks from climate change under scenarios with no mitigation [149, 172].

Scenarios where SAI is used for rapid temperature reduction cluster on the left side of the figure above the Last Millennium baseline and expose large amounts of global area to high climate speeds from rapid cooling. The individual scenarios (see Table 3.1 in Methods for details) each depict a unique potential design choice that could produce a deployment shock. One pathway would be through a delayed start with deployment after a temperature target has been surpassed, either through the choice to deliberately postpone deployment (ARISE-DelayedStart) or if the temperature threshold is breached early due to high climate sensitivity (UKESM1-ARISE-1.5 [166]). Alternatively, the intervention could be deployed with the explicit goal of obtaining a low temperature target below the starting global mean value (CESM2-ARISE-1.0 [30, 134], or the simulations of [173] [not shown]). Regardless of the underlying strategic logic, the salient point is that every SAI scenario with rapid temperature reduction exposes more global area to the threshold climate speed than its corresponding no-SAI climate change reference scenario: CESM2-ARISE-1.0 and CESM2-ARISE-DelayedStart compared to CESM2-SSP2-4.5, and UKESM1-ARISE-1.5 compared to UKESM1-SSP2-4.5.

SAI scenarios where the intervention is used to maintain global mean temperature (CESM2-ARISE-1.5, CESM1-GLENS-SAI) remain near the origin, with ensemble means within the bounds of Last Millennium conditions. These SAI scenarios essentially eliminate the most extreme risks to ecosystems from climate speeds occurring in the no-SAI climate change scenarios. However, a 10-year delay in deployment is the predominant difference between ARISE-1.5 and ARISE-

DelayedStart. This short delay is sufficient to produce a highly distinct profile of extreme ecological risk.

3.3 Discussion

This work demonstrates a key difference between scenarios where SAI is used to maintain global temperature, and those where SAI causes rapid temperature reduction. Scenarios that maintain global temperature greatly reduce risks from climate speeds, with global-scale parameters statistically indistinguishable from Last Millennium conditions. In contrast, rapid temperature reduction scenarios increase ecological risk ("deployment shock") relative to their corresponding no-SAI scenarios. The design of the ARISE scenarios allow these conclusions to be connected to specific potential decisions: a policy-relevant delay in deployment can turn a scenario that would otherwise greatly reduce ecological risk from climate speeds by maintaining temperature (ARISE-1.5) into one with a deployment shock that worsens this risk relative to no-SAI climate change (ARISE-DelayedStart).

Our results arise in policy-relevant scenarios designed for plausibility [30, 134], as opposed to termination scenarios created to illustrate risks of SAI [141]. Deployment shock demonstrates a risk that intrinsically accompanies the ability to rapidly change temperature. This may restrict the ability to safely return to a temperature target after it has been surpassed. It is theoretically possible to design a strategy with sufficiently slow ramp-up of SAI to allow ecosystems to respond to the forcing. However, SAI scenarios where global temperature is reduced are usually framed as an aggressive response option to relieve some severe impact of climate change [21, 174], prevent tipping points [175], or to facilitate rapid detection by providing a large signal-to-noise ratio [30, 168]. The strategic choice to slowly implement a low temperature target may be in tension with these same goals.

Climate speeds are typically used for measuring ecosystem responses and risks in a warming climate [9, 10, 149], which raises the question of whether they are as meaningful for a cooling climate. Observed range shifts track temperature trends from internal climate variability regardless

of their sign, strongly indicating both cooling and warming are ecologically relevant [38,40]. While relicts that temporarily survive warming through persistence or by sheltering in microclimates [16, 151] would likely benefit from rapid cooling, numerous ecosystems that have transitioned to a new state under warming may be suddenly jeopardized. Paleoclimatic data indicates periods with rapid (interannual to multidecadal) large-scale cooling following a long-term warming trend coincide with planetary-scale changes to ecosystems [8, 176]. These findings support the possibility that abrupt global cooling embedded in an antecedent warming trend could cause a large disturbance to ecosystems.

Insight from climate speeds can help inform future scenario design and decision-making. Designing scenarios to avoid deployment shock constrains both global temperature target and deployment year, which helps prevent a combinatorial explosion in scenario design [30]. We note two scenarios within these constraints that have not yet been simulated: delayed start maintenance with deployment dates past 2035 and higher temperature targets to avoid rapid temperature reduction, and slow starts where the intervention is implemented over sufficient time to moderate climate speeds. Decisions about global environmental policy involve complex tradeoffs of risk from many processes and phenomena [174]. As research concretely identifies sources of these tradeoffs in SAI scenarios, the relative prioritization of risks should be transparently documented during the design of a given scenario to help aid in analysis and effective decision-making.

3.4 Methods

3.4.1 Primary simulations

Our work draws on data from three simulations (SSP2-4.5, ARISE-1.5, and ARISE- Delayed-Start) using the Community Earth System Model Version 2 with Whole Atmosphere Community Climate Model version 6 (CESM2[WACCM6]) [57, 143]. CESM2(WACCM6) is a fully-interactive Earth system model with a high-fidelity depiction of the climate, including the stratospheric processes thought to be most relevant to SAI [57, 58, 143]. For all simulations here, CESM2(WACCM6) was run with 70 vertical levels (model top $\approx$140 km) and 1.25° longitude

$\times 0.9^\circ$ latitude horizontal resolution [134]. This spatial scale (Table 3.1) is considered adequate to analyze global ecosystem risk in the broader ecology literature [10, 17, 136].

The CESM2(WACCM6ma) Last Millennium dataset is a simulation of the 1000-year interval 850 through 1849, immediately preceding the Industrial Revolution which is defined to begin in 1850 by convention in the climate modeling community [143, 146] Relatively abundant paleoclimate data allows for a well-constrained long-record depiction of this period including natural variability, realistic natural forcings including volcanoes and solar cycles, and anthropogenic land use changes [147]. We use the Last Millennium to provide an ecologically-relevant baseline of climate variability and change before anthropogenic climate change through greenhouse gas emissions and industrialization became large. CESM2(WACCM6ma) is a middle-atmosphere configuration of CESM2(WACCM6), and includes a simplified chemistry scheme to reduce computational complexity. The climate of CESM2(WACCM6ma) is very similar to CESM2(WACCM6) apart from the tropospheric chemistry [177].

The SSP2-4.5 simulations depict a no-SAI future with moderate mitigation of climate change and the slow deployment of negative emissions technologies [148]. Five ensemble members were created for the Coupled Model Intercomparison Project Phase 6 [129]. An additional five ensemble members were created to augment the sample size for the ARISE project [134]. All 10 realizations are available from 2015-2069. SSP2-4.5 is consistent with present-day policy pledges by the global community, though it still results in warming beyond Paris Agreement targets in CESM2 and other climate models [121, 178].

We use the ARISE-1.5 and ARISE-DelayedStart datasets to explore two policy-relevant SAI scenarios [134, 144]. These simulations are often referred to as ARISE-SAI-1.5 and ARISE-SAI-1.37-DelayedStart. We use the names ARISE-1.5 and ARISE-DelayedStart for brevity, or CESM2-ARISE-1.5 and CESM2-ARISE-DelayedStart when necessary to distinguish from scenarios run in other models. SAI in ARISE-1.5 is deployed in 2035 to maintain global mean temperature at the 2020-2039 average in CESM2(WACCM6) ($\approx$1.5°C above the IPCC AR6 preindustrial value) [134, 179]. In ARISE-DelayedStart, SAI is deployed 10 years later in 2045 with a similar global

mean temperature target of the 2020-2039 average from CESM1(WACCM5) (≈1.37 °C above the IPCC AR6 preindustrial value) to depict the impacts of a policy-relevant delay in deployment [30]. ARISE-DelayedStart requires a larger stratospheric sulfate burden than ARISE-1.5 due both to the delayed start and the slightly lower temperature target [30, 144].

Other design choices are constant between ARISE-1.5 and ARISE-DelayedStart: sulfur dioxide is injected at the same height (≈21 km), SSP2-4.5 greenhouse forcing is used in both, and each ensemble has ten members. Injections occur continuously from four locations (30° and 15° N/S, all at 180°E) with a proportional-integral feedback-control algorithm to maintain the pole-to-pole and pole-to-equator temperature gradients alongside the global temperature target [134, 180]. Controlling for these goals with off-equatorial injections is intended to reduce side effects by compensating for the planetary-scale spatial patterns of greenhouse warming: the increase in global mean temperature, hemispheric asymmetry, and polar amplification [181].

ARISE-1.5 and ARISE-DelayedStart are identical to SSP2-4.5 in every way except for the SAI intervention. Therefore, consistent differences between the simulations are likely due to the SAI strategies. The effect sizes of the SAI interventions in ARISE-1.5 and ARISE-DelayedStart relative to SSP2-4.5 are large enough that the global-scale results are clearly due to the SAI intervention (i.e., ensemble mean global temperature trend changing sign worldwide). Where useful, we additionally use the robustness test as a non-parametric method to identify where the forced response to the SAI intervention is large [165]. We refer to results as robust when they pass this test (corresponding to $p < 0.1$ under a binomial test).

The CESM2(WACCM6) Preindustrial control (Unforced) provides a single 500-year integration of the Earth system with perpetual 1850 greenhouse gas forcing [143]. This simulation illustrates the range of internal climate variability over an extended period of time without external forcings [129]. The small climate speeds in the Unforced simulation (Figure B.2) raise confidence that the model is adequate for our analysis: while internal climate variability can produce pronounced ecosystem impacts in individual regions, planetary-scale risk to ecosystems would be implausible under unforced variability alone [38, 40]. We use Unforced as a reference to perfectly-

unforced conditions under internal variability alone, although land-use changes during and before 1850 imply it does not perfectly represent true equilibrium conditions [164].

3.4.2 Climate velocity

The climate velocity of a geophysical quantity describes the movement of the isopleths of that variable in a changing climate [9]. Formally, the climate velocity is defined as the ratio of the temporal gradient of a variable A ($\frac{dA}{dt}$, units time^{-1}) to the spatial gradient of that same variable ($\vec{\nabla}A$, units space^{-1}) [9]. The resultant variable ($\vec{C_A}$) has units of space per time–that is, a velocity (Equation 3.1) [9].

$$\frac{\frac{dA}{dt}}{\vec{\nabla}A} = \vec{C_A} \tag{3.1}$$

Climate velocity can be calculated for any variable, but is most frequently applied to temperature [10]. Temperature exhibits a clear large-scale response to both climate change and SAI, and has relatively well-understood spatiotemporal behavior in both observations and model output [10]. We use 2m temperature rather than sea surface temperature over the ocean due to data availability limitations in ARISE-DelayedStart at time of writing. On climatological spatiotemporal scales, 2m temperature is similar to sea surface temperature and is often used for aquatic ecosystem analysis [182, 183].

The climate velocity is a vector quantity, with both a magnitude and a direction. The scalar magnitude alone (climate speed) can be used separately from the vector quantity to quantify the high-level degree of disturbance to ecosystems [136, 149, 184, 185]. This degree of disturbance is the quantity of interest for our research questions, and we use the climate speed exclusively in our analysis. We provide climate velocity vector maps for additional context (Figure B.11), however, we caution readers that local analysis of these vectors would require a much finer-resolution dataset to better capture spatial gradients [9, 10, 154, 185].

Following standard methods, we calculate the temporal gradient of temperature using linear regression and the spatial gradient of temperature using the 3x3 neighborhood slope algorithm [9, 10, 136, 149]. In the accompanying Python code (`fun_calc_var.py`), we implement the

Sobel operator (mathematically equivalent to the 3x3 neighborhood slope algorithm) to obtain the spatial gradient of temperature. We calculate both our temporal gradient and spatial gradient directly from each dataset. At each point for each ensemble member, we divide the local 20-year temporal gradient (10-year for UKESM1 only, see below) by the spatial gradient and take the vector magnitude to obtain the climate speed. We impose a sign on the climate speed to denote whether it is associated with a warming or cooling trend. For all figures, we take the ensemble mean after the calculation of the climate speed. Climate speeds may be overestimated around complex topography in datasets with coarse spatial resolution [10]. Our results are robust to the choice of spatial resolution at the scale of all datasets used in this work (demonstrated for ERA5 in Figure B.10).

By convention, climate velocities and climate speeds are assessed over time periods of 10 years or longer [9, 10, 136]. We calculate the climate speed over time periods chosen to be relevant to each scenario. For the scenarios with SAI in CESM2, this is the 20-year period immediately following deployment: 2035-2054 in ARISE-1.5, and 2045-2064 in ARISE-DelayedStart. 20-year timespans encompass the entire period when global mean temperature is decreasing in ARISE-DelayedStart. For no-SAI SSP2-4.5, we use the period 2045-2064 to compare to results from ARISE-DelayedStart. The time period 2035-2054 (corresponding to ARISE-1.5) is very similar in CESM2 simulations of SSP2-4.5, as the rate of change in global mean temperature does not alter substantially between 2035 and 2064. The time period spanning the interval when global mean temperature is decreasing in an SAI scenario is model-dependent, and needs to be adjusted to correspond to the model that generated a given dataset. In UKESM1, a 10-year period fully encompasses the cooling after deployment due to its high aerosol sensitivity [166, 186]. Thus, we calculate climate speeds over 10-year periods for output from UKESM1 as opposed to 20-year periods for all other products on Figure 3.4. Using 20-year periods for UKESM1 would artificially reduce the climate speeds during its deployment shock by spreading the cooling out past the time horizon when global mean temperature has stabilized. In contrast, using the shorter 10-year periods for CESM2 would overlook the substantial cooling that continues past this horizon (Figure 3.2).

The 10-member ensemble size of ARISE-1.5, ARISE-DelayedStart, and SSP2-4.5 enlarges the number of years available for analysis over each 20-year period to an effective size of 200 years [46]. Since the Last Millennium has only one ensemble member but a 1000-year simulation period, we choose ten 20-year time periods to avoid large volcanic eruptions (10 teragrams of stratospheric sulfate injection [147]): years 851-870, 871-890, 891-910, 911-930, 945-964, 971-990, 991-1010, 1011-1030, 1031-1050, 1051-1070. Avoiding such eruptions is necessary due to their large, but brief, impacts on global climate, which violate the linear trend assumptions underlying the definition of the climate velocity [10]. We additionally calculate the full distribution of non-overlapping 20-year climate speeds (again omitting large volcanic eruptions) in the Last Millennium for use in Figure 3.4. Similarly, we choose ten 20-year time periods (years 5-24, 43-62, 95-114, 124-143, 164-183, 259-278, 280-299, 336-355, 379-398, 465-484) from the Unforced simulation to obtain a comparable sample size of 200 years, where relevant.

There is a wealth of ecological literature pertaining to the question of which climate speed values and periods of time correspond to ecosystem impacts on land and in the ocean. We cite only the most critical literature in the main body of the paper to remain within citation count restrictions, and provide references here for a fuller selection of this body of work for terrestrial ecosystems [9, 11, 149, 187–190], marine ecosystems [11, 131, 149, 187, 189], and interannual to multidecadal range shifts [38–40, 191–195].

3.4.3 Additional data

We use a broad selection of data in Figure 3.4 to discuss the relative risk between a variety of future scenarios of climate change and climate intervention and various depictions of the historical period. Table 3.1 enumerates all datasets used with a brief description of each.

3.5 Data Availability

The 2-meter temperature data from Earth system models and reanalysis used in this study (see Table 3.1 for compendium) have been deposited in the Open Science Framework database under

Table 3.1: Table of all datasets used to calculate climate speeds.

Name	Brief description	Time used	Resolution (lon x lat)
Last Millennium [143, 146, 147]	CESM2(WACCM6ma) simulation of the millennium prior to 1850	Ten 20-year periods, and all non-overlapping 20-year periods	2.5° x1.89°
SSP2-4.5 [134, 148]	CESM2(WACCM6) simulation of future climate change with moderate mitigation and slow deployment of negative emissions technologies	2045-2064 (10 ensemble members)	1.25° x0.9°
ARISE-1.5 [134]	CESM2(WACCM6) simulation with SAI deployed in 2035 to maintain global mean temperature, pole-to-pole temperature gradient, and pole-to-equator temperature gradient at 2020-2039 mean against SSP2-4.5 forcing	2035-2054 (10 ensemble members)	1.25° x0.9°
ARISE-DelayedStart [144]	CESM2(WACCM6) simulation with SAI deployed in 2045 to return global mean temperature, pole-to-pole temperature gradient, and pole-to-equator temperature gradient to 2020-2039 CESM1(WACCM5) mean against SSP2-4.5 forcing	2045-2064 (10 ensemble members)	1.25° x0.9°
CESM1-GLENS [196]	CESM1(WACCM5) simulation with SAI deployed in 2020 to maintain global mean temperature, pole-to-pole temperature gradient, and pole-to-equator temperature gradient at 2010-2030 mean against RCP8.5 forcing	2020-2039 (21 ensemble members)	1.25° x0.9°
ARISE-1.0 [144]	CESM2(WACCM6) simulation with SAI deployed in 2035 to return global mean temperature, pole-to-pole temperature gradient, and pole-to-equator temperature gradient to 2000-2019 mean against SSP2-4.5 forcing	2035-2054 (10 ensemble members)	1.25° x0.9°
UKESM1-ARISE-1.5 [166]	UKESM1 simulation with SAI deployed in 2035 to return global mean temperature, pole-to-pole temperature gradient, and pole-to-equator temperature gradient to 2015-2034 mean against SSP2-4.5 forcing	2035-2044 (5 ensemble members)	1.875° x1.25°
RCP8.5 [196, 197]	CESM1(WACCM5) simulation of future climate change with no mitigation	2045-2064 (3 ensemble members)	1.25° x0.9°
UKESM1-SSP2-4.5 [148, 166]	UKESM1 simulation of future climate change with moderate mitigation and slow deployment of negative emissions technologies	2035-2044 (5 ensemble members)	1.875° x1.25°
SSP1-2.6 [148]	CESM2(WACCM6) simulation of future climate change with high mitigation and rapid deployment of negative emissions technologies	2045-2064 (1 ensemble member)	1.25° x0.9°
CESM2-Historical [57]	CESM2(WACCM6) simulation of the climate state over the historical period	1996-2015 (3 ensemble members)	1.25° x0.9°
ERA5 [169]	Observationally-constrained estimate of the historical Earth system	1996-2015 (1 reanalysis)	0.25° x0.25°, remapped to 1.25° x0.9° to match CESM simulations
Unforced [129, 143]	CESM2(WACCM6) simulation of preindustrial conditions without external forcings	10 randomly-selected 20-year periods	1.25° x0.9°

accession code 10.17605/OSF.IO/Z37ES: doi.org/10.17605/OSF.IO/Z37ES [198]. This archive includes all data used in our figures and analysis, along with a datasheet that provides additional documentation of relevant biases and technical characteristics [199].

Additionally, the complete raw datasets can be obtained at the following repositories and citations. ARISE-1.5 is available at the National Center for Atmospheric Research (NCAR) Climate Data Gateway under accession code 10.5065/9kcn-9y79 [200]. CESM2-SSP2-4.5 is available at the NCAR Climate Data Gateway under accession code 10.26024/0cs0-ev98 [201]. The CESM2 Last Millennium is available at the NCAR Climate Data Gateway under accession code 10.26024/5dgt-qf16 [146]. CESM1-GLENS-SAI and CESM1-RCP8.5 are available together at the NCAR Climate Data Gateway under accession code 10.5065/D6JH3JXX [196]. ARISE-DelayedStart and ARISE-1.0 are located on the NCAR Globally Accessible Data Environment file space while post-processing is conducted. The public permanent archive will be provided at the ARISE community page: cesm.ucar.edu/community-projects/arise-sai. ARISE-DelayedStart and ARISE-1.0 data used in our study is included at the Open Science Framework repository [198]. UKESM1-ARISE-1.5 is available at the Centre for Environmental Data Analysis under ac-

cession code 26b89d8d76bd40bfbaf9fedfa383e9cf [202]. UKESM1-SSP2-4.5 is available at the World Data Center for Climate under accession code 10.26050/WDCC/AR6.C6SPMOU0 [203]. CESM2-SSP1-2.6 is available at the World Data Center for Climate under accession code 10.22033 /ESGF/CMIP6.10100 [204]. CESM2-Historical is available at the World Data Center for Climate under accession code 10.22033/ESGF/CMIP6.10071 [205]. The CESM2 Unforced (preindustrial control) is available at the World Data Center for Climate under accession code 10.22033 /ESGF/CMIP6.10094 [206]. ERA5 is available at the Copernicus Climate Data Store under accession code 10.22033/ESGF/CMIP6.10094 [207].

3.6 Code Availability

Code used to process data and make all figures has been deposited at the Open Science Framework under accession code 10.17605/OSF.IO/Z37ES [198]. This code is licensed under the Open Software License 3.0.

Chapter 4

Potential distribution of a top Arctic predator under multiple climate futures

See footnote for publication information.[3]

4.1 Introduction

The impact of climate change on ecosystems is well-established around the globe [11, 19, 76, 131, 187]. Climate impacts to ecosystems can arise extrinsically, through the direct effects of changing environmental conditions, or intrinsically, by altering species interactions within the ecosystem [8]. Intrinsic changes frequently arise through impacts to specific species, known as "biotic multipliers," that have disproportionate influence on other organisms [12]. Top consumers are often biotic multipliers as changes to their distribution or abundance disrupts vertical interactions within the trophic web and lead to nonlinear impacts on the ecosystem as a whole [12, 13, 208].

Worsening climate impacts and the ongoing failure of global efforts to reduce emissions to international targets [120, 121, 178] have motivated research into hypothetical climate intervention methods to intervene in the Earth system to reduce climate risks [20, 21]. Stratospheric aerosol injection (SAI) is one hypothetical proposal to emit reflective particles into the upper atmosphere to reduce temperatures relative to a greenhouse forcing [20]. SAI has a low theoretical cost of deployment and is the only known method by which global temperatures could be reduced within a few years using near-future technology [21].

Potential extrinsic and intrinsic ecological impacts of SAI remain poorly understood. While averting future warming would benefit ecosystems [209], SAI adds the potential for rapid changes in temperature if the intervention were to be stopped while masking a higher radiative equilibrium

[3]This work is in preparation for publication as: Hueholt, D.M., E.A. Barnes, J.W. Hurrell, & A.L. Morrison. Potential distribution of a top Arctic predator under multiple climate futures. To be submitted.

("termination shock") or deployed to rapidly reduce global temperatures ("deployment shock") [136, 210]. There have been no studies to date on potential intrinsic changes or species-level impacts under SAI; these were highlighted as key knowledge gaps by a recent community review [37].

Species-level projections are often made using ecological niche models (ENMs), which estimate the potential distribution of a species based on its niche as learned from statistical relationships between historical observations of species occurrence and paired environmental data [211–214]. A trained ENM can then predict the potential distribution based on environmental data alone, which allows projection into past or future climates under the assumption that historical relationships between distribution and environment remain stable [213, 215, 216]. Maxent is one widely-used ENM method which estimates the relative suitability for a species given species detection information and a background field of environmental data [212, 215, 217]. In general, ENMs such as Maxent are a robust method to project species occurrence into out-of-sample environments [215, 218, 219].

Studies projecting future ecosystem change usually focus on the response to external forcings such as climate warming or SAI (e.g., [9, 41–44]. The climate state at any given time is produced by the combination of the response to external forcings and the influence of natural internal climate variability, for example, the El Niño-Southern Oscillation or Pacific Decadal Variability [46, 47, 108, 220]. Internal variability is known to influence the distribution and abundance of many species–especially in the Arctic, where organisms are often temperature-limited [38,39,187]. Hence, to anticipate ecological impacts, it is critical to characterize contributions from internal variability in addition to the forced response. In climate science, storyline approaches examine individual ensemble members to describe the combination of the forced response and internal variability together in creating a plausible future [50–53]. These methods have not yet been applied to study ecosystem impacts.

We create a Maxent ENM [211] trained on citizen science observations from the eBird database [221] and historical climate reanalysis [169] to explore impacts of climate change and SAI in the

presence of natural variability on the potential distribution of a top Arctic predator, the Gyrfalcon (*Falco rusticolus*) [222]. The Gyrfalcon is a large, predatory bird which has a top-down predator-prey relationship with other tundra species (most notably two grouse species, the Willow Ptarmigan [*Lagopus lagopus*] and Rock Ptarmigan [*Lagopus muta*]) [222–224]. This implies the Gyrfalcon is a biotic multiplier and thus may be of outsize importance to the greater Arctic ecosystem. We project the potential distribution of the Gyrfalcon under three ensemble simulations in the Community Earth System Model 2 with Whole Atmosphere Community Climate Model 6 (CESM2[WACCM6]) [57, 143] to explore various climate change futures with and without SAI. The Shared Socioeconomic Pathway 2-4.5 (SSP2-4.5) provides a moderate-mitigation climate change future without SAI, consistent with present policy [120, 121, 148]. Simulations from the Assessing Responses and Impacts of Solar climate intervention on the Earth system (ARISE) project where SAI is deployed in 2035 to maintain temperature at 1.5 °C above preindustrial near the Paris Agreement target (ARISE-1.5) or to rapidly reduce temperature to 1.0 °C above preindustrial (ARISE-1.0) depict two potential futures with climate intervention [134, 144].

4.2 Data

4.2.1 Reanalysis

We use 2m temperature from the European Reanalysis Version 5 (ERA5) as an observationally-constrained estimate of the climate state [169, 170]. ERA5 horizontal resolution is 0.25° x 0.25°; this is coarse relative to the scale of individual bird observations, but adequate to represent regional environmental conditions relevant to ecosystems [10]. The ERA5 record extends from 1940 to present (2025 at time of writing). We choose the period 2013-2022 to pair with citizen science observations from eBird as training data for the Maxent model. 10-year periods are recommended for ENM training and eBird record density is greatest in more recent years [225,226]. We calculate seasonal averages from May, June, and July to cover the peak breeding season of the Gyrfalcon, when relationships between species distribution and climate are likely to be strongest [222, 227].

4.2.2 Climate model output

We use 2m temperature from large ensemble simulations with the Community Earth System Model 2 (CESM2) with Whole Atmosphere Community Climate Model 6 (WACCM6). CESM2 (WACCM6) is a high-top model (70 vertical layers, model top ≈140km) that explicitly simulates the stratosphere and includes representations of the chemical and microphysical processes thought to be relevant to SAI [58, 143]. CESM2(WACCM6) is an extensively validated model which shows reasonable agreement to mean-state stratospheric observations and those following volcanic eruptions including Pinatubo and Hunga Tonga-Hunga Ha'apai; it has been used to submit simulations to the United Nations Intergovernmental Panel on Climate Change Coupled Model Intercomparison Project [31, 57, 143, 228]. The horizontal resolution of the model is 1.25° longitude x 0.94° latitude in all simulations used in this work.

The Shared Socioeconomic Pathway 2-4.5 (SSP2-4.5) scenario follows a moderate-mitigation trajectory with no use of SAI [148]. SSP2-4.5 is consistent with present policy commitments by governments and is projected to result in warming beyond international targets by the mid-21st century [120, 121, 178]. The SSP2-4.5 simulations used here contain ten ensemble members between 2015-2069; five ensemble members continue to 2100 [134]. A set of three Historical simulations with the same model depict the 1850-2014 period. [57].

Two simulations from the Assessing Responses and Impacts of Solar climate intervention on the Earth system (ARISE) project depict different scenarios where SAI is used to oppose greenhouse warming. In ARISE-1.5, SAI is deployed in 2035 to maintain temperatures at the 2020-2039 average (≈1.5°C above the model preindustrial value) against SSP2-4.5 forcings [134]. This illustrates a scenario where SAI is used to maintain the temperature target of the Paris Agreement. In ARISE-1.0, SAI is deployed in 2035 to rapidly reduce global mean temperature to the 2000-2019 average (≈1.0°C above the model preindustrial value) [144]. In both simulations, sulfur dioxide is injected above the tropopause (≈21km) at 15° and 30° in both hemispheres with a proportional-integral feedback-control algorithm used to maintain multiple climate targets: global temperature, the pole-to-pole temperature gradient, and the pole-to-equator temperature gradient [134,144,181].

These controller targets reduce unintended side effects on planetary circulations [36,134,181,196]. In both scenarios, SAI is assumed to be a global effort ("collective actor" scenario) deployed without interruption [134]. Arctic mean (poleward of 50°N, land-only) temperatures steadily increase for SSP2-4.5, are maintained near the 2035 value for ARISE-1.5, and are rapidly reduced to the lower target for ARISE-1.0 (Figure 4.1). Both ARISE-1.5 and ARISE-1.0 have 10 ensemble members which run from 2035-2069.

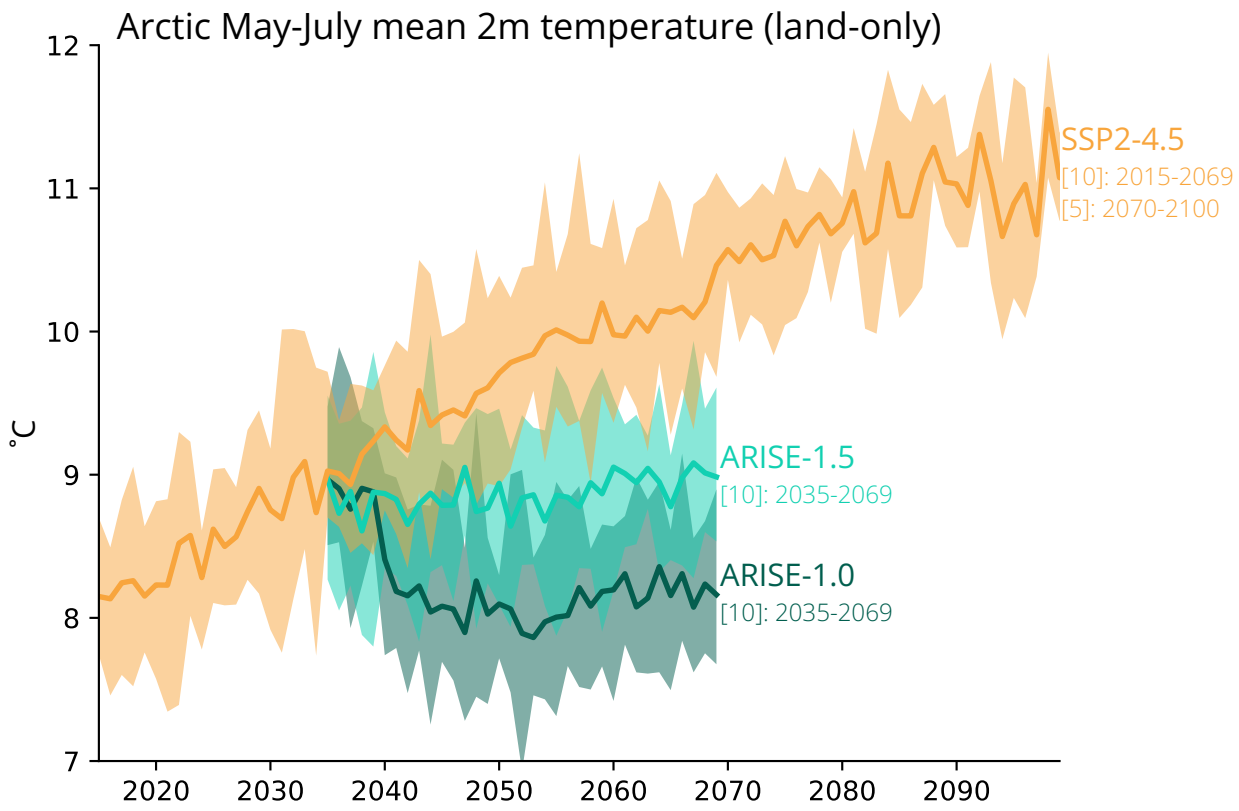

Figure 4.1: Seasonal May-July mean land-only 2m temperature for the Arctic region (poleward of 50°N) in the SSP2-4.5 (10 members 2015-2069, 5 members 2070-2100), ARISE-1.5 (10 members 2035-2069), and ARISE-1.0 (10 members 2035-2069) simulations. Thick lines denote ensemble mean and shading encompasses maximum to minimum value across the ensemble. Ensemble size over time period is given in label below the simulation name.

4.2.3 Bias adjustment of climate model output

We use quantile mapping to bias-adjust all simulations from the ensemble mean of the CESM2 (WACCM6) Historical simulations to the 1940-1970 period in ERA5 [229, 230]. This period is less reliable than data later in ERA5 as it predates the satellite record; we choose this period as a baseline in order to compare the two datasets before climate change becomes large. We bias-adjust to the ensemble mean of CESM2(WACCM6) to identify the biases originating from structural differences between this model and ERA5. As a plausibility check relative to the ERA5 baseline (Figure C.1a), the bias-adjusted 2m temperature fields result in much more realistic ENM output on years outside the training data (Figure C.1b) than the raw fields produce on their own (Figure C.1c).

The future simulations with and without SAI use the same bias adjustment calculated from the historical period. This methodology assumes the structural bias of the model remains the same under future warmer climate states and those under SAI, and does not aim to adjust for biases in warming trends or climate sensitivity.

4.2.4 Gyrfalcon detection data

We take observations of Gyrfalcons from May, June, and July (MJJ) between 2013-2022 from the eBird database for our training data [221]. eBird is a semi-structured citizen science database consisting of user-submitted "checklists," which describe observations of bird species, quantity, and survey effort metadata including location information [231, 232]. eBird is quality-controlled by a combination of automated statistical filters and volunteer reviewers to ensure reliability for scientific applications [226]. While the Gyrfalcon breeding season extends from April to August, we use the MJJ months to avoid records of migratory individuals in April and August which may distort population-climate relationships during ENM training [222, 227, 233, 234].

To ensure representative matching between eBird observations and environmental data from ERA5, we remove checklists where the distance traveled is greater than 20km, or where the speed is greater than 100 km/hr. We do not filter based on the checklist duration. These restrictions are looser than standard recommendations for niche modeling with eBird data [231, 232], as these are

intended for use with higher-resolution satellite datasets. The coarser grid sizes of our environmental datasets permit matching with coarser-resolution checklists. To account for sampling biases in space and time, we subsample to a space-time grid of 25 km in space and 92 days in time using the Auk package [235] to reflect the nominal resolution of ERA5 reanalysis per MJJ season [232].

We include checklists under the Stationary, Traveling, and Historical protocols. Many Gyrfalcon observations are entered under the Historical protocol as they originate from historical data that did not record metadata required by the eBird database. We do not apply a filter based on the number of observers. While large numbers of observers ($\gtrapprox 10$) impede detectability for many species [232], our analysis of the dataset indicate that many Gyrfalcon records come from large ecotourism expeditions which specifically visit breeding locations.

We exclusively use detection data for the Gyrfalcons and do not infer nondetections using the full eBird dataset. Thus, our modeling framework takes a presence-background (or detection-background) approach rather than a presence-absence (or detection-nondetection) approach [217]. Using eBird as a presence-background dataset loses affordances of the full detection-nondetection dataset–most notably, it precludes modeling of the encounter rate [215, 217, 231]. However, it allows the inclusion of records which would otherwise be filtered out due to incomplete metadata. This is an asset for studying species such as the Gyrfalcon which occupy remote locations with sparse records.

4.3 Model

4.3.1 Maxent modeling

The Maxent model (version 3.4.4 [236]) is a machine learning method to predict the potential distribution of a species based on paired georeferenced observations and environmental data [211, 212]. Maxent is a presence-background method: given paired detection-environmental observations as well as a background field of environmental data over the region of interest, Maxent learns the distribution that fits the detection data while minimizing departures from uniform distribution over the area [211, 217]. Maxent has been extensively used, validated, and docu-

mented within ecology. We briefly summarize the model construction below (derived from [212] and [217]), and refer readers to previous work in statistical ecology for more comprehensive discussion [211, 212, 217, 237].

Maxent uses an exponential model to estimate the ratio of the probability distribution function (pdf) of environmental data over sites with detections to the background field of all environmental data (Equation 4.1).

$$e^{\alpha+\beta\cdot h(\boldsymbol{z})} = \frac{f_1(\boldsymbol{z})}{f(\boldsymbol{z})} \tag{4.1}$$

In Equation 4.1, α is a normalizing constant, β refers to the weights optimized by maximizing the penalized log likelihood objective function, and $h(\boldsymbol{z})$ the feature vector of environmental data. $f_1(\boldsymbol{z})$ refers to the pdf of environmental variables across locations where the species is detected, and $f(\boldsymbol{z})$ the pdf of environmental variables at all locations in the domain of interest. By Bayes' rule (Equation 4.2), $\frac{f_1(\boldsymbol{z})}{f(\boldsymbol{z})}$ is proportional to the encounter rate $Pr(\text{detection}|\boldsymbol{z})$.

$$Pr(\text{detection}|\boldsymbol{z}) = \frac{f_1(\boldsymbol{z})}{f(\boldsymbol{z})} Pr(\text{detection}) \tag{4.2}$$

Obtaining $Pr(\text{detection})$ to calculate the encounter rate requires further assumptions about the sampling strategy which are not straightforward with the combination of citizen science records and coarse environmental data we use here [215, 217]. Without this term, the raw output from Maxent represents a qualitative metric of "relative suitability." Relative suitability sums to 1 over the domain, with higher and lower values denoting regions of greater and lesser suitability for the species [217, 236]. Since this provides sufficient information for our purpose of qualitatively illustrating future changes in potential distribution, we use the raw output from Maxent directly without attempting to derive the encounter rate.

The presence data for the model consists of checklists with Gyrfalcon detections from the eBird database between 2013-2022 (processed as described in Section 4.2.4) matched with MJJ-average 2m temperatures from ERA5 at the closest grid cell. The background dataset consists of all ERA5 MJJ-average 2m temperature data above 50 °N from the time period matching the

eBird observations. This provides a regular sample of the background climate state. A 10-year period of training data is standard for ecological niche modeling [225]. Once trained, we project the model to various periods in the bias-adjusted climate model simulations. This assumes that the population-climate relationships identified in the reanalysis apply to the bias-adjusted model output. Training on the CESM2 Historical simulations directly is not possible, as contributions from climate variability in the free-running simulations will be out of phase with those from the real-world realization implicit in the eBird observations. If the environmental data and the species observations are not drawn from the same climate state, the ENM may learn spurious statistical relationships during training [225].

Qualitatively, the model successfully represents Gyrfalcon detections in an out-of-sample testing year from the ERA5 dataset (2024, Figure 4.2a). Detections overlap with the regions of high

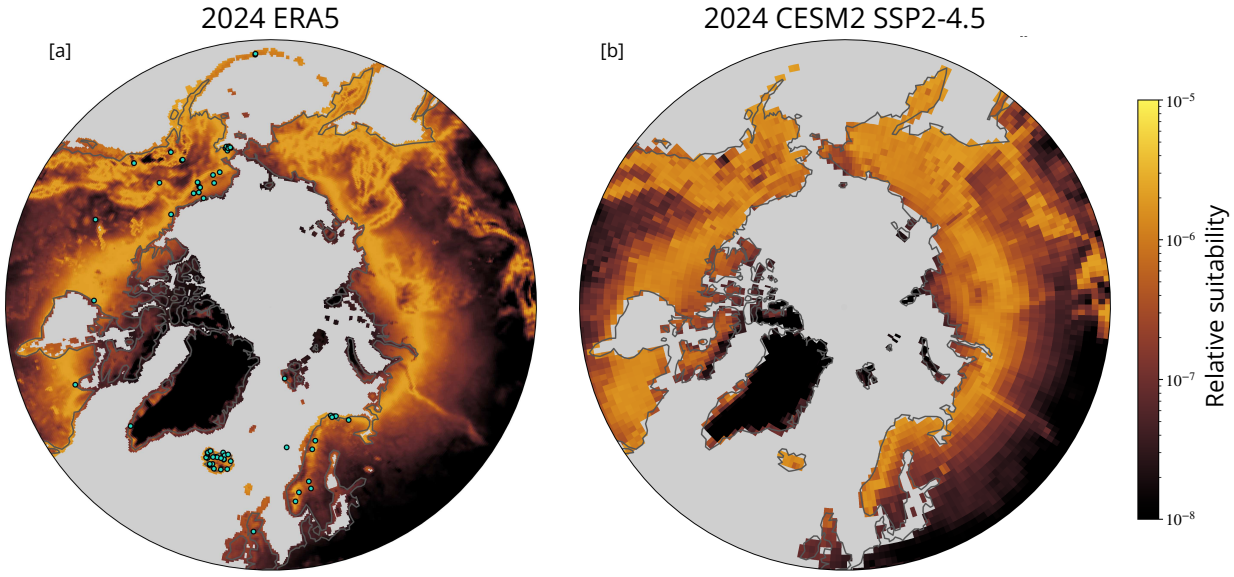

Figure 4.2: Relative suitability from Maxent model for 2024 in ERA5 (a), and projected to the ensemble mean of 2024 in SSP2-4.5 (b). Dots in [a] represent locations of eBird checklists with Gyrfalcon detections in 2024 (n=127). Ocean area is masked.

suitability, with no detections in regions where suitability is low. Since the simulated realizations of climate variability do not match the real world, output from the Maxent model projected to 2024 in SSP2-4.5 (Figure 4.2b) cannot be compared directly to ERA5 (Figure 4.2a) to evaluate

local model performance. On a broad scale, both figures align with maps created by expert judgment reflecting current and historical average distribution of the species [222]. The Area Under the Curve (AUC) score for the model on its training data is 0.868, consistent with standard guidelines for adequate performance of an ENM [211].

The default hyperparameters of Maxent are intended to apply to most species without tuning [211]. Given the above performance, we have no compelling reason to change these default values: a regularization multiplier of 1, a maximum of 500 iterations, a convergence threshold of 0.00001, and no adjustment to sample radius. In the Open Science Framework archive accompanying this work, we provide a completed Overview, Data, Model, Assessment and Prediction (ODMAP) protocol [216] for further transparency around our modeling approach.

4.4 Results

4.4.1 Substantial shifts in habitat suitability over the historical record

Over the 84-year ERA5 record, habitat suitability for the Gyrfalcon generally contracts poleward around the circumpolar region (Figure 4.3a). In regions with complex topography, such as the Rocky Mountains in Canada, suitability shifts up the elevation gradient toward cooler temperatures. Suitable area contracts in low-latitude mountainous regions (e.g., the Stanovoy Range); here, warming temperatures render the elevated topography less suitable and the nearby lowland regions remain unsuitable. This region is south of the present-day breeding range of the Gyrfalcon, though within their range during the Last Glacial Maximum [227]. Overall, these results are consistent with a climate velocity framework where species follow their thermal niches poleward and upslope, with contraction at transport barriers [9, 18].

Some regions, such as the Brooks Coast of Alaska, show trends counter to expectations of poleward range shifts from the forced response to warming (Figure 4.3a). This is likely due to the influence of climate variability, which will be large across the difference of any two single years. The ensemble mean of CESM2 estimates the forced response over the historical period (Figure 4.3b), and shows a uniform shift in range poleward and upslope to within the limitations

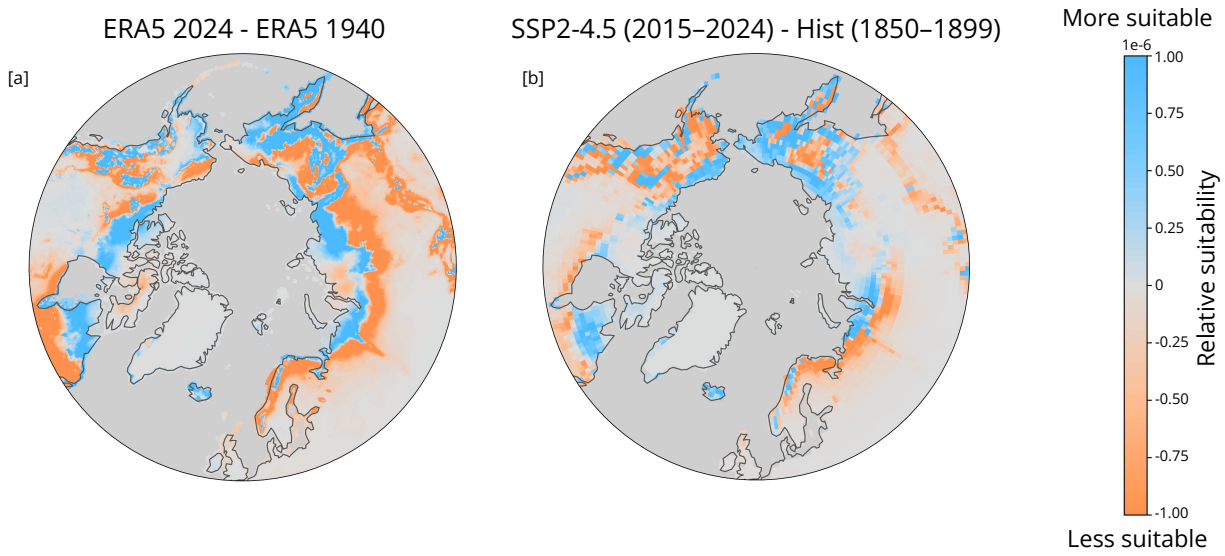

Figure 4.3: Difference in relative suitability from Maxent model between 2024 and 1940 in ERA5 (a), and between the 2015-2024 (SSP2-4.5) and 1850-1899 (Historical) periods in the ensemble mean. Ocean area is masked.

of the coarse model topography. Isolating the forced response in the single realization of climate variability in ERA5 for a direct comparison is challenging. A difference of 30-year periods is conventionally taken to provide an estimate of the forced response (Figure C.2), but may be questionable in the Arctic given high regional climate variability [122]. The 30-year difference does show a more uniform poleward and upslope shift (Figure C.2), similar to the forced response in CESM2 (Figure 4.3b).

4.4.2 Distinct forced responses to climate change and intervention

The difference of mid-century 5-year time periods in the ensemble mean in SSP2-4.5 shows a continued uniform poleward contraction in the habitat suitability (Figure 4.4a). Low-latitude sites in Alaska and Canada (Figure 4.2a, [222]) without connectivity to suitable area at higher latitudes may be vulnerable to local extinctions in the mid-century, similar to the retreat from the Stanovoy Range after the Last Glacial Maximum [227]. Studying suitability in 5-year time periods is consistent with the known interannual variability of Gyrfalcon populations [222–224].

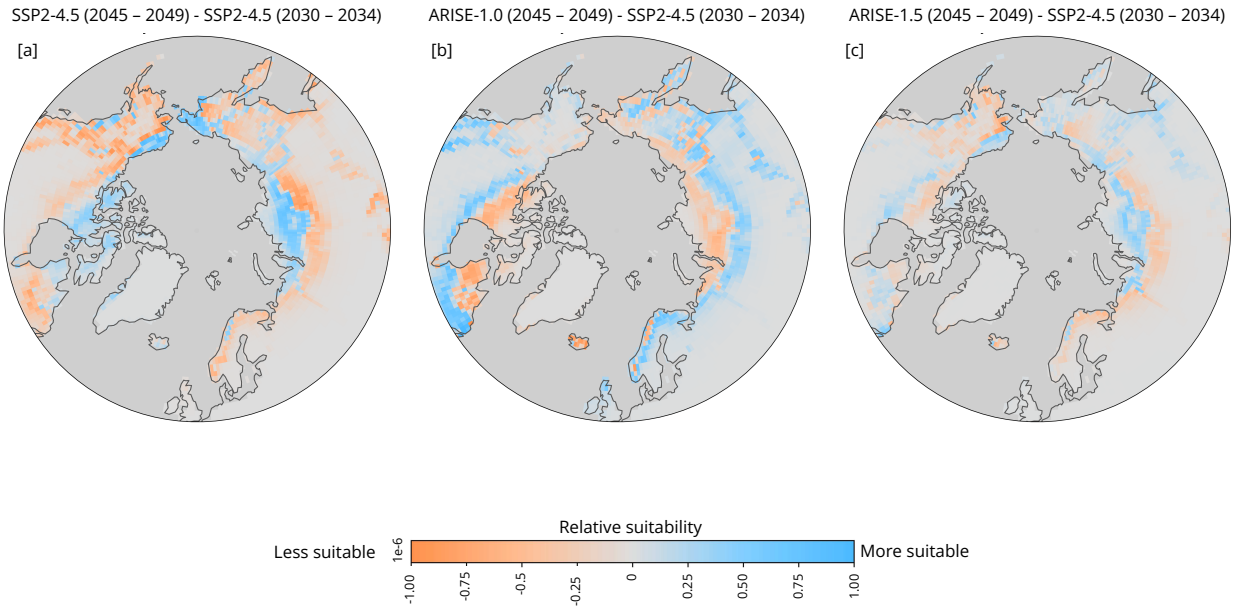

Figure 4.4: Ensemble mean of relative suitability from Maxent model for the difference of 2045-2049 and 2030-2034 in SSP2-4.5 (a), ARISE-1.0 (b), and ARISE-1.5 (c). Ocean area is masked.

To isolate the effect of the SAI intervention in the ARISE simulations, we take the difference of the ensemble mean of 5-year time periods immediately before SAI deployment (2030-2034) and beginning 15 years after deployment (2045-2049). This comparison captures the greatest change during the deployment shock in the first 20 years of ARISE-1.0 [210], and depicts how suitability would change before and after the SAI deployment (i.e., a "snapshot around deployment" [165]). The 10-member ensemble effectively increases the sample size of these 5-year periods to 50 years which likely provides an effective estimate of the forced response in temperature [238]. Together with the very large signal-to-noise ratio in the ARISE-1.0 scenario, it is thus unlikely that trends in these difference maps (Figure 4.4b) are due to internal variability alone.

In some regions, ARISE-1.0 shows the opposite trend (Figure 4.4b) as compared to SSP2-4.5 (Figure 4.4a) in response to the rapid temperature reduction (Figure 4.1). Eurasia and much of Canada exhibit a strong equatorward shift under ARISE-1.0 (Figure 4.4b), in contrast to the poleward contraction under SSP2-4.5 (Figure 4.4a). Other regions show distinct responses between the two simulations. Alaska shows a contraction in suitable area poleward and upslope under SSP2-4.5 (Figure 4.4a), but no clear trend in ARISE-1.0 (Figure 4.4b); Iceland exhibits no strong trend

under SSP2-4.5 (Figure 4.4a), but loses suitability in ARISE-1.0 (Figure 4.4b). These distinct trends in habitat suitability illustrate the importance of studying potential SAI impacts across a range of variables and modeling frameworks, rather than assuming that these will follow global mean target values in opposing no-SAI climate change trends.

In ARISE-1.5, changes are smaller in magnitude (Figure 4.4c) than ARISE-1.0 (Figure 4.4b) or SSP2-4.5 (Figure 4.4a). On a circumpolar scale, there is no clear directionality to the response in ARISE-1.5; different regions exhibit both poleward and equatorward shifts. This shows forced trends are much smaller in a scenario where global temperature is maintained than when SAI is used for rapid temperature reduction.

4.4.3 Suitability storylines

We take a storyline approach by exploring two individual realizations under the SSP2-4.5 and ARISE-1.0 scenarios. These storylines illustrate plausible cases of how the habitat suitability of this species may evolve under different forced responses and realizations of natural variability.

In member 4 of SSP2-4.5, the overall poleward shift associated with the warming trend (Figure 4.5a,b,c) is both opposed and amplified by contributions from internal variability at different times (Figure 4.5d,e,f). The poleward shift in the coastline of central Asia is amplified by internal variability in the 2045-2049 period, but subsequently suppressed in 2060-2064. In Arctic Canada, equatorward trends from internal variability suppress the poleward shift from the forced response in the 2060-2064 period (Figure 4.5f), with smaller effects in the other periods (Figure 4.5d,e).

Member 7 of ARISE-1.0 shows how internal variability can act to amplify the forced response. Poleward shifts driven by internal variability increase the equatorward shift forced by the deployment shock (Figure 4.6d,e,f). This contributes to large movement equatorward in habitat suitability; in central Asia, the primary band of highest suitability values do not overlap between 2030-2034 (Figure 4.6d) and 2045-2049 (Figure 4.6e). This is a remarkable shift in suitability for such a short time period.

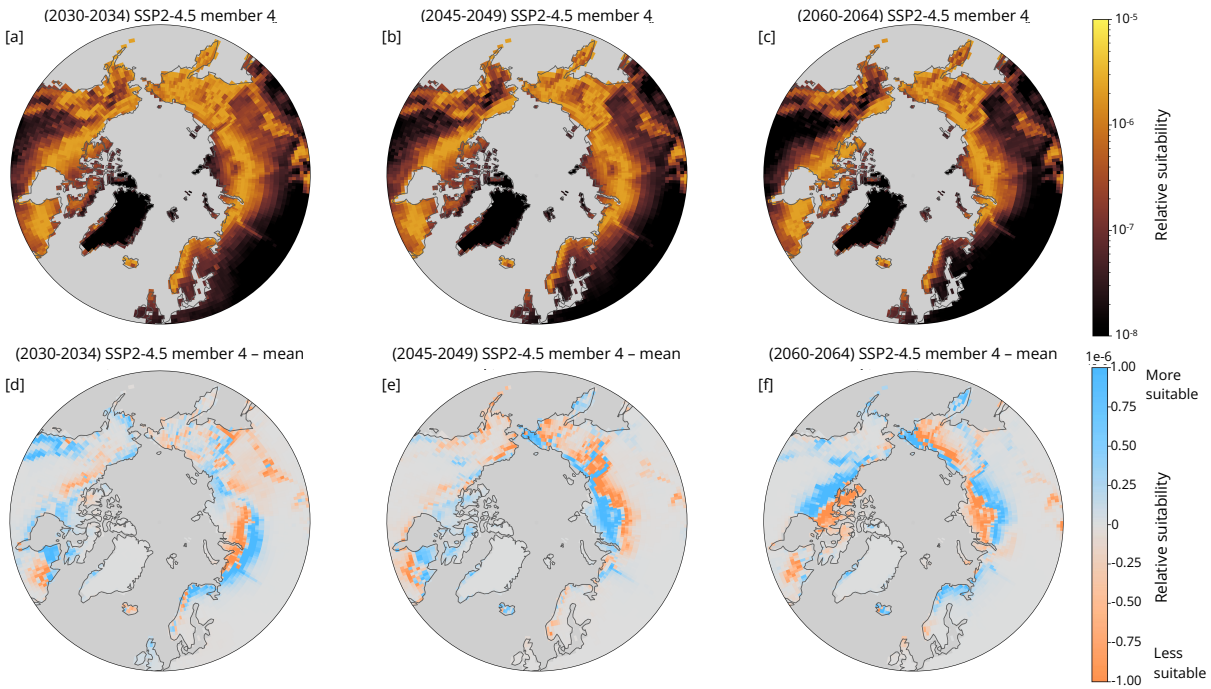

Figure 4.5: Storyline of relative suitability from Maxent model for member 4 of the SSP2-4.5 ensemble (a, b, c) and the difference between each time slice and the ensemble mean in the same period (d, e, f). Ocean area is masked out.

These storylines demonstrate substantial contributions from internal variability to regional patterns of species-level suitability in a given climate state, even under very large external forcings such as the ARISE-1.0 scenario (Figure 4.6). While the ensemble mean is important for understanding the forced response (Figure 4.4), storylines illustrate the realized climate conditions that may affect an ecosystem (Figure 4.5, Figure 4.6).

4.5 Discussion

Our results show large, short-term forced change in habitat suitability associated with a single species during the deployment shock associated with the use of SAI for rapid temperature reduction (Figure 4.4b), which equals or exceeds the forced response under climate change with present policy and no SAI (Figure 4.4a). When SAI is used to maintain temperature, in contrast, forced trends in suitability are much weaker (Figure 4.4c). The contrast in the forced response between SAI sce-

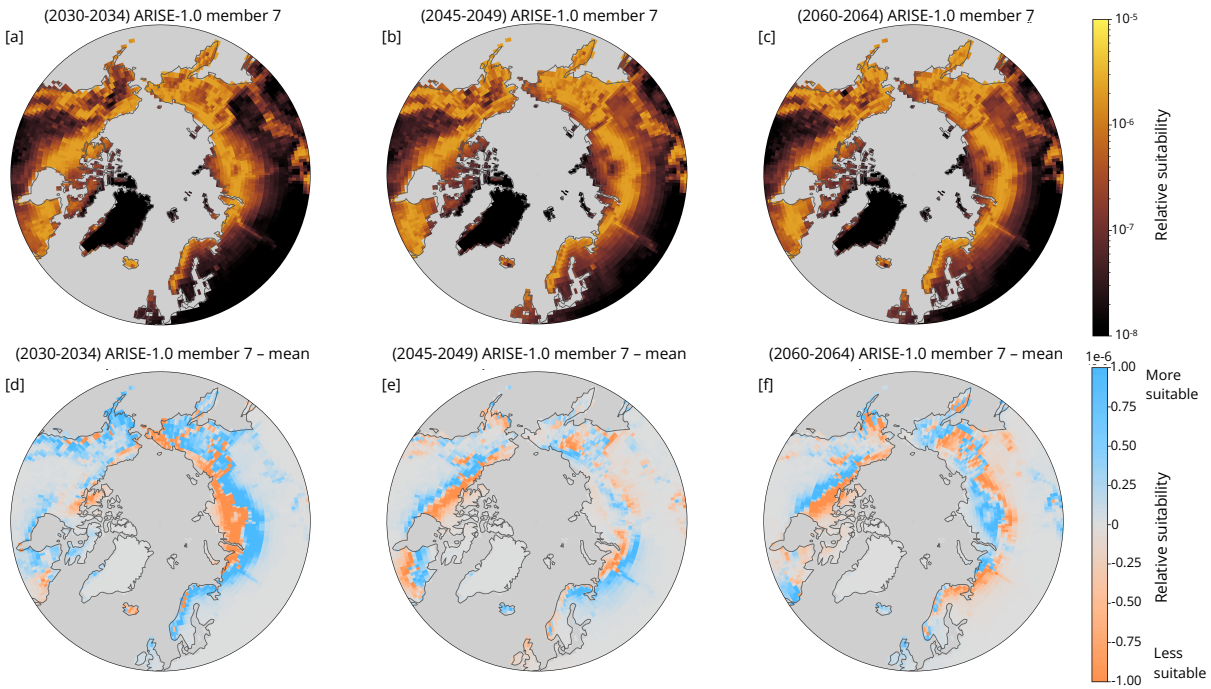

Figure 4.6: Storyline of relative suitability from Maxent model for member 7 of the ARISE-1.0 ensemble (a, b, c) and the difference between each time slice and the ensemble mean in the same period (d, e, f). Ocean area is masked out.

narios where the intervention is used to rapidly reduce temperature and those where temperature is maintained are consistent with high-level findings based on thermal conditions alone [210].

Effective ecological niche modeling relies on identifying robust relationships between the species of interest and environmental conditions. Following standard methods, we use a 10-year period (2013-2022) of paired species observations and environmental data for training [225]. Ideally, the training data for an ENM is drawn from a stationary climate state to ensure that the relationships between species detections and environmental data are in pseudo-equilibrium. Arctic environmental change in the early 21st century was already large; in particular, this is the period where the Arctic climate state became dominated by the warming trend over internal variability (e.g., Chapter 2, or [239]). Therefore, 2013-2022 is not an ideal baseline for training; still, good performance on out-of-sample observations (Figure 4.2a) suggests the model is qualitatively reliable despite these challenges. Future work could compare models trained over different time

periods throughout the 20th century to identify tradeoffs between sparser training data and a more stationary climate.

Many avenues exist to enrich our niche modeling approach. Formally modeling the encounter rate by using eBird data in a detection-nondetection framework would facilitate quantitative analysis that may be more directly interpretable for conservation. Including more variables in the ENM, such as seasonal temperature extremes, growing degree days, and precipitation metrics, would provide further environmental covariates relevant for the historical distribution and future climate scenarios [222]. We stress that our results are not meant as a predictive model, but to provide a starting point to consider the impacts and relative risks of climate change and SAI on an ecologically-significant top consumer species.

The Maxent approach we use illustrates changes in potential distribution, but cannot answer the question of whether this would necessarily induce range shifts in the Gyrfalcon. Gyrfalcons are known to be sensitive to interannual climate variability both directly and through impacts to prey species [222–224]. Previous ENM approaches have successfully represented Gyrfalcon distribution shifts on paleoclimate timescales [227]. If the Gyrfalcon distribution does change, it is possible that nonlinear impacts would occur to the rest of the tundra ecosystem through disruption to vertical trophic interactions. In the context of SAI deployment, it is unclear what the impacts would be if distribution of the top predator contracts poleward on short timescales followed by a subsequent rapid shift back into its former range. While the Gyrfalcon may simply recolonize the region, it is also possible that state changes in the ecosystem are not fully reversible [8]. Future work could explicitly model species interactions within the tundra, such as the predator-prey system between the Gyrfalcon and ptarmigan species.

Chapter 5

Summary and Future Research

5.1 Summary

We demonstrate the use of large ensembles to study climate conditions that are known to lead to extrinsic and intrinsic ecosystem change. In Chapter 2, we applied this approach with growing degree days to disentangle contributions of forced change and internal variability from Arctic greening under climate change. In Chapter 3, we examined climate speeds to understand the effect of very large extrinsic changes imposed by rapid temperature reduction under SAI. Finally, in Chapter 4, we carried out a species-level analysis of changes in the Gyrfalcon, a biotic multiplier which leads to intrinsic change in the Arctic tundra.

5.2 Future research

It is well-established that many large-scale climate conditions lead to ecological impacts in ecosystems beyond those studied in this dissertation. Examples of candidate climate conditions for further study include: hyperthermic thresholds linked to mass mortality events [240], anoxic thresholds of marine species survival [10], and growing degree days connected to alpine greening [241]. The framework that we demonstrate here to study these climate conditions through storylines and statistics in large ensembles could be immediately applied to such cases. Targeted ecosystem dynamical modeling and process-based modeling would complement these studies by exploring how climate-driven changes in individual ecosystems evolve in finer detail.

The “crossover" metric from Chapter 2 shows promise as a statistical method to more broadly explore changes to the climate state. Due to its lack of necessary prior assumptions, crossover may be particularly well suited to studying polar climate variables which often exhibit nonlinearity, heteroscedasticity, and non-normal distributions. In systems such as Arctic sea ice where time of emergence has been characterized with other methods (e.g., [239]), future work could intercom-

pare the results of these methods with those of the crossover statistic. Identifying the sources of differences between these methods may provide new insight into how forced change emerges from climate variability, and characterize when to use different methods of determining emergence with a given quantity of interest.

Storylines provide a rich tool to study and anticipate future ecosystem change and could be applied to many more ecosystems and modeled datasets. Larger ensembles provide more climate states to help anticipate extreme or otherwise surprising contributions from climate variability. Machine learning-based emulators with rapid generation times of very large ensembles raise the possibility of sampling a much wider distribution of climate statistics [49], although these models presently are limited in their output variables and not coupled on climate timescales [242]. Storylines have proven effective at communicating uncertainty in climate hazards to non-scientist stakeholders [52], and may be similarly beneficial in ecological settings where collaborations with planning practitioners and land managers are important.

There are many avenues to further incorporate climate information into ecological projections and forecasting. Storyline and composite analysis may help identify sources of coupled climate variability that can be applied for predicting ecological change on subseasonal to decadal timescales. Few studies have examined how uncertainty in the climate data used as inputs to niche models influences the projections of potential distribution. In particular, it has not been quantified how the relative contributions of the four major forms of climate uncertainty–internal variability, choice of scenario or forcing, structural uncertainty, and pattern uncertainty [123, 124]–impact output from niche modeling. The impact of providing climate information to niche models on different timescales (annual to multidecadal) is not well constrained. These different timescales will reflect different contributions from internal variability and the forced response, and will have distinct species-level impacts. For example, many animals are highly sensitive to variability between individual years [38, 40], while certain trees respond only on multidecadal time horizons [112]. Interdisciplinary collaboration between ecologists and climate scientists could ensure the best match between the environmental data and species of interest for a given analysis. Discussions with land

managers and wildlife scientists would be key to producing information from climate-informed ecological analysis that supports conservation goals for vulnerable ecosystems and species.

Bibliography

[1] Eric Dinerstein, David Olson, Anup Joshi, Carly Vynne, Neil D. Burgess, Eric Wikramanayake, Nathan Hahn, Suzanne Palminteri, Prashant Hedao, Reed Noss, Matt Hansen, Harvey Locke, Erle C Ellis, Benjamin Jones, Charles Victor Barber, Randy Hayes, Cyril Kormos, Vance Martin, Eileen Crist, Wes Sechrest, Lori Price, Jonathan E. M. Baillie, Don Weeden, Kierán Suckling, Crystal Davis, Nigel Sizer, Rebecca Moore, David Thau, Tanya Birch, Peter Potapov, Svetlana Turubanova, Alexandra Tyukavina, Nadia de Souza, Lilian Pintea, José C. Brito, Othman A. Llewellyn, Anthony G. Miller, Annette Patzelt, Shahina A. Ghazanfar, Jonathan Timberlake, Heinz Klöser, Yara Shennan-Farpón, Roeland Kindt, Jens-Peter Barnekow Lillesø, Paulo van Breugel, Lars Graudal, Maianna Voge, Khalaf F. Al-Shammari, and Muhammad Saleem. An Ecoregion-Based Approach to Protecting Half the Terrestrial Realm. *BioScience*, 67(6):534–545, June 2017.

[2] Irene D. Alabia, Jorge García Molinos, Sei-Ichi Saitoh, Toru Hirawake, Takafumi Hirata, and Franz J. Mueter. Distribution shifts of marine taxa in the Pacific Arctic under contemporary climate changes. *Diversity and Distributions*, 24(11):1583–1597, 2018. _eprint: https://onlinelibrary.wiley.com/doi/pdf/10.1111/ddi.12788.

[3] Logan T. Berner and Scott J. Goetz. Satellite observations document trends consistent with a boreal forest biome shift. *Global Change Biology*, 28(10):3275–3292, 2022. _eprint: https://onlinelibrary.wiley.com/doi/pdf/10.1111/gcb.16121.

[4] Thomas P. Roland, Oliver T. Bartlett, Dan J. Charman, Karen Anderson, Dominic A. Hodgson, Matthew J. Amesbury, Ilya Maclean, Peter T. Fretwell, and Andrew Fleming. Sustained greening of the Antarctic Peninsula observed from satellites. *Nat. Geosci.*, pages 1–6, October 2024. Publisher: Nature Publishing Group.

[5] Lindsey S. Smart, Paul J. Taillie, Benjamin Poulter, Jelena Vukomanovic, Kunwar K. Singh, Jennifer J. Swenson, Helena Mitasova, Jordan W. Smith, and Ross K. Meentemeyer. Above-

ground carbon loss associated with the spread of ghost forests as sea levels rise. *Environ. Res. Lett.*, 15(10):104028, September 2020. Publisher: IOP Publishing.

[6] Camille S. Stevens-Rumann, Kerry B. Kemp, Philip E. Higuera, Brian J. Harvey, Monica T. Rother, Daniel C. Donato, Penelope Morgan, and Thomas T. Veblen. Evidence for declining forest resilience to wildfires under climate change. *Ecology Letters*, 21(2):243–252, 2018. _eprint: https://onlinelibrary.wiley.com/doi/pdf/10.1111/ele.12889.

[7] Sarah H. Watts, David K. Mardon, Catherine Mercer, Dan Watson, Helen Cole, Rosalind F. Shaw, and Alistair S. Jump. Riding the elevator to extinction: Disjunct arctic-alpine plants of open habitats decline as their more competitive neighbours expand. *Biological Conservation*, 272:109620, August 2022.

[8] John W. Williams, Jessica L. Blois, and Bryan N. Shuman. Extrinsic and intrinsic forcing of abrupt ecological change: case studies from the late Quaternary. *Journal of Ecology*, 99(3):664–677, 2011. _eprint: https://onlinelibrary.wiley.com/doi/pdf/10.1111/j.1365-2745.2011.01810.x.

[9] Scott R. Loarie, Philip B. Duffy, Healy Hamilton, Gregory P. Asner, Christopher B. Field, and David D. Ackerly. The velocity of climate change. *Nature*, 462(7276):1052–1055, December 2009. Number: 7276 Publisher: Nature Publishing Group.

[10] Isaac Brito-Morales, Jorge García Molinos, David S. Schoeman, Michael T. Burrows, Elvira S. Poloczanska, Christopher J. Brown, Simon Ferrier, Tom D. Harwood, Carissa J. Klein, Eve McDonald-Madden, Pippa J. Moore, John M. Pandolfi, James E. M. Watson, Amelia S. Wenger, and Anthony J. Richardson. Climate Velocity Can Inform Conservation in a Warming World. *Trends in Ecology & Evolution*, 33(6):441–457, June 2018.

[11] Jonathan Lenoir, Romain Bertrand, Lise Comte, Luana Bourgeaud, Tarek Hattab, Jérôme Murienne, and Gaël Grenouillet. Species better track climate warming in the oceans than

on land. *Nat Ecol Evol*, 4(8):1044–1059, August 2020. Number: 8 Publisher: Nature Publishing Group.

[12] Phoebe L. Zarnetske, David K. Skelly, and Mark C. Urban. Biotic Multipliers of Climate Change. *Science*, 336(6088):1516–1518, June 2012. Publisher: American Association for the Advancement of Science.

[13] Mark C. Urban, Phoebe L. Zarnetske, and David K. Skelly. Searching for Biotic Multipliers of Climate Change. *Integrative and Comparative Biology*, 57(1):134–147, July 2017.

[14] Jessica L. Allen and James C. Lendemer. Climate change impacts on endemic, high-elevation lichens in a biodiversity hotspot. *Biodivers Conserv*, 25(3):555–568, March 2016.

[15] K. Frieler, M. Meinshausen, A. Golly, M. Mengel, K. Lebek, S. D. Donner, and O. Hoegh-Guldberg. Limiting global warming to 2 °C is unlikely to save most coral reefs. *Nature Clim Change*, 3(2):165–170, February 2013. Number: 2 Publisher: Nature Publishing Group.

[16] Johan Reyes-Chávez, Megan Quail, Stephanie Tarvin, Michael Kessler, and Sven P. Batke. Nowhere to escape – Diversity and community composition of ferns and lycophytes on the highest mountain in Honduras. *Journal of Tropical Ecology*, 37(2):72–81, March 2021. Publisher: Cambridge University Press.

[17] Michael T. Burrows, David S. Schoeman, Anthony J. Richardson, Jorge García Molinos, Ary Hoffmann, Lauren B. Buckley, Pippa J. Moore, Christopher J. Brown, John F. Bruno, Carlos M. Duarte, Benjamin S. Halpern, Ove Hoegh-Guldberg, Carrie V. Kappel, Wolfgang Kiessling, Mary I. O'Connor, John M. Pandolfi, Camille Parmesan, William J. Sydeman, Simon Ferrier, Kristen J. Williams, and Elvira S. Poloczanska. Geographical limits to species-range shifts are suggested by climate velocity. *Nature*, 507(7493):492–495, March 2014. Number: 7493 Publisher: Nature Publishing Group.

[18] Mark C. Urban. Escalator to extinction. *Proceedings of the National Academy of Sciences*, 115(47):11871–11873, November 2018. Publisher: Proceedings of the National Academy of Sciences.

[19] Sally N. Aitken, Sam Yeaman, Jason A. Holliday, Tongli Wang, and Sierra Curtis-McLane. Adaptation, migration or extirpation: climate change outcomes for tree populations. *Evolutionary Applications*, 1(1):95–111, 2008. _eprint: https://onlinelibrary.wiley.com/doi/pdf/10.1111/j.1752-4571.2007.00013.x.

[20] NASEM. Reflecting Sunlight: Recommendations for Solar Geoengineering Research and Research Governance. Technical report, National Academies of Science, Engineering, and Medicine, 2021.

[21] UNEP. One Atmosphere: An independent expert review on Solar Radiation Modification research and deployment. Technical report, UNEP, 2023.

[22] AMS Council. Climate Intervention: A Policy Statement of the American Meteorological Society Adopted by the Council 2 February 2022. Technical report, American Meteorological Society, Boston, MA, 2022.

[23] AGU. Position Statement on Climate Intervention. Technical report, American Geophysical Union, Washington, DC, 2023.

[24] Sampa Das, Peter R. Colarco, Luke D. Oman, Ghassan Taha, and Omar Torres. The long-term transport and radiative impacts of the 2017 British Columbia pyrocumulonimbus smoke aerosols in the stratosphere. *Atmospheric Chemistry and Physics*, 21(15):12069–12090, August 2021. Publisher: Copernicus GmbH.

[25] C. Timmreck. Modeling the climatic effects of large explosive volcanic eruptions. *WIREs Climate Change*, 3(6):545–564, 2012. _eprint: https://onlinelibrary.wiley.com/doi/pdf/10.1002/wcc.192.

[26] Alan Robock and Jianping Mao. The Volcanic Signal in Surface Temperature Observations. *Journal of Climate*, 8(5):1086–1103, May 1995. Publisher: American Meteorological Society Section: Journal of Climate.

[27] Antonios Mamalakis, Elizabeth A. Barnes, and James Wilson Hurrell. Quantifying "climate distinguishability" after stratospheric aerosol injection using explainable artificial intelligence, June 2023.

[28] Curtis M Bell and Patrick W Keys. Strategic logic of unilateral climate intervention. *Environ. Res. Lett.*, 2023.

[29] Holly Jean Buck. Environmental Peacebuilding and Solar Geoengineering. *Frontiers in Climate*, 4, 2022.

[30] D. G. MacMartin, D. Visioni, B. Kravitz, J.H. Richter, T. Felgenhauer, W. R. Lee, D. R. Morrow, E. A. Parson, and M. Sugiyama. Scenarios for modeling solar radiation modification. *Proceedings of the National Academy of Sciences*, 119(33):e2202230119, August 2022. Publisher: Proceedings of the National Academy of Sciences.

[31] Yunqian Zhu, Charles G. Bardeen, Simone Tilmes, Michael J. Mills, Xinyue Wang, V. Lynn Harvey, Ghassan Taha, Douglas Kinnison, Robert W. Portmann, Pengfei Yu, Karen H. Rosenlof, Melody Avery, Corinna Kloss, Can Li, Anne S. Glanville, Luis Millán, Terry Deshler, Nickolay Krotkov, and Owen B. Toon. Perturbations in stratospheric aerosol evolution due to the water-rich plume of the 2022 Hunga-Tonga eruption. *Commun Earth Environ*, 3(1):1–7, October 2022. Publisher: Nature Publishing Group.

[32] Mengying Zhao, Long Cao, Daniele Visioni, and Douglas G. MacMartin. Carbon Cycle Response to Stratospheric Aerosol Injection With Multiple Temperature Stabilization Targets and Strategies. *Earth's Future*, 12(6):e2024EF004474, 2024. _eprint: https://onlinelibrary.wiley.com/doi/pdf/10.1029/2024EF004474.

[33] Patrick W. Keys, Elizabeth A. Barnes, Noah S. Diffenbaugh, James W. Hurrell, and Curtis M. Bell. Potential for perceived failure of stratospheric aerosol injection deployment. *Proceedings of the National Academy of Sciences*, 119(40):e2210036119, October 2022. Publisher: Proceedings of the National Academy of Sciences.

[34] Michelle Simões Reboita, João Gabriel Martins Ribeiro, Natália Machado Crespo, Rosmeri Portfírio da Rocha, Romaric C Odoulami, Windmanagda Sawadogo, and John C Moore. Response of the Southern Hemisphere extratropical cyclone climatology to climate intervention with stratospheric aerosol injection. *Environ. Res.: Climate*, 2024.

[35] Heri Kuswanto, Ben Kravitz, Brina Miftahurrohmah, Fatkhurokhman Fauzi, Ardhasena Sopahaluwaken, and John Moore. Impact of solar geoengineering on temperatures over the Indonesian Maritime Continent. *International Journal of Climatology*, 42(5), 2022.

[36] Alice F. Wells, Matthew Henry, Ewa M. Bednarz, Douglas G. MacMartin, Andy Jones, Mohit Dalvi, and James M. Haywood. Identifying Climate Impacts From Different Stratospheric Aerosol Injection Strategies in UKESM1. *Earth's Future*, 12(3):e2023EF004358, 2024. _eprint: https://onlinelibrary.wiley.com/doi/pdf/10.1029/2023EF004358.

[37] Phoebe L. Zarnetske, Jessica Gurevitch, Janet Franklin, Peter M. Groffman, Cheryl S. Harrison, Jessica J. Hellmann, Forrest M. Hoffman, Shan Kothari, Alan Robock, Simone Tilmes, Daniele Visioni, Jin Wu, Lili Xia, and Cheng-En Yang. Potential ecological impacts of climate intervention by reflecting sunlight to cool Earth. *Proceedings of the National Academy of Sciences*, 118(15):e1921854118, April 2021. Publisher: Proceedings of the National Academy of Sciences.

[38] Nils C. Stenseth, Atle Mysterud, Geir Ottersen, James W. Hurrell, Kung-Sik Chan, and Mauricio Lima. Ecological Effects of Climate Fluctuations. *Science*, 297(5585):1292–1296, August 2002. Publisher: American Association for the Advancement of Science.

[39] Geir Ottersen, Benjamin Planque, Andrea Belgrano, Eric Post, Philip C. Reid, and Nils C. Stenseth. Ecological effects of the North Atlantic Oscillation. *Oecologia*, 128(1):1–14, June 2001.

[40] Camille Parmesan. Ecological and Evolutionary Responses to Recent Climate Change. *Annu. Rev. Ecol. Evol. Syst.*, 37(1):637–669, December 2006. Publisher: Annual Reviews.

[41] Signe Normand, Christophe Randin, Ralf Ohlemüller, Christian Bay, Toke T. Høye, Erik D. Kjær, Christian Körner, Heike Lischke, Luigi Maiorano, Jens Paulsen, Peter B. Pearman, Achilleas Psomas, Urs A. Treier, Niklaus E. Zimmermann, and Jens-Christian Svenning. A greener Greenland? Climatic potential and long-term constraints on future expansions of trees and shrubs. *Philosophical Transactions of the Royal Society B: Biological Sciences*, 368(1624):20120479, August 2013. Publisher: Royal Society.

[42] Richard G. Pearson, Steven J. Phillips, Michael M. Loranty, Pieter S. A. Beck, Theodoros Damoulas, Sarah J. Knight, and Scott J. Goetz. Shifts in Arctic vegetation and associated feedbacks under climate change. *Nature Clim Change*, 3(7):673–677, July 2013. Number: 7 Publisher: Nature Publishing Group.

[43] Eric C. J. Oliver, Michael T. Burrows, Markus G. Donat, Alex Sen Gupta, Lisa V. Alexander, Sarah E. Perkins-Kirkpatrick, Jessica A. Benthuysen, Alistair J. Hobday, Neil J. Holbrook, Pippa J. Moore, Mads S. Thomsen, Thomas Wernberg, and Dan A. Smale. Projected Marine Heatwaves in the 21st Century and the Potential for Ecological Impact. *Front. Mar. Sci.*, 6, 2019. Publisher: Frontiers.

[44] David S. Schoeman, Alex Sen Gupta, Cheryl S. Harrison, Jason D. Everett, Isaac Brito-Morales, Lee Hannah, Laurent Bopp, Patrick R. Roehrdanz, and Anthony J. Richardson. Demystifying global climate models for use in the life sciences. *Trends in Ecology & Evolution*, 38(9):843–858, September 2023. Publisher: Elsevier.

[45] Jamin K Rader, Charlotte J Connolly, M A Fernandez, and Emily M Gordon. Attribution of the record-high 2023 SST using a deep-learning framework. *Environ. Res. Commun.*, 7(5):051005, May 2025. Publisher: IOP Publishing.

[46] Clara Deser, Adam Phillips, Vincent Bourdette, and Haiyan Teng. Uncertainty in climate change projections: the role of internal variability. *Clim Dyn*, 38(3):527–546, February 2012.

[47] Nicola Maher, Sebastian Milinski, and Ralf Ludwig. Large ensemble climate model simulations: introduction, overview, and future prospects for utilising multiple types of large ensemble. *Earth System Dynamics*, 12(2):401–418, April 2021. Publisher: Copernicus GmbH.

[48] Keith B. Rodgers, Sun-Seon Lee, Nan Rosenbloom, Axel Timmermann, Gokhan Danabasoglu, Clara Deser, Jim Edwards, Ji-Eun Kim, Isla R. Simpson, Karl Stein, Malte F. Stuecker, Ryohei Yamaguchi, Tamás Bódai, Eui-Seok Chung, Lei Huang, Who M. Kim, Jean-François Lamarque, Danica L. Lombardozzi, William R. Wieder, and Stephen G. Yeager. Ubiquity of human-induced changes in climate variability. *Earth System Dynamics*, 12(4):1393–1411, December 2021. Publisher: Copernicus GmbH.

[49] Ankur Mahesh, William Collins, Boris Bonev, Noah Brenowitz, Yair Cohen, Peter Harrington, Karthik Kashinath, Thorsten Kurth, Joshua North, Travis OBrien, Michael Pritchard, David Pruitt, Mark Risser, Shashank Subramanian, and Jared Willard. Huge Ensembles Part II: Properties of a Huge Ensemble of Hindcasts Generated with Spherical Fourier Neural Operators, August 2024. arXiv:2408.01581 [physics].

[50] Jana Sillmann, Theodore G. Shepherd, Bart van den Hurk, Wilco Hazeleger, Olivia Martius, Julia Slingo, and Jakob Zscheischler. Event-Based Storylines to Address Climate Risk. *Earth's Future*, 9(2):e2020EF001783, 2021. _eprint: https://onlinelibrary.wiley.com/doi/pdf/10.1029/2020EF001783.

[51] E. M. Fischer, U. Beyerle, L. Bloin-Wibe, C. Gessner, V. Humphrey, F. Lehner, A. G. Pendergrass, S. Sippel, J. Zeder, and R. Knutti. Storylines for unprecedented heatwaves based on ensemble boosting. *Nat Commun*, 14(1):4643, August 2023. Number: 1 Publisher: Nature Publishing Group.

[52] Theodore G. Shepherd, Emily Boyd, Raphael A. Calel, Sandra C. Chapman, Suraje Dessai, Ioana M. Dima-West, Hayley J. Fowler, Rachel James, Douglas Maraun, Olivia Martius, Catherine A. Senior, Adam H. Sobel, David A. Stainforth, Simon F. B. Tett, Kevin E. Trenberth, Bart J. J. M. van den Hurk, Nicholas W. Watkins, Robert L. Wilby, and Dimitri A. Zenghelis. Storylines: an alternative approach to representing uncertainty in physical aspects of climate change. *Climatic Change*, 151(3):555–571, December 2018.

[53] Karen A. McKinnon and Isla R. Simpson. How Unexpected Was the 2021 Pacific Northwest Heatwave? *Geophysical Research Letters*, 49(18):e2022GL100380, 2022. _eprint: https://onlinelibrary.wiley.com/doi/pdf/10.1029/2022GL100380.

[54] Patrick W. Keys. The plot must thicken: a call for increased attention to social surprises in scenarios of climate futures. *Environ. Res. Lett.*, 18(8):081003, July 2023. Publisher: IOP Publishing.

[55] David M. Lawrence, Rosie A. Fisher, Charles D. Koven, Keith W. Oleson, Sean C. Swenson, Gordon Bonan, Nathan Collier, Bardan Ghimire, Leo van Kampenhout, Daniel Kennedy, Erik Kluzek, Peter J. Lawrence, Fang Li, Hongyi Li, Danica Lombardozzi, William J. Riley, William J. Sacks, Mingjie Shi, Mariana Vertenstein, William R. Wieder, Chonggang Xu, Ashehad A. Ali, Andrew M. Badger, Gautam Bisht, Michiel van den Broeke, Michael A. Brunke, Sean P. Burns, Jonathan Buzan, Martyn Clark, Anthony Craig, Kyla Dahlin, Beth Drewniak, Joshua B. Fisher, Mark Flanner, Andrew M. Fox, Pierre Gentine, Forrest Hoffman, Gretchen Keppel-Aleks, Ryan Knox, Sanjiv Kumar, Jan Lenaerts, L. Ruby Leung, William H. Lipscomb, Yaqiong Lu, Ashutosh Pandey, Jon D. Pelletier, Justin Perket, James T. Randerson, Daniel M. Ricciuto, Benjamin M. Sanderson, Andrew Slater,

Zachary M. Subin, Jinyun Tang, R. Quinn Thomas, Maria Val Martin, and Xubin Zeng. The Community Land Model Version 5: Description of New Features, Benchmarking, and Impact of Forcing Uncertainty. *Journal of Advances in Modeling Earth Systems*, 11(12):4245–4287, 2019. _eprint: https://onlinelibrary.wiley.com/doi/pdf/10.1029/2018MS001583.

[56] Rosie A. Fisher and Charles D. Koven. Perspectives on the Future of Land Surface Models and the Challenges of Representing Complex Terrestrial Systems. *Journal of Advances in Modeling Earth Systems*, 12(4):e2018MS001453, 2020. _eprint: https://onlinelibrary.wiley.com/doi/pdf/10.1029/2018MS001453.

[57] G. Danabasoglu, J.-F. Lamarque, J. Bacmeister, D. A. Bailey, A. K. DuVivier, J. Edwards, L. K. Emmons, J. Fasullo, R. Garcia, A. Gettelman, C. Hannay, M. M. Holland, W. G. Large, P. H. Lauritzen, D. M. Lawrence, J. T. M. Lenaerts, K. Lindsay, W. H. Lipscomb, M. J. Mills, R. Neale, K. W. Oleson, B. Otto-Bliesner, A. S. Phillips, W. Sacks, S. Tilmes, L. van Kampenhout, M. Vertenstein, A. Bertini, J. Dennis, C. Deser, C. Fischer, B. Fox-Kemper, J. E. Kay, D. Kinnison, P. J. Kushner, V. E. Larson, M. C. Long, S. Mickelson, J. K. Moore, E. Nienhouse, L. Polvani, P. J. Rasch, and W. G. Strand. The Community Earth System Model Version 2 (CESM2). *Journal of Advances in Modeling Earth Systems*, 12(2):e2019MS001916, 2020. _eprint: https://onlinelibrary.wiley.com/doi/pdf/10.1029/2019MS001916.

[58] John T. Fasullo. Evaluating simulated climate patterns from the CMIP archives using satellite and reanalysis datasets using the Climate Model Assessment Tool (CMATv1). *Geoscientific Model Development*, 13(8):3627–3642, August 2020. Publisher: Copernicus GmbH.

[59] Isabelle Gamache and Serge Payette. Latitudinal response of subarctic tree lines to recent climate change in eastern Canada. *Journal of Biogeography*, 32(5):849–862, 2005. _eprint: https://onlinelibrary.wiley.com/doi/pdf/10.1111/j.1365-2699.2004.01182.x.

[60] G.m MacDonald, K.v Kremenetski, and D.w Beilman. Climate change and the northern Russian treeline zone. *Philosophical Transactions of the Royal Society B: Biological Sciences*, 363(1501):2283–2299, November 2007. Publisher: Royal Society.

[61] Megan E. Franke, James W. Hurrell, Kristen L. Rasmussen, and Lantao Sun. Impacts of Forced and Internal Climate Variability on Changes in Convective Environments Over the Eastern United States. *Front. Clim.*, 6, October 2024. Publisher: Frontiers.

[62] Isla H. Myers-Smith, Meagan M. Grabowski, Haydn J. D. Thomas, Sandra Angers-Blondin, Gergana N. Daskalova, Anne D. Bjorkman, Andrew M. Cunliffe, Jakob J. Assmann, Joseph S. Boyle, Edward McLeod, Samuel McLeod, Ricky Joe, Paden Lennie, Deon Arey, Richard R. Gordon, and Cameron D. Eckert. Eighteen years of ecological monitoring reveals multiple lines of evidence for tundra vegetation change. *Ecological Monographs*, 89(2):e01351, 2019. _eprint: https://esajournals.onlinelibrary.wiley.com/doi/pdf/10.1002/ecm.1351.

[63] Shilong Piao, Xuhui Wang, Taejin Park, Chi Chen, Xu Lian, Yue He, Jarle W. Bjerke, Anping Chen, Philippe Ciais, Hans Tømmervik, Ramakrishna R. Nemani, and Ranga B. Myneni. Characteristics, drivers and feedbacks of global greening. *Nat Rev Earth Environ*, 1(1):14–27, January 2020. Publisher: Nature Publishing Group.

[64] F. S. Chapin III, M. Sturm, M. C. Serreze, J. P. McFadden, J. R. Key, A. H. Lloyd, A. D. McGuire, T. S. Rupp, A. H. Lynch, J. P. Schimel, J. Beringer, W. L. Chapman, H. E. Epstein, E. S. Euskirchen, L. D. Hinzman, G. Jia, C.-L. Ping, K. D. Tape, C. D. C. Thompson, D. A. Walker, and J. M. Welker. Role of Land-Surface Changes in Arctic Summer Warming. *Science*, 310(5748):657–660, October 2005. Publisher: American Association for the Advancement of Science.

[65] Bruce C. Forbes, Marc Macias Fauria, and Pentti Zetterberg. Russian Arctic warming and 'greening' are closely tracked by tundra shrub willows. *Global Change Biology*,

16(5):1542–1554, 2010. _eprint: https://onlinelibrary.wiley.com/doi/pdf/10.1111/j.1365-2486.2009.02047.x.

[66] Logan T. Berner, Richard Massey, Patrick Jantz, Bruce C. Forbes, Marc Macias-Fauria, Isla Myers-Smith, Timo Kumpula, Gilles Gauthier, Laia Andreu-Hayles, Benjamin V. Gaglioti, Patrick Burns, Pentti Zetterberg, Rosanne D'Arrigo, and Scott J. Goetz. Summer warming explains widespread but not uniform greening in the Arctic tundra biome. *Nat Commun*, 11(1):4621, September 2020. Publisher: Nature Publishing Group.

[67] Gensuo J. Jia, Howard E. Epstein, and Donald A. Walker. Greening of arctic Alaska, 1981–2001. *Geophysical Research Letters*, 30(20), 2003. _eprint: https://onlinelibrary.wiley.com/doi/pdf/10.1029/2003GL018268.

[68] T. A. Moon, R. Thoman, M. L. Druckenmiller, Brandon Ahmasuk, Stacia A. Backensto, Thomas J. Ballinger, Rasmus Benestad, Logan T. Berner, Germar H. Bernhard, Uma S. Bhatt, Siiri Bigalke, W. BjerkeJarle, Brian Brettschneider, Hanne H. Christiansen, Judah L. Cohen, Bertrand Decharme, Chris Derksen, Dmitry Divine, Jensen Drost, Matthew L. Druckenmiller, Alesksandra EliasChereque, Howard E. Epstein, Robert S. Fausto, Xavier Fettweis, Vitali E. Fioletov, Bruce C. Forbes, Gerald V. (JJ) Frost, Sebastian Gerland, Scott J. Goetz, Jens-Uwe Grooß, Edward Hanna, Inger Hanssen-Bauer, Stefan Hendricks, Robert M. Holmes, Iolanda Ialongo, Ketil Isaksen, Bjørn Johnsen, Timothy Jones, Robb S. A. Kaler, Lars Kaleschke, Seong-Joong Kim, Zachary M. Labe, Rick Lader, Kaisa Lakkala, Mark J. Lara, Jackie Lindsey, Bryant D. Loomis, Kari Luojus, Matthew J. Macander, Jostein Mamen, Ken D. Mankoff, Gloria L. Manney, Stephanie A. McAfee, James W. McClelland, Walter N. Meier, Twila A. Moon, G. W. K. Moore, Thomas L. Mote, Lawrence Mudryk, Rolf Müller, Kelsey E. Nyland, James E. Overland, Julia K. Parrish, Donald K. Perovich, Guðrún Nína Petersen, Alek Petty, Gareth K. Phoenix, Kristin Poinar, Mika Rantanen, Robert Ricker, Vladimir E. Romanovsky, Shawn P. Serbin, Mark C. Serreze, Gay Sheffield, Alexander I. Shiklomanov, Nikolay I. Shiklomanov, Sharon L. Smith, Robert

G. M. Spencer, Dmitry A. Streletskiy, Anya Suslova, Tove Svendby, Suzanne E. Tank, Marco Tedesco, Richard L. Thoman, Xiangshan Tian-Kunze, Mary-Louise Timmermans, Hans Tømmervik, Mikhail Tretiakov, Donald (Skip) A. Walker, John E. Walsh, Muyin Wang, Melinda Webster, Adrian Wehrlé, Daqing Yang, Scott Zolkos, Jessicca Allen, Amy V. Camper, Bridgette O. Haley, Gregory Hammer, S. Love-Brotak, Laura Ohlmann, Lukas Noguchi, Deborah B. Riddle, and Sara W. Veasey. The Arctic. *Bulletin of the American Meteorological Society*, 104(9):S271–S321, September 2023. Publisher: American Meteorological Society Section: Bulletin of the American Meteorological Society.

[69] Mika Rantanen, Alexey Yu Karpechko, Antti Lipponen, Kalle Nordling, Otto Hyvärinen, Kimmo Ruosteenoja, Timo Vihma, and Ari Laaksonen. The Arctic has warmed nearly four times faster than the globe since 1979. *Commun Earth Environ*, 3(1):1–10, August 2022. Number: 1 Publisher: Nature Publishing Group.

[70] Melanie A. Harsch, Philip E. Hulme, Matt S. McGlone, and Richard P. Duncan. Are treelines advancing? A global meta-analysis of treeline response to climate warming. *Ecology Letters*, 12(10):1040–1049, 2009. _eprint: https://onlinelibrary.wiley.com/doi/pdf/10.1111/j.1461-0248.2009.01355.x.

[71] Benoît Tremblay, Esther Lévesque, and Stéphane Boudreau. Recent expansion of erect shrubs in the Low Arctic: evidence from Eastern Nunavik. *Environ. Res. Lett.*, 7(3):035501, July 2012. Publisher: IOP Publishing.

[72] Sarah C. Elmendorf, Gregory H. R. Henry, Robert D. Hollister, Robert G. Björk, Noémie Boulanger-Lapointe, Elisabeth J. Cooper, Johannes H. C. Cornelissen, Thomas A. Day, Ellen Dorrepaal, Tatiana G. Elumeeva, Mike Gill, William A. Gould, John Harte, David S. Hik, Annika Hofgaard, David R. Johnson, Jill F. Johnstone, Ingibjörg Svala Jónsdóttir, Janet C. Jorgenson, Kari Klanderud, Julia A. Klein, Saewan Koh, Gaku Kudo, Mark Lara, Esther Lévesque, Borgthor Magnússon, Jeremy L. May, Joel A. Mercado-Dı´az, Anders Michelsen, Ulf Molau, Isla H. Myers-Smith, Steven F. Oberbauer, Vladimir G. Onipchenko,

Christian Rixen, Niels Martin Schmidt, Gaius R. Shaver, Marko J. Spasojevic, Þóra Ellen Þórhallsdóttir, Anne Tolvanen, Tiffany Troxler, Craig E. Tweedie, Sandra Villareal, Carl-Henrik Wahren, Xanthe Walker, Patrick J. Webber, Jeffrey M. Welker, and Sonja Wipf. Plot-scale evidence of tundra vegetation change and links to recent summer warming. *Nature Clim Change*, 2(6):453–457, June 2012. Number: 6 Publisher: Nature Publishing Group.

[73] Stef Weijers, Friederike Wagner-Cremer, Ute Sass-Klaassen, Rob Broekman, and Jelte Rozema. Reconstructing High Arctic growing season intensity from shoot length growth of a dwarf shrub. *The Holocene*, 23(5):721–731, May 2013. Publisher: SAGE Publications Ltd.

[74] Marco Caccianiga and Serge Payette. Recent advance of white spruce (Picea glauca) in the coastal tundra of the eastern shore of Hudson Bay (Québec, Canada). *Journal of Biogeography*, 33(12):2120–2135, 2006. _eprint: https://onlinelibrary.wiley.com/doi/pdf/10.1111/j.1365-2699.2006.01563.x.

[75] Roman J. Dial, Colin T. Maher, Rebecca E. Hewitt, and Patrick F. Sullivan. Sufficient conditions for rapid range expansion of a boreal conifer. *Nature*, pages 1–6, August 2022. Publisher: Nature Publishing Group.

[76] K. Fred Huemmrich, John Gamon, Petya Campbell, Marianna Mora, Sergio Vargas Z, Brenda Almanza, and Craig Tweedie. 20 years of change in tundra NDVI from coupled field and satellite observations. *Environ. Res. Lett.*, 18(9):094022, August 2023. Publisher: IOP Publishing.

[77] Stein Rune Karlsen, Arve Elvebakk, Laura Stendardi, Kjell Arild Høgda, and Marc Macias-Fauria. Greening of Svalbard. *Science of The Total Environment*, 945:174130, October 2024.

[78] Geneviève Dufour-Tremblay, Esther Lévesque, and Stéphane Boudreau. Dynamics at the treeline: differential responses of Picea mariana and Larix laricina to climate change in eastern subarctic Québec. *Environ. Res. Lett.*, 7(4):044038, December 2012. Publisher: IOP Publishing.

[79] Isla H. Myers-Smith, Jeffrey T. Kerby, Gareth K. Phoenix, Jarle W. Bjerke, Howard E. Epstein, Jakob J. Assmann, Christian John, Laia Andreu-Hayles, Sandra Angers-Blondin, Pieter S. A. Beck, Logan T. Berner, Uma S. Bhatt, Anne D. Bjorkman, Daan Blok, Anders Bryn, Casper T. Christiansen, J. Hans C. Cornelissen, Andrew M. Cunliffe, Sarah C. Elmendorf, Bruce C. Forbes, Scott J. Goetz, Robert D. Hollister, Rogier de Jong, Michael M. Loranty, Marc Macias-Fauria, Kadmiel Maseyk, Signe Normand, Johan Olofsson, Thomas C. Parker, Frans-Jan W. Parmentier, Eric Post, Gabriela Schaepman-Strub, Frode Stordal, Patrick F. Sullivan, Haydn J. D. Thomas, Hans Tømmervik, Rachael Treharne, Craig E. Tweedie, Donald A. Walker, Martin Wilmking, and Sonja Wipf. Complexity revealed in the greening of the Arctic. *Nat. Clim. Chang.*, 10(2):106–117, February 2020. Number: 2 Publisher: Nature Publishing Group.

[80] Logan T. Berner, Pieter S. A. Beck, Andrew G. Bunn, and Scott J. Goetz. Plant response to climate change along the forest-tundra ecotone in northeastern Siberia. *Global Change Biology*, 19(11):3449–3462, 2013. _eprint: https://onlinelibrary.wiley.com/doi/pdf/10.1111/gcb.12304.

[81] Rebecca Edwards and Paul Treitz. Vegetation Greening Trends at Two Sites in the Canadian Arctic: 1984–2015. *Arctic, Antarctic, and Alpine Research*, 49(4):601–619, November 2017. Publisher: Taylor & Francis _eprint: https://doi.org/10.1657/AAAR0016-075.

[82] Robert H. Fraser, Trevor C. Lantz, Ian Olthof, Steven V. Kokelj, and Richard A. Sims. Warming-Induced Shrub Expansion and Lichen Decline in the Western Canadian Arctic. *Ecosystems*, 17(7):1151–1168, November 2014.

[83] T. F. Keenan and W. J. Riley. Greening of the land surface in the world's cold regions consistent with recent warming. *Nature Clim Change*, 8(9):825–828, September 2018. Publisher: Nature Publishing Group.

[84] Matthew Sturm, Charles Racine, and Kenneth Tape. Increasing shrub abundance in the Arctic. *Nature*, 411(6837):546–547, May 2001. Number: 6837 Publisher: Nature Publishing Group.

[85] Ryan K. Danby and David S. Hik. Evidence of Recent Treeline Dynamics in Southwest Yukon from Aerial Photographs. *Arctic*, 60(4):411–420, 2007. Publisher: Arctic Institute of North America.

[86] Ulf Büntgen, Lena Hellmann, Willy Tegel, Signe Normand, Isla Myers-Smith, Alexander V. Kirdyanov, Daniel Nievergelt, and Fritz H. Schweingruber. Temperature-induced recruitment pulses of Arctic dwarf shrub communities. *Journal of Ecology*, 103(2):489–501, 2015. _eprint: https://onlinelibrary.wiley.com/doi/pdf/10.1111/1365-2745.12361.

[87] Laia Andreu-Hayles, Benjamin V. Gaglioti, Logan T. Berner, Mathieu Levesque, Kevin J. Anchukaitis, Scott J. Goetz, and Rosanne D'Arrigo. A narrow window of summer temperatures associated with shrub growth in Arctic Alaska. *Environ. Res. Lett.*, 15(10):105012, October 2020. Publisher: IOP Publishing.

[88] Stéphane Boudreau and Marie-Pascale Villeneuve-Simard. Dendrochronological evidence of shrub growth suppression by trees in a subarctic lichen woodland. *Botany*, 90(2):151–156, February 2012. Publisher: NRC Research Press.

[89] Jan Esper and Fritz H. Schweingruber. Large-scale treeline changes recorded in Siberia. *Geophysical Research Letters*, 31(6), 2004. _eprint: https://onlinelibrary.wiley.com/doi/pdf/10.1029/2003GL019178.

[90] Andrea H. Lloyd and Christopher L. Fastie. Recent changes in treeline forest distribution and structure in interior Alaska. *Écoscience*, 10(2):176–185, 2003. Publisher: Taylor & Francis, Ltd.

[91] Evelyn C. Pielou. *After the ice age: the return of life to glaciated North America*. University of Chicago Press, 2008.

[92] Sarah E. Crump, Bianca Fréchette, Matthew Power, Sam Cutler, Gregory de Wet, Martha K. Raynolds, Jonathan H. Raberg, Jason P. Briner, Elizabeth K. Thomas, Julio Sepúlveda, Beth Shapiro, Michael Bunce, and Gifford H. Miller. Ancient plant DNA reveals High Arctic greening during the Last Interglacial. *Proceedings of the National Academy of Sciences*, 118(13):e2019069118, March 2021. Publisher: Proceedings of the National Academy of Sciences.

[93] Paul R. Bierman, Halley M. Mastro, Dorothy M. Peteet, Lee B. Corbett, Eric J. Steig, Chris T. Halsted, Marc M. Caffee, Alan J. Hidy, Greg Balco, Ole Bennike, and Barry Rock. Plant, insect, and fungi fossils under the center of Greenland's ice sheet are evidence of ice-free times. *Proceedings of the National Academy of Sciences*, 121(33):e2407465121, August 2024. Publisher: Proceedings of the National Academy of Sciences.

[94] Sarah C. Elmendorf, Gregory H. R. Henry, Robert D. Hollister, Robert G. Björk, Anne D. Bjorkman, Terry V. Callaghan, Laura Siegwart Collier, Elisabeth J. Cooper, Johannes H. C. Cornelissen, Thomas A. Day, Anna Maria Fosaa, William A. Gould, Járngerður Grétarsdóttir, John Harte, Luise Hermanutz, David S. Hik, Annika Hofgaard, Frith Jarrad, Ingibjörg Svala Jónsdóttir, Frida Keuper, Kari Klanderud, Julia A. Klein, Saewan Koh, Gaku Kudo, Simone I. Lang, Val Loewen, Jeremy L. May, Joel Mercado, Anders Michelsen, Ulf Molau, Isla H. Myers-Smith, Steven F. Oberbauer, Sara Pieper, Eric Post, Christian Rixen, Clare H. Robinson, Niels Martin Schmidt, Gaius R. Shaver, Anna Stenström, Anne Tolvanen, Ørjan Totland, Tiffany Troxler, Carl-Henrik Wahren, Patrick J. Webber, Jeffery M. Welker, and Philip A. Wookey. Global assessment of experimental climate warming on tun-

dra vegetation: heterogeneity over space and time. *Ecology Letters*, 15(2):164–175, 2012. _eprint: https://onlinelibrary.wiley.com/doi/pdf/10.1111/j.1461-0248.2011.01716.x.

[95] Marilyn D. Walker, C. Henrik Wahren, Robert D. Hollister, Greg H. R. Henry, Lorraine E. Ahlquist, Juha M. Alatalo, M. Syndonia Bret-Harte, Monika P. Calef, Terry V. Callaghan, Amy B. Carroll, Howard E. Epstein, Ingibjörg S. Jónsdóttir, Julia A. Klein, Borgþór Magnússon, Ulf Molau, Steven F. Oberbauer, Steven P. Rewa, Clare H. Robinson, Gaius R. Shaver, Katharine N. Suding, Catharine C. Thompson, Anne Tolvanen, Ørjan Totland, P. Lee Turner, Craig E. Tweedie, Patrick J. Webber, and Philip A. Wookey. Plant community responses to experimental warming across the tundra biome. *Proceedings of the National Academy of Sciences*, 103(5):1342–1346, January 2006. Publisher: Proceedings of the National Academy of Sciences.

[96] Alain Cuerrier, Nicolas D. Brunet, José Gérin-Lajoie, Ashleigh Downing, and Esther Lévesque. The Study of Inuit Knowledge of Climate Change in Nunavik, Quebec: A Mixed Methods Approach. *Hum Ecol*, 43(3):379–394, June 2015.

[97] ITEX. ITEX Manual, Second Edition. Technical report, Danish Polar Center, 1996.

[98] Matthew J. Menne, Imke Durre, Russell S. Vose, Byron E. Gleason, and Tamara G. Houston. An Overview of the Global Historical Climatology Network-Daily Database. *Journal of Atmospheric and Oceanic Technology*, 29(7):897–910, July 2012. Publisher: American Meteorological Society Section: Journal of Atmospheric and Oceanic Technology.

[99] Matthew Newman, Michael A. Alexander, Toby R. Ault, Kim M. Cobb, Clara Deser, Emanuele Di Lorenzo, Nathan J. Mantua, Arthur J. Miller, Shoshiro Minobe, Hisashi Nakamura, Niklas Schneider, Daniel J. Vimont, Adam S. Phillips, James D. Scott, and Catherine A. Smith. The Pacific Decadal Oscillation, Revisited. *Journal of Climate*, 29(12):4399–4427, June 2016. Publisher: American Meteorological Society Section: Journal of Climate.

[100] Gerald A. Meehl, Jadwiga H. Richter, Haiyan Teng, Antonietta Capotondi, Kim Cobb, Francisco Doblas-Reyes, Markus G. Donat, Matthew H. England, John C. Fyfe, Weiqing Han, Hyemi Kim, Ben P. Kirtman, Yochanan Kushnir, Nicole S. Lovenduski, Michael E. Mann, William J. Merryfield, Veronica Nieves, Kathy Pegion, Nan Rosenbloom, Sara C. Sanchez, Adam A. Scaife, Doug Smith, Aneesh C. Subramanian, Lantao Sun, Diane Thompson, Caroline C. Ummenhofer, and Shang-Ping Xie. Initialized Earth System prediction from subseasonal to decadal timescales. *Nature Reviews Earth & Environment*, pages 1–18, April 2021. Publisher: Nature Publishing Group.

[101] John W. Williams, Bryan N. Shuman, and Thompson Webb III. Dissimilarity Analyses of Late-Quaternary Vegetation and Climate in Eastern North America. *Ecology*, 82(12):3346–3362, 2001. _eprint: https://onlinelibrary.wiley.com/doi/pdf/10.1890/0012-9658%282001%29082%5B3346%3ADAOLQV%5D2.0.CO%3B2.

[102] John W. Williams, Stephen T. Jackson, and John E. Kutzbach. Projected distributions of novel and disappearing climates by 2100 AD. *Proceedings of the National Academy of Sciences*, 104(14):5738–5742, April 2007. Publisher: Proceedings of the National Academy of Sciences.

[103] Diana Stralberg, Dennis Jongsomjit, Christine A. Howell, Mark A. Snyder, John D. Alexander, John A. Wiens, and Terry L. Root. Re-Shuffling of Species with Climate Disruption: A No-Analog Future for California Birds? *PLOS ONE*, 4(9):e6825, September 2009. Publisher: Public Library of Science.

[104] John T. Fasullo and Jadwiga H. Richter. Dependence of strategic solar climate intervention on background scenario and model physics. *Atmospheric Chemistry and Physics*, 23(1):163–182, January 2023. Publisher: Copernicus GmbH.

[105] T. Janjić, N. Bormann, M. Bocquet, J. A Carton, S. E. Cohn, S. L. Dance, S. N. Losa, N. K. Nichols, R. Potthast, J. A. Waller, and P. Weston. On the representation error in data

assimilation. *Quarterly Journal of the Royal Meteorological Society*, 144(713):1257–1278, 2018. _eprint: https://onlinelibrary.wiley.com/doi/pdf/10.1002/qj.3130.

[106] J. A. Waller, S. L. Dance, A. S. Lawless, N. K. Nichols, and J. R. Eyre. Representativity error for temperature and humidity using the Met Office high-resolution model. *Quarterly Journal of the Royal Meteorological Society*, 140(681):1189–1197, 2014. _eprint: https://onlinelibrary.wiley.com/doi/pdf/10.1002/qj.2207.

[107] Ben Tustison, Daniel Harris, and Efi Foufoula-Georgiou. Scale issues in verification of precipitation forecasts. *Journal of Geophysical Research: Atmospheres*, 106(D11):11775–11784, 2001. _eprint: https://onlinelibrary.wiley.com/doi/pdf/10.1029/2001JD900066.

[108] Shipra Jain, Adam A. Scaife, Theodore G. Shepherd, Clara Deser, Nick Dunstone, Gavin A. Schmidt, Kevin E. Trenberth, and Thea Turkington. Importance of internal variability for climate model assessment. *npj Clim Atmos Sci*, 6(1):1–7, June 2023. Number: 1 Publisher: Nature Publishing Group.

[109] Richard Seager, Naomi Henderson, and Mark Cane. Persistent Discrepancies between Observed and Modeled Trends in the Tropical Pacific Ocean. *Journal of Climate*, 35(14):4571–4584, July 2022. Publisher: American Meteorological Society Section: Journal of Climate.

[110] Maria Rugenstein, Shreya Dhame, Dirk Olonscheck, Robert Jnglin Wills, Masahiro Watanabe, and Richard Seager. Connecting the SST Pattern Problem and the Hot Model Problem. *Geophysical Research Letters*, 50(22):e2023GL105488, 2023. _eprint: https://onlinelibrary.wiley.com/doi/pdf/10.1029/2023GL105488.

[111] Andrea H. Lloyd, Paul A. Duffy, and Daniel H. Mann. Nonlinear responses of white spruce growth to climate variability in interior Alaska. *Can. J. For. Res.*, 43(4):331–343, April 2013. Publisher: NRC Research Press.

[112] Allison M. Jensen, David Fastovich, Ben I. Watson, Jacquelyn L. Gill, Stephen T. Jackson, James M. Russell, Joseph Bevington, Katherine Hayes, Katherine B. Lininger, Claire

Rubbelke, Grace C. Schellinger, and John W. Williams. More than one way to kill a spruce forest: The role of fire and climate in the late-glacial termination of spruce woodlands across the southern Great Lakes. *Journal of Ecology*, 109(1):459–477, 2021. _eprint: https://onlinelibrary.wiley.com/doi/pdf/10.1111/1365-2745.13517.

[113] Katherine Hayes and Brian Buma. Effects of short-interval disturbances continue to accumulate, overwhelming variability in local resilience. *Ecosphere*, 12(3):e03379, 2021. _eprint: https://onlinelibrary.wiley.com/doi/pdf/10.1002/ecs2.3379.

[114] Ryan G. Jameson, Andrew J. Trant, and Luise Hermanutz. Insects can limit seed productivity at the treeline. *Can. J. For. Res.*, 45(3):286–296, March 2015. Publisher: NRC Research Press.

[115] Anna L. Crofts and Carissa D. Brown. The importance of biotic filtering on boreal conifer recruitment at alpine treeline. *Ecography*, 43(6):914–929, 2020. _eprint: https://onlinelibrary.wiley.com/doi/pdf/10.1111/ecog.04899.

[116] Johan Olofsson, Lauri Oksanen, Terry Callaghan, Philip E. Hulme, Tarja Oksanen, and Otso Suominen. Herbivores inhibit climate-driven shrub expansion on the tundra. *Global Change Biology*, 15(11):2681–2693, 2009. _eprint: https://onlinelibrary.wiley.com/doi/pdf/10.1111/j.1365-2486.2009.01935.x.

[117] Kari Anne Bråthen, Virve Tuulia Ravolainen, Audun Stien, Torkild Tveraa, and Rolf A. Ims. Rangifer management controls a climate-sensitive tundra state transition. *Ecological Applications*, 27(8):2416–2427, 2017. _eprint: https://onlinelibrary.wiley.com/doi/pdf/10.1002/eap.1618.

[118] Brian C. O'Neill, Elmar Kriegler, Keywan Riahi, Kristie L. Ebi, Stephane Hallegatte, Timothy R. Carter, Ritu Mathur, and Detlef P. van Vuuren. A new scenario framework for climate change research: the concept of shared socioeconomic pathways. *Climatic Change*, 122(3):387–400, February 2014.

[119] Alice K. DuVivier, Marika M. Holland, Jennifer E. Kay, Simone Tilmes, Andrew Gettelman, and David A. Bailey. Arctic and Antarctic Sea Ice Mean State in the Community Earth System Model Version 2 and the Influence of Atmospheric Chemistry. *Journal of Geophysical Research: Oceans*, 125(8):e2019JC015934, 2020. _eprint: https://onlinelibrary.wiley.com/doi/pdf/10.1029/2019JC015934.

[120] Zeke Hausfather. An assessment of current policy scenarios over the 21st century and the reduced plausibility of high-emissions pathways. *Dialogues on Climate Change*, page 29768659241304854, January 2025. Publisher: SAGE Publications.

[121] H. Damon Matthews and Seth Wynes. Current global efforts are insufficient to limit warming to 1.5°C. *Science*, 376(6600):1404–1409, June 2022. Publisher: American Association for the Advancement of Science.

[122] Jennifer E. Kay, Patricia DeRepentigny, Marika M. Holland, David A. Bailey, Alice K. DuVivier, Ed Blanchard-Wrigglesworth, Clara Deser, Alexandra Jahn, Hansi Singh, Madison M. Smith, Melinda A. Webster, Jim Edwards, Sun-Seon Lee, Keith B. Rodgers, and Nan Rosenbloom. Less Surface Sea Ice Melt in the CESM2 Improves Arctic Sea Ice Simulation With Minimal Non-Polar Climate Impacts. *Journal of Advances in Modeling Earth Systems*, 14(4):e2021MS002679, 2022. _eprint: https://onlinelibrary.wiley.com/doi/pdf/10.1029/2021MS002679.

[123] Ed Hawkins and Rowan Sutton. The Potential to Narrow Uncertainty in Regional Climate Predictions. *Bulletin of the American Meteorological Society*, 90(8):1095–1108, August 2009. Publisher: American Meteorological Society Section: Bulletin of the American Meteorological Society.

[124] Marc J. Alessi and Maria A. A. Rugenstein. Surface Temperature Pattern Scenarios Suggest Higher Warming Rates Than Current Projections. *Geophysical Research Letters*, 50(23):e2023GL105795, 2023. _eprint: https://onlinelibrary.wiley.com/doi/pdf/10.1029/2023GL105795.

[125] Ana Bastos, Philippe Ciais, Taejin Park, Jakob Zscheischler, Chao Yue, Jonathan Barichivich, Ranga B. Myneni, Shushi Peng, Shilong Piao, and Zaichun Zhu. Was the extreme Northern Hemisphere greening in 2015 predictable? *Environ. Res. Lett.*, 12(4):044016, April 2017. Publisher: IOP Publishing.

[126] EPA. Technical Documentation: Growing Degree Days. Technical report, United States Environmental Protection Agency, 2024.

[127] J. T. Fasullo, Jean-Francois Lamarque, Cecile Hannay, Nan Rosenbloom, Simone Tilmes, Patricia DeRepentigny, Alexandra Jahn, and Clara Deser. Spurious Late Historical-Era Warming in CESM2 Driven by Prescribed Biomass Burning Emissions. *Geophysical Research Letters*, page e2021GL097420, January 2022. Publisher: John Wiley & Sons, Ltd.

[128] Laura Landrum, Bette L. Otto-Bliesner, Eugene R. Wahl, Andrew Conley, Peter J. Lawrence, Nan Rosenbloom, and Haiyan Teng. Last Millennium Climate and Its Variability in CCSM4. *Journal of Climate*, 26(4):1085–1111, February 2013. Publisher: American Meteorological Society Section: Journal of Climate.

[129] Veronika Eyring, Sandrine Bony, Gerald A. Meehl, Catherine A. Senior, Bjorn Stevens, Ronald J. Stouffer, and Karl E. Taylor. Overview of the Coupled Model Intercomparison Project Phase 6 (CMIP6) experimental design and organization. *Geoscientific Model Development*, 9(5):1937–1958, May 2016. Publisher: Copernicus GmbH.

[130] Ellert van der Velden. CMasher: Scientific colormaps for making accessible, informative and 'cmashing' plots. *Journal of Open Source Software*, 5(46):2004, February 2020.

[131] Elvira S. Poloczanska, Christopher J. Brown, William J. Sydeman, Wolfgang Kiessling, David S. Schoeman, Pippa J. Moore, Keith Brander, John F. Bruno, Lauren B. Buckley, Michael T. Burrows, Carlos M. Duarte, Benjamin S. Halpern, Johnna Holding, Carrie V. Kappel, Mary I. O'Connor, John M. Pandolfi, Camille Parmesan, Franklin Schwing, Sarah Ann Thompson, and Anthony J. Richardson. Global imprint of climate change on

marine life. *Nature Clim Change*, 3(10):919–925, October 2013. Number: 10 Publisher: Nature Publishing Group.

[132] Jorge García Molinos, Benjamin S. Halpern, David S. Schoeman, Christopher J. Brown, Wolfgang Kiessling, Pippa J. Moore, John M. Pandolfi, Elvira S. Poloczanska, Anthony J. Richardson, and Michael T. Burrows. Climate velocity and the future global redistribution of marine biodiversity. *Nature Clim Change*, 6(1):83–88, January 2016. Number: 1 Publisher: Nature Publishing Group.

[133] Jane C. S. Long and John G. Shepherd. The Strategic Value of Geoengineering Research. In Bill Freedman, editor, *Global Environmental Change*, Handbook of Global Environmental Pollution, pages 757–770. Springer Netherlands, Dordrecht, 2014.

[134] Jadwiga H. Richter, Daniele Visioni, Douglas G. MacMartin, David A. Bailey, Nan Rosenbloom, Brian Dobbins, Walker R. Lee, Mari Tye, and Jean-Francois Lamarque. Assessing Responses and Impacts of Solar climate intervention on the Earth system with stratospheric aerosol injection (ARISE-SAI): protocol and initial results from the first simulations. *Geoscientific Model Development*, 15(22):8221–8243, November 2022. Publisher: Copernicus GmbH.

[135] Holly Jean Buck. Rapid scale-up of negative emissions technologies: social barriers and social implications. *Climatic Change*, 139(2):155–167, November 2016.

[136] Christopher H. Trisos, Giuseppe Amatulli, Jessica Gurevitch, Alan Robock, Lili Xia, and Brian Zambri. Potentially dangerous consequences for biodiversity of solar geoengineering implementation and termination. *Nat Ecol Evol*, 2(3):475–482, March 2018. Number: 3 Publisher: Nature Publishing Group.

[137] Ailene K. Ettinger and Janneke HilleRisLambers. Climate isn't everything: Competitive interactions and variation by life stage will also affect range shifts in a

warming world. *American Journal of Botany*, 100(7):1344–1355, 2013. _eprint: https://onlinelibrary.wiley.com/doi/pdf/10.3732/ajb.1200489.

[138] Erik A Beever, L Embere Hall, Johanna Varner, Anne E Loosen, Jason B Dunham, Megan K Gahl, Felisa A Smith, and Joshua J Lawler. Behavioral flexibility as a mechanism for coping with climate change. *Frontiers in Ecology and the Environment*, 15(6):299–308, 2017. _eprint: https://onlinelibrary.wiley.com/doi/pdf/10.1002/fee.1502.

[139] Elsa Youngsteadt, Sara Guiti Prado, Kirsten Joanna Keleher, and Michelle Kirchner. Can behaviour and physiology mitigate effects of warming on ectotherms? A test in urban ants. *Journal of Animal Ecology*, n/a(n/a), 2023. _eprint: https://onlinelibrary.wiley.com/doi/pdf/10.1111/1365-2656.13860.

[140] Jill F Johnstone, Craig D Allen, Jerry F Franklin, Lee E Frelich, Brian J Harvey, Philip E Higuera, Michelle C Mack, Ross K Meentemeyer, Margaret R Metz, George LW Perry, Tania Schoennagel, and Monica G Turner. Changing disturbance regimes, ecological memory, and forest resilience. *Frontiers in Ecology and the Environment*, 14(7):369–378, 2016. _eprint: https://onlinelibrary.wiley.com/doi/pdf/10.1002/fee.1311.

[141] Kelly E. McCusker, Kyle C. Armour, Cecilia M. Bitz, and David S. Battisti. Rapid and extensive warming following cessation of solar radiation management. *Environ. Res. Lett.*, 9(2):024005, January 2014. Publisher: IOP Publishing.

[142] Andy Parker and Peter J. Irvine. The Risk of Termination Shock From Solar Geoengineering. *Earth's Future*, 6(3):456–467, 2018. _eprint: https://onlinelibrary.wiley.com/doi/pdf/10.1002/2017EF000735.

[143] A. Gettelman, M. J. Mills, D. E. Kinnison, R. R. Garcia, A. K. Smith, D. R. Marsh, S. Tilmes, F. Vitt, C. G. Bardeen, J. McInerny, H.-L. Liu, S. C. Solomon, L. M. Polvani, L. K. Emmons, J.-F. Lamarque, J. H. Richter, A. S. Glanville, J. T. Bacmeister, A. S. Phillips, R. B. Neale, I. R. Simpson, A. K. DuVivier, A. Hodzic, and W. J.

Randel. The Whole Atmosphere Community Climate Model Version 6 (WACCM6). *Journal of Geophysical Research: Atmospheres*, 124(23):12380–12403, 2019. _eprint: https://agupubs.onlinelibrary.wiley.com/doi/pdf/10.1029/2019JD030943.

[144] Ezra Brody, Daniele Visioni, Ewa M. Bednarz, Ben Kravitz, Douglas G. MacMartin, Jadwiga H. Richter, and Mari R. Tye. Kicking the Can Down the Road: Understanding the Effects of Delaying the Deployment of Stratospheric Aerosol Injection, February 2024. arXiv:2402.11992 [physics].

[145] Noémie Laurens. Institutional Adaptation in Slow Motion: Zooming In on Desertification Governance. *Global Environmental Politics*, 23(2):31–53, 2023. Publisher: The MIT Press.

[146] B. Otto-Bliesner, M. J. Mills, E.C. Brady, A. Schmidt, R. R. Garcia, and J. Zhu. CESM2-WACCM6ma Last Millennium, 2023.

[147] Johann H. Jungclaus, Edouard Bard, Mélanie Baroni, Pascale Braconnot, Jian Cao, Louise P. Chini, Tania Egorova, Michael Evans, J. Fidel González-Rouco, Hugues Goosse, George C. Hurtt, Fortunat Joos, Jed O. Kaplan, Myriam Khodri, Kees Klein Goldewijk, Natalie Krivova, Allegra N. LeGrande, Stephan J. Lorenz, Jürg Luterbacher, Wenmin Man, Amanda C. Maycock, Malte Meinshausen, Anders Moberg, Raimund Muscheler, Christoph Nehrbass-Ahles, Bette I. Otto-Bliesner, Steven J. Phipps, Julia Pongratz, Eugene Rozanov, Gavin A. Schmidt, Hauke Schmidt, Werner Schmutz, Andrew Schurer, Alexander I. Shapiro, Michael Sigl, Jason E. Smerdon, Sami K. Solanki, Claudia Timmreck, Matthew Toohey, Ilya G. Usoskin, Sebastian Wagner, Chi-Ju Wu, Kok Leng Yeo, Davide Zanchettin, Qiong Zhang, and Eduardo Zorita. The PMIP4 contribution to CMIP6 – Part 3: The last millennium, scientific objective, and experimental design for the PMIP4 past1000 simulations. *Geoscientific Model Development*, 10(11):4005–4033, November 2017. Publisher: Copernicus GmbH.

[148] Keywan Riahi, Detlef P. van Vuuren, Elmar Kriegler, Jae Edmonds, Brian C. O'Neill, Shinichiro Fujimori, Nico Bauer, Katherine Calvin, Rob Dellink, Oliver Fricko, Wolfgang

Lutz, Alexander Popp, Jesus Crespo Cuaresma, Samir Kc, Marian Leimbach, Leiwen Jiang, Tom Kram, Shilpa Rao, Johannes Emmerling, Kristie Ebi, Tomoko Hasegawa, Petr Havlik, Florian Humpenöder, Lara Aleluia Da Silva, Steve Smith, Elke Stehfest, Valentina Bosetti, Jiyong Eom, David Gernaat, Toshihiko Masui, Joeri Rogelj, Jessica Strefler, Laurent Drouet, Volker Krey, Gunnar Luderer, Mathijs Harmsen, Kiyoshi Takahashi, Lavinia Baumstark, Jonathan C. Doelman, Mikiko Kainuma, Zbigniew Klimont, Giacomo Marangoni, Hermann Lotze-Campen, Michael Obersteiner, Andrzej Tabeau, and Massimo Tavoni. The Shared Socioeconomic Pathways and their energy, land use, and greenhouse gas emissions implications: An overview. *Global Environmental Change*, 42:153–168, January 2017.

[149] Michael T. Burrows, David S. Schoeman, Lauren B. Buckley, Pippa Moore, Elvira S. Poloczanska, Keith M. Brander, Chris Brown, John F. Bruno, Carlos M. Duarte, Benjamin S. Halpern, Johnna Holding, Carrie V. Kappel, Wolfgang Kiessling, Mary I. O'Connor, John M. Pandolfi, Camille Parmesan, Franklin B. Schwing, William J. Sydeman, and Anthony J. Richardson. The Pace of Shifting Climate in Marine and Terrestrial Ecosystems. *Science*, 334(6056):652–655, November 2011. Publisher: American Association for the Advancement of Science.

[150] Geert Jan van Oldenborgh, Matthew Collins, Julie Arblaster, Jens Hesselbjerg Christensen, Jochem Marotzke, Scott B. Power, Markku Rummukainen, and Tianjun Zhou. Annex I: Atlas of Global and Regional Climate Projections. In Thomas F. Stocker, Dahe Qin, Gian-Kasper Plattner, Melinda M. B. Tignor, Simon K. Allen, Judith Boschung, Alexander Nauels, Yu Xia, Vincent Bex, and Pauline M. Midgley, editors, *Climate Change 2013: The Physical Science Basis. Contribution of Working Group I to the Fifth Assessment Report of the Intergovernmental Panel on Climate Change*, pages 1311–1393. Cambridge University Press, Cambridge, United Kingdom, 2013. Num Pages: 84.

[151] Austin M. Thomas, Mark E. Johns, and Robert M. Jetton. Characterization of a Disjunct Population of Eastern Hemlock (Tsuga canadensis) and Surrounding Plant Communities in

the North Carolina Piedmont after 65 Years of Forest Change. *sena*, 20(3):377–398, August 2021. Publisher: Eagle Hill Institute.

[152] Jenny L. McGuire, Joshua J. Lawler, Brad H. McRae, Tristan A. Nuñez, and David M. Theobald. Achieving climate connectivity in a fragmented landscape. *Proceedings of the National Academy of Sciences*, 113(26):7195–7200, June 2016. Publisher: Proceedings of the National Academy of Sciences.

[153] Michelle Ward, Santiago Saura, Brooke Williams, Juan Pablo Ramírez-Delgado, Nur Arafeh-Dalmau, James R. Allan, Oscar Venter, Grégoire Dubois, and James E. M. Watson. Just ten percent of the global terrestrial protected area network is structurally connected via intact land. *Nat Commun*, 11(1):4563, September 2020. Number: 1 Publisher: Nature Publishing Group.

[154] Nur Arafeh-Dalmau, Isaac Brito-Morales, David S. Schoeman, Hugh P. Possingham, Carissa J. Klein, and Anthony J. Richardson. Incorporating climate velocity into the design of climate-smart networks of marine protected areas. *Methods in Ecology and Evolution*, 12(10):1969–1983, 2021. _eprint: https://onlinelibrary.wiley.com/doi/pdf/10.1111/2041-210X.13675.

[155] Romain Bertrand, Gabriela Riofrío-Dillon, Jonathan Lenoir, Jacques Drapier, Patrice de Ruffray, Jean-Claude Gégout, and Michel Loreau. Ecological constraints increase the climatic debt in forests. *Nat Commun*, 7(1):12643, August 2016. Number: 1 Publisher: Nature Publishing Group.

[156] Gabriel Jorda, Núria Marbà, Scott Bennett, Julia Santana-Garcon, Susana Agusti, and Carlos M. Duarte. Ocean warming compresses the three-dimensional habitat of marine life. *Nat Ecol Evol*, 4(1):109–114, January 2020. Number: 1 Publisher: Nature Publishing Group.

[157] Mark C. Serreze and Roger G. Barry. Processes and impacts of Arctic amplification: A research synthesis. *Global and Planetary Change*, 77(1):85–96, May 2011.

[158] Maria Fossheim, Raul Primicerio, Edda Johannesen, Randi B. Ingvaldsen, Michaela M. Aschan, and Andrey V. Dolgov. Recent warming leads to a rapid borealization of fish communities in the Arctic. *Nature Clim Change*, 5(7):673–677, July 2015. Number: 7 Publisher: Nature Publishing Group.

[159] Hui Li, Jadwiga H. Richter, Aixue Hu, Gerald A. Meehl, and Douglas MacMartin. Responses in the subpolar North Atlantic in two climate model sensitivity experiments with increased stratospheric aerosols. *Journal of Climate*, -1(aop):1–31, August 2023. Publisher: American Meteorological Society Section: Journal of Climate.

[160] Brian J. Soden, Richard T. Wetherald, Georgiy L. Stenchikov, and Alan Robock. Global Cooling After the Eruption of Mount Pinatubo: A Test of Climate Feedback by Water Vapor. *Science*, 296(5568):727–730, April 2002. Publisher: American Association for the Advancement of Science.

[161] Benjamin A. Black, Jean-François Lamarque, Daniel R. Marsh, Anja Schmidt, and Charles G. Bardeen. Global climate disruption and regional climate shelters after the Toba supereruption. *Proceedings of the National Academy of Sciences*, 118(29):e2013046118, July 2021. Publisher: Proceedings of the National Academy of Sciences.

[162] L. J. Gray, J. Beer, M. Geller, J. D. Haigh, M. Lockwood, K. Matthes, U. Cubasch, D. Fleitmann, G. Harrison, L. Hood, J. Luterbacher, G. A. Meehl, D. Shindell, B. van Geel, and W. White. Solar Influences on Climate. *Reviews of Geophysics*, 48(4), 2010. _eprint: https://onlinelibrary.wiley.com/doi/pdf/10.1029/2009RG000282.

[163] S. Solomon, J. S. Daniel, R. R. Neely, J.-P. Vernier, E. G. Dutton, and L. W. Thomason. The Persistently Variable "Background" Stratospheric Aerosol Layer and Global Climate Change. *Science*, 333(6044):866–870, August 2011. Publisher: American Association for the Advancement of Science.

[164] Julia Pongratz and Ken Caldeira. Attribution of atmospheric CO2 and temperature increases to regions: importance of preindustrial land use change. *Environ. Res. Lett.*, 7(3):034001, July 2012. Publisher: IOP Publishing.

[165] Daniel M. Hueholt, Elizabeth A. Barnes, James W. Hurrell, Jadwiga H. Richter, and Lantao Sun. Assessing Outcomes in Stratospheric Aerosol Injection Scenarios Shortly After Deployment. *Earth's Future*, 11(5):e2023EF003488, 2023. _eprint: https://onlinelibrary.wiley.com/doi/pdf/10.1029/2023EF003488.

[166] Matthew Henry, Jim Haywood, Andy Jones, Mohit Dalvi, Alice Wells, Daniele Visioni, Ewa Bednarz, Douglas MacMartin, Walker Lee, and Mari Tye. Comparison of UKESM1 and CESM2 Simulations Using the Same Multi-Target Stratospheric Aerosol Injection Strategy. *EGUsphere*, pages 1–22, June 2023. Publisher: Copernicus GmbH.

[167] Devin A. Lyons and Robert E. Scheibling. Range expansion by invasive marine algae: rates and patterns of spread at a regional scale. *Diversity and Distributions*, 15(5):762–775, 2009. _eprint: https://onlinelibrary.wiley.com/doi/pdf/10.1111/j.1472-4642.2009.00580.x.

[168] Elizabeth A. Barnes, James W. Hurrell, and Lantao Sun. Detecting changes in global extremes under the GLENS-SAI climate intervention strategy. *Geophysical Research Letters*, n/a(n/a):e2022GL100198, 2022. _eprint: https://onlinelibrary.wiley.com/doi/pdf/10.1029/2022GL100198.

[169] Hans Hersbach, Bill Bell, Paul Berrisford, Shoji Hirahara, András Horányi, Joaquín Muñoz-Sabater, Julien Nicolas, Carole Peubey, Raluca Radu, Dinand Schepers, Adrian Simmons, Cornel Soci, Saleh Abdalla, Xavier Abellan, Gianpaolo Balsamo, Peter Bechtold, Gionata Biavati, Jean Bidlot, Massimo Bonavita, Giovanna De Chiara, Per Dahlgren, Dick Dee, Michail Diamantakis, Rossana Dragani, Johannes Flemming, Richard Forbes, Manuel Fuentes, Alan Geer, Leo Haimberger, Sean Healy, Robin J. Hogan, Elías Hólm, Marta Janisková, Sarah Keeley, Patrick Laloyaux, Philippe Lopez,

Cristina Lupu, Gabor Radnoti, Patricia de Rosnay, Iryna Rozum, Freja Vamborg, Sebastien Villaume, and Jean-Noël Thépaut. The ERA5 global reanalysis. *Quarterly Journal of the Royal Meteorological Society*, 146(730):1999–2049, 2020. _eprint: https://rmets.onlinelibrary.wiley.com/doi/pdf/10.1002/qj.3803.

[170] Wendy S. Parker. Reanalyses and Observations: What's the Difference? *Bulletin of the American Meteorological Society*, 97(9):1565–1572, September 2016. Publisher: American Meteorological Society Section: Bulletin of the American Meteorological Society.

[171] Yue Dong, Kyle C. Armour, Mark D. Zelinka, Cristian Proistosescu, David S. Battisti, Chen Zhou, and Timothy Andrews. Intermodel Spread in the Pattern Effect and Its Contribution to Climate Sensitivity in CMIP5 and CMIP6 Models. *Journal of Climate*, 33(18):7755–7775, September 2020. Publisher: American Meteorological Society Section: Journal of Climate.

[172] Haijun Song, David B. Kemp, Li Tian, Daoliang Chu, Huyue Song, and Xu Dai. Thresholds of temperature change for mass extinctions. *Nat Commun*, 12(1):4694, August 2021. Bandiera_abtest: a Cc_license_type: cc_by Cg_type: Nature Research Journals Number: 1 Primary_atype: Research Publisher: Nature Publishing Group Subject_term: Biodiversity;Palaeoecology;Palaeontology Subject_term_id: biodiversity;palaeoecology;palaeontology.

[173] D. Visioni, E. M. Bednarz, D. G. MacMartin, B. Kravitz, and P. B. Goddard. The Choice of Baseline Period Influences the Assessments of the Outcomes of Stratospheric Aerosol Injection. *Earth's Future*, 11(8):e2023EF003851, 2023. _eprint: https://onlinelibrary.wiley.com/doi/pdf/10.1029/2023EF003851.

[174] Holly Jean Buck, Laura Jane Martin, Oliver Geden, Peter Kareiva, Liz Koslov, Will Krantz, Ben Kravitz, John Noël, Edward A. Parson, Christopher J. Preston, Daniel L. Sanchez, Lynn Scarlett, and Shuchi Talati. Evaluating the efficacy and equity of environmental stopgap measures. *Nat Sustain*, 3(7):499–504, July 2020. Number: 7 Publisher: Nature Publishing Group.

[175] A. L. Morrison, E. A. Barnes, and J. W. Hurrell. Stratospheric Aerosol Injection to Stabilize Northern Hemisphere Terrestrial Permafrost Under the ARISE-SAI-1.5 Scenario. *Earth's Future*, 12(4):e2023EF004151, 2024. _eprint: https://onlinelibrary.wiley.com/doi/pdf/10.1029/2023EF004151.

[176] Willy Tinner and André F. Lotter. Central European vegetation response to abrupt climate change at 8.2 ka. *Geology*, 29(6):551–554, June 2001.

[177] N. A. Davis, D. Visioni, R. R. Garcia, D. E. Kinnison, D. R. Marsh, M. Mills, J. H. Richter, S. Tilmes, C. G. Bardeen, A. Gettelman, A. A. Glanville, D. G. MacMartin, A. K. Smith, and F. Vitt. Climate, Variability, and Climate Sensitivity of "Middle Atmosphere" Chemistry Configurations of the Community Earth System Model Version 2, Whole Atmosphere Community Climate Model Version 6 (CESM2(WACCM6)). *Journal of Advances in Modeling Earth Systems*, 15(9):e2022MS003579, 2023. _eprint: https://onlinelibrary.wiley.com/doi/pdf/10.1029/2022MS003579.

[178] Noah S. Diffenbaugh and Elizabeth A. Barnes. Data-driven predictions of the time remaining until critical global warming thresholds are reached. *Proceedings of the National Academy of Sciences*, 120(6):e2207183120, February 2023. Publisher: Proceedings of the National Academy of Sciences.

[179] IPCC. Climate Change 2021: The Physical Science Basis. Contribution of Working Group I to the Sixth Assessment Report of the Intergovernmental Panel on Climate Change; Technical Summary. Technical report, Intergovernmental Panel on Climate Change, 2021.

[180] Douglas G. MacMartin, Ben Kravitz, David W. Keith, and Andrew Jarvis. Dynamics of the coupled human–climate system resulting from closed-loop control of solar geoengineering. *Clim Dyn*, 43(1):243–258, July 2014.

[181] Ben Kravitz, Douglas G. MacMartin, Michael J. Mills, Jadwiga H. Richter, Simone Tilmes, Jean-Francois Lamarque, Joseph J. Tribbia, and Francis Vitt. First Simulations of Design-

ing Stratospheric Sulfate Aerosol Geoengineering to Meet Multiple Simultaneous Climate Objectives. *Journal of Geophysical Research: Atmospheres*, 122(23):12,616–12,634, 2017. _eprint: https://onlinelibrary.wiley.com/doi/pdf/10.1002/2017JD026874.

[182] Daniel R. Cayan. Large-Scale Relationships between Sea Surface Temperature and Surface Air Temperature. *Monthly Weather Review*, 108(9):1293–1301, September 1980. Publisher: American Meteorological Society Section: Monthly Weather Review.

[183] Dominique Alò, Shaw Nozaki Lacy, Andrea Castillo, Horacio A. Samaniego, and Pablo A. Marquet. The macroecology of fish migration. *Global Ecology and Biogeography*, 30(1):99–116, 2021. _eprint: https://onlinelibrary.wiley.com/doi/pdf/10.1111/geb.13199.

[184] Jennifer M. Sunday, Gretta T. Pecl, Stewart Frusher, Alistair J. Hobday, Nicole Hill, Neil J. Holbrook, Graham J. Edgar, Rick Stuart-Smith, Neville Barrett, Thomas Wernberg, Reg A. Watson, Dan A. Smale, Elizabeth A. Fulton, Dirk Slawinski, Ming Feng, Ben T. Radford, Peter A. Thompson, and Amanda E. Bates. Species traits and climate velocity explain geographic range shifts in an ocean-warming hotspot. *Ecology Letters*, 18(9):944–953, 2015. _eprint: https://onlinelibrary.wiley.com/doi/pdf/10.1111/ele.12474.

[185] Disha Sachan, Pankaj Kumar, and Md. Saquib Saharwardi. Contemporary climate change velocity for near-surface temperatures over India. *Climatic Change*, 173(3):24, August 2022.

[186] Andrew G. Pauling, Cecilia M. Bitz, and Kyle C. Armour. The Climate Response to the Mt. Pinatubo Eruption Does Not Constrain Climate Sensitivity. *Geophysical Research Letters*, 50(7):e2023GL102946, 2023. _eprint: https://onlinelibrary.wiley.com/doi/pdf/10.1029/2023GL102946.

[187] Camille Parmesan and Gary Yohe. A globally coherent fingerprint of climate change impacts across natural systems. *Nature*, 421(6918):37–42, January 2003. Number: 6918 Publisher: Nature Publishing Group.

[188] Craig Moritz, James L. Patton, Chris J. Conroy, Juan L. Parra, Gary C. White, and Steven R. Beissinger. Impact of a Century of Climate Change on Small-Mammal Communities in Yosemite National Park, USA. *Science*, 322(5899):261–264, October 2008. Publisher: American Association for the Advancement of Science.

[189] I-Ching Chen, Jane K. Hill, Ralf Ohlemüller, David B. Roy, and Chris D. Thomas. Rapid Range Shifts of Species Associated with High Levels of Climate Warming. *Science*, 333(6045):1024–1026, August 2011. Publisher: American Association for the Advancement of Science.

[190] Hanna A. Nomoto and Jake M. Alexander. Drivers of local extinction risk in alpine plants under warming climate. *Ecology Letters*, 24(6):1157–1166, 2021. _eprint: https://onlinelibrary.wiley.com/doi/pdf/10.1111/ele.13727.

[191] M.J. Tegner, P.K. Dayton, P.B. Edwards, and K.L. Riser. Large-scale, low-frequency oceanographic effects on kelp forest succession: a tale of two cohorts. *Marine Ecology Progress Series*, 146:117–134, January 1997.

[192] Alan J Southward, Olivia Langmead, Nicholas J Hardman-Mountford, James Aiken, Gerald T Boalch, Paul R Dando, Martin J Genner, Ian Joint, Michael A Kendall, Nicholas C Halliday, Roger P Harris, Rebecca Leaper, Nova Mieszkowska, Robin D Pingree, Anthony J Richardson, David W Sims, Tania Smith, Anthony W Walne, and Stephen J Hawkins. Long-term oceanographic and ecological research in the Western English Channel. *Adv Mar Biol*, 47:1–105, 2005.

[193] Angela D. Anders and Eric Post. Distribution-wide effects of climate on population densities of a declining migratory landbird. *Journal of Animal Ecology*, 75(1):221–227, 2006. _eprint: https://onlinelibrary.wiley.com/doi/pdf/10.1111/j.1365-2656.2006.01034.x.

[194] Valerie J. Loeb, Eileen E. Hofmann, John M. Klinck, Osmund Holm-Hansen, and Warren B. White. ENSO and variability of the Antarctic Peninsula pelagic marine ecosystem. *Antarctic Science*, 21(2):135–148, April 2009. Publisher: Cambridge University Press.

[195] P. Gonzalez, C. J. Tucker, and H. Sy. Tree density and species decline in the African Sahel attributable to climate. *Journal of Arid Environments*, 78:55–64, March 2012.

[196] Simone Tilmes, Jadwiga H. Richter, Ben Kravitz, Douglas G. MacMartin, Michael J. Mills, Isla R. Simpson, Anne S. Glanville, John T. Fasullo, Adam S. Phillips, Jean-Francois Lamarque, Joseph Tribbia, Jim Edwards, Sheri Mickelson, and Siddhartha Ghosh. CESM1(WACCM) Stratospheric Aerosol Geoengineering Large Ensemble Project. *Bulletin of the American Meteorological Society*, 99(11):2361–2371, November 2018. Publisher: American Meteorological Society Section: Bulletin of the American Meteorological Society.

[197] Keywan Riahi, Shilpa Rao, Volker Krey, Cheolhung Cho, Vadim Chirkov, Guenther Fischer, Georg Kindermann, Nebojsa Nakicenovic, and Peter Rafaj. RCP 8.5—A scenario of comparatively high greenhouse gas emissions. *Climatic Change*, 109(1):33, August 2011.

[198] Daniel Hueholt. Archive accompanying "Speed of environmental change frames relative ecological risk in climate change and climate intervention scenarios", 2024.

[199] Charlotte J. Connolly, Daniel M. Hueholt, and Melissa A. Burt. Datasheets for Earth Science Datasets. *Bulletin of the American Meteorological Society*, 106(4):E642–E648, April 2025. Publisher: American Meteorological Society Section: Bulletin of the American Meteorological Society.

[200] Jadwiga H. Richter. Assessing Responses and Impacts of Solar climate intervention on the Earth system with stratospheric aerosol injection simulations (ARISE-SAI-1.5) [Dataset], 2022.

[201] Mike Mills, Daniele Visioni, and Jadwiga Richter. CESM2-WACCM-SSP245 simulations [Dataset], 2022.

[202] J. Haywood, A. Jones, and M. Dalvi. Dataset Record: UKESM1 ARISE-SAI climate simulations, 2022.

[203] Peter Good, Alistair Sellar, Yongming Tang, Steve Rumbold, Rich Ellis, Douglas Kelley, Till Kuhlbrodt, and Jeremy Walton. IPCC DDC: MOHC UKESM1.0-LL model output prepared for CMIP6 ScenarioMIP, March 2019.

[204] Gokhan Danabasoglu. NCAR CESM2-WACCM model output prepared for CMIP6 ScenarioMIP ssp126, 2019.

[205] Gokhan Danabasoglu. NCAR CESM2-WACCM model output prepared for CMIP6 CMIP historical, 2019.

[206] Gokhan Danabasoglu. NCAR CESM2-WACCM model output prepared for CMIP6 CMIP piControl, 2019.

[207] H. Hersbach, B. Bell, P. Berrisford, G. Biavati, A. Horányi, J. Muñoz-Sabater, J. Nicolas, C. Peubey, R. Radu, I. Rozum, D. Schepers, A. Simmons, C. Soci, D. Dee, and J-N Thépaut. ERA5 monthly averaged data on single levels from 1979 to present, 2023.

[208] Kristy J. Kroeker and Eric Sanford. Ecological Leverage Points: Species Interactions Amplify the Physiological Effects of Global Environmental Change in the Ocean. *Annual Review of Marine Science*, 14(1):75–103, 2022. _eprint: https://doi.org/10.1146/annurev-marine-042021-051211.

[209] Katherine Dagon and Daniel P. Schrag. Quantifying the effects of solar geoengineering on vegetation. *Climatic Change*, 153(1-2):235–251, March 2019. Num Pages: 235-251 Place: Dordrecht, Netherlands Publisher: Springer Nature B.V.

[210] Daniel M. Hueholt, Elizabeth A. Barnes, James W. Hurrell, and Ariel L. Morrison. Speed of environmental change frames relative ecological risk in climate change and climate intervention scenarios. *Nat Commun*, 15(1):3332, April 2024. Publisher: Nature Publishing Group.

[211] Steven J. Phillips, Robert P. Anderson, Miroslav Dudík, Robert E. Schapire, and Mary E. Blair. Opening the black box: an open-source release of Maxent. *Ecography*, 40(7):887–893, 2017. _eprint: https://onlinelibrary.wiley.com/doi/pdf/10.1111/ecog.03049.

[212] Jane Elith, Steven J. Phillips, Trevor Hastie, Miroslav Dudík, Yung En Chee, and Colin J. Yates. A statistical explanation of MaxEnt for ecologists. *Diversity and Distributions*, 17(1):43–57, 2011. _eprint: https://onlinelibrary.wiley.com/doi/pdf/10.1111/j.1472-4642.2010.00725.x.

[213] A. Townsend Peterson and Jorge Soberón. Species distribution modeling and ecological niche modeling: getting the concepts right. *Natureza & Conservação*, 10(2):102–107, 2012. Publisher: Elsevier BV.

[214] A. A. Lissovsky, S. V. Dudov, and E. V. Obolenskaya. Species-Distribution Modeling: Advantages and Limitations of Its Application. 1. General Approaches. *Biol Bull Rev*, 11(3):254–264, May 2021.

[215] Charles B. Yackulic, Richard Chandler, Elise F. Zipkin, J. Andrew Royle, James D. Nichols, Evan H. Campbell Grant, and Sophie Veran. Presence-only modelling using MAXENT: when can we trust the inferences? *Methods in Ecology and Evolution*, 4(3):236–243, 2013. _eprint: https://onlinelibrary.wiley.com/doi/pdf/10.1111/2041-210x.12004.

[216] Damaris Zurell, Janet Franklin, Christian König, Phil J. Bouchet, Carsten F. Dormann, Jane Elith, Guillermo Fandos, Xiao Feng, Gurutzeta Guillera-Arroita, Antoine Guisan, José J. Lahoz-Monfort, Pedro J. Leitão, Daniel S. Park, A. Townsend Peterson, Giovanni Rapacciuolo, Dirk R. Schmatz, Boris Schröder, Josep M. Serra-Diaz, Wilfried Thuiller,

Katherine L. Yates, Niklaus E. Zimmermann, and Cory Merow. A standard protocol for reporting species distribution models. *Ecography*, 43(9):1261–1277, 2020. _eprint: https://onlinelibrary.wiley.com/doi/pdf/10.1111/ecog.04960.

[217] Gurutzeta Guillera-Arroita, José J. Lahoz-Monfort, and Jane Elith. Maxent is not a presence–absence method: a comment on Thibaud et al. *Methods in Ecology and Evolution*, 5(11):1192–1197, 2014. _eprint: https://onlinelibrary.wiley.com/doi/pdf/10.1111/2041-210X.12252.

[218] Gurutzeta Guillera-Arroita, José J. Lahoz-Monfort, Jane Elith, Ascelin Gordon, Heini Kujala, Pia E. Lentini, Michael A. McCarthy, Reid Tingley, and Brendan A. Wintle. Is my species distribution model fit for purpose? Matching data and models to applications. *Global Ecology and Biogeography*, 24(3):276–292, 2015. _eprint: https://onlinelibrary.wiley.com/doi/pdf/10.1111/geb.12268.

[219] Julie A. Lee-Yaw, Jenny L. McCune, Samuel Pironon, and Seema N. Sheth. Species distribution models rarely predict the biology of real populations. *Ecography*, 2022(6):e05877, 2022. _eprint: https://onlinelibrary.wiley.com/doi/pdf/10.1111/ecog.05877.

[220] C. Deser, F. Lehner, K. B. Rodgers, T. Ault, T. L. Delworth, P. N. DiNezio, A. Fiore, C. Frankignoul, J. C. Fyfe, D. E. Horton, J. E. Kay, R. Knutti, N. S. Lovenduski, J. Marotzke, K. A. McKinnon, S. Minobe, J. Randerson, J. A. Screen, I. R. Simpson, and M. Ting. Insights from Earth system model initial-condition large ensembles and future prospects. *Nat. Clim. Chang.*, 10(4):277–286, April 2020. Number: 4 Publisher: Nature Publishing Group.

[221] Brian L. Sullivan, Christopher L. Wood, Marshall J. Iliff, Rick E. Bonney, Daniel Fink, and Steve Kelling. eBird: A citizen-based bird observation network in the biological sciences. *Biological Conservation*, 142(10):2282–2292, October 2009.

[222] Travis L. Booms, Tom J. Cade, and Nancy J. Clum. Gyrfalcon (Falco rusticolus), version 1.0. *Birds of the World*, 2020. Publisher: Cornell Lab of Ornithology, Ithaca, NY, USA.

[223] O. K. Nielsen and Tom J. Cade. Gyrfalcon and ptarmigan predator-prey relationship. *Applied Raptor Ecology: Essentials from Gyrfalcon Research (DL Anderson, CJW McClure, and A. Franke, Editors). The Peregrine Fund, Boise, ID, USA*, pages 43–74, 2017.

[224] Kathy Martin and Scott Wilson. Ptarmigan in North America: Influence of life history and environmental conditions on population persistence. *Gyrfalcons and ptarmigan in a changing world*, 1:45–54, 2011. Publisher: The Peregrine Fund Boise.

[225] A. J. Roubicek, J. VanDerWal, L. J. Beaumont, A. J. Pitman, P. Wilson, and L. Hughes. Does the choice of climate baseline matter in ecological niche modelling? *Ecological Modelling*, 221(19):2280–2286, September 2010.

[226] Brian L. Sullivan, Jocelyn L. Aycrigg, Jessie H. Barry, Rick E. Bonney, Nicholas Bruns, Caren B. Cooper, Theo Damoulas, André A. Dhondt, Tom Dietterich, Andrew Farnsworth, Daniel Fink, John W. Fitzpatrick, Thomas Fredericks, Jeff Gerbracht, Carla Gomes, Wesley M. Hochachka, Marshall J. Iliff, Carl Lagoze, Frank A. La Sorte, Matthew Merrifield, Will Morris, Tina B. Phillips, Mark Reynolds, Amanda D. Rodewald, Kenneth V. Rosenberg, Nancy M. Trautmann, Andrea Wiggins, David W. Winkler, Weng-Keen Wong, Christopher L. Wood, Jun Yu, and Steve Kelling. The eBird enterprise: An integrated approach to development and application of citizen science. *Biological Conservation*, 169:31–40, January 2014.

[227] Li Hu, Juan Long, Yi Lin, Zhongru Gu, Han Su, Xuemin Dong, Zhenzhen Lin, Qian Xiao, Nyambayar Batbayar, Batbayar Bold, Lucia Deutschová, Sergey Ganusevich, Vasiliy Sokolov, Aleksandr Sokolov, Hardip R. Patel, Paul D. Waters, Jennifer Ann Marshall Graves, Andrew Dixon, Shengkai Pan, and Xiangjiang Zhan. Arctic introgression and chromatin regulation facilitated rapid Qinghai-Tibet Plateau colonization by an avian predator. *Nat Commun*, 13(1):6413, October 2022. Number: 1 Publisher: Nature Publishing Group.

[228] Simone Tilmes, Michael J. Mills, Yunqian Zhu, Charles G. Bardeen, Francis Vitt, Pengfei Yu, David Fillmore, Xiaohong Liu, Brian Toon, and Terry Deshler. Description and perfor-

mance of a sectional aerosol microphysical model in the Community Earth System Model (CESM2). *Geoscientific Model Development*, 16(21):6087–6125, November 2023. Publisher: Copernicus GmbH.

[229] Weijia Qian and Howard H. Chang. Projecting Health Impacts of Future Temperature: A Comparison of Quantile-Mapping Bias-Correction Methods. *International Journal of Environmental Research and Public Health*, 18(4):1992, January 2021. Number: 4 Publisher: Multidisciplinary Digital Publishing Institute.

[230] Alex J. Cannon, Stephen R. Sobie, and Trevor Q. Murdock. Bias Correction of GCM Precipitation by Quantile Mapping: How Well Do Methods Preserve Changes in Quantiles and Extremes? *Journal of Climate*, 28(17):6938–6959, September 2015. Publisher: American Meteorological Society Section: Journal of Climate.

[231] Alison Johnston, Wesley M. Hochachka, Matthew E. Strimas-Mackey, Viviana Ruiz Gutierrez, Orin J. Robinson, Eliot T. Miller, Tom Auer, Steve T. Kelling, and Daniel Fink. Analytical guidelines to increase the value of community science data: An example using eBird data to estimate species distributions. *Diversity and Distributions*, 27(7):1265–1277, 2021. _eprint: https://onlinelibrary.wiley.com/doi/pdf/10.1111/ddi.13271.

[232] Matthew Strimas-Mackey, Wesley M. Hochachka, Viviana Ruiz-Gutierrez, Orin J. Robinson, Eliot T. Miller, Tom Auer, Steve Kelling, Daniel Fink, and Alison Johnston. *Best Practices for Using eBird Data v1.0*. Zenodo, 2023. Version Number: v1.0.

[233] Carol L. McIntyre, David C. Douglas, and Layne G. Adams. Movements of Juvenile Gyrfalcons from Western and Interior Alaska Following Departure from Their Natal Areas. *rapt*, 43(2):99–109, June 2009. Publisher: Raptor Research Foundation.

[234] Kurt K. Burnham and Ian Newton. Seasonal movements of Gyrfalcons Falco rusticolus include extensive periods at sea. *Ibis*, 153(3):468–484, 2011. _eprint: https://onlinelibrary.wiley.com/doi/pdf/10.1111/j.1474-919X.2011.01141.x.

[235] Matthew Strimas-Mackey, Eliot Miller, and Wesley Hochachka. *auk: eBird Data Extraction and Processing in R*, 2025. R package version 0.8.1.

[236] Stephen J. Phillips, Miroslav Dudík, and Robert E. Schapire. Maxent software for modeling species niches and distributions (Version 3.4.1), 2017.

[237] Steven J. Phillips, Miroslav Dudík, and Robert E. Schapire. A maximum entropy approach to species distribution modeling. In *Proceedings of the twenty-first international conference on Machine learning*, page 83, 2004.

[238] Claudia Tebaldi, Kalyn Dorheim, Michael Wehner, and Ruby Leung. Extreme metrics from large ensembles: investigating the effects of ensemble size on their estimates. *Earth System Dynamics*, 12(4):1427–1501, December 2021. Publisher: Copernicus GmbH.

[239] Laura Landrum and Marika M. Holland. Extremes become routine in an emerging new Arctic. *Nat. Clim. Chang.*, 10(12):1108–1115, December 2020. Publisher: Nature Publishing Group.

[240] Andrew E. McKechnie, Philip AR Hockey, and Blair O. Wolf. *Feeling the heat: Australian landbirds and climate change*, volume 112. Taylor & Francis, 2012. Issue: 2 Pages: i-vii Publication Title: Emu-Austral Ornithology.

[241] Lilin Zheng, Jianhua Xu, Dahui Li, Zilong Xia, Yaning Chen, Guoyu Xu, and Debin Lu. Increasing control of climate warming on the greening of alpine pastures in central Asia. *International Journal of Applied Earth Observation and Geoinformation*, 105:102606, December 2021.

[242] Oliver Watt-Meyer, Brian Henn, Jeremy McGibbon, Spencer K. Clark, Anna Kwa, W. Andre Perkins, Elynn Wu, Lucas Harris, and Christopher S. Bretherton. ACE2: Accurately learning subseasonal to decadal atmospheric variability and forced responses, November 2024. arXiv:2411.11268 [physics].

Appendix A

Supplementary Information for Chapter 2

A.1 Supplementary Figure for Chapter 2

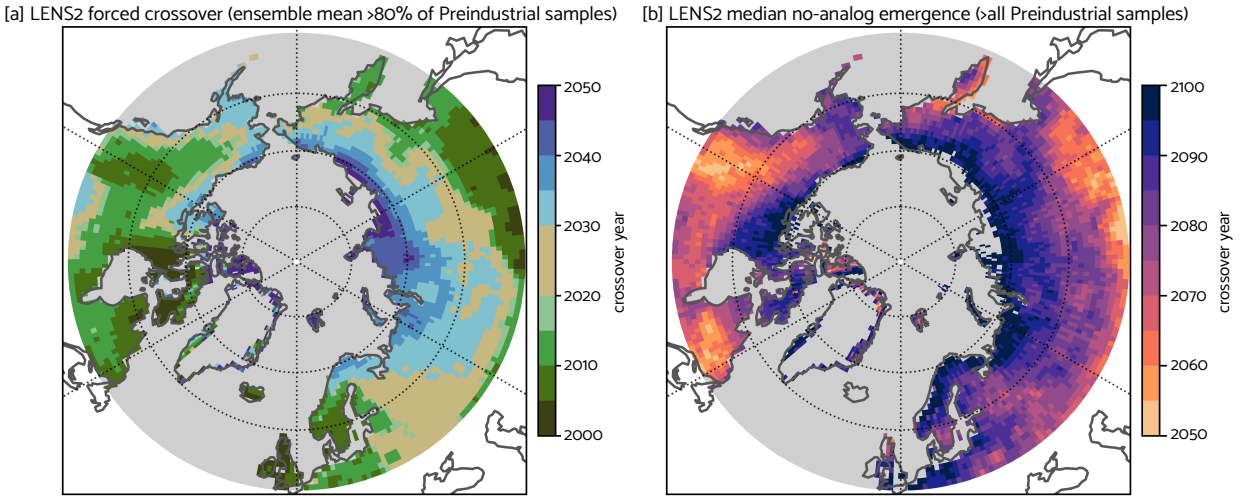

Figure A.1: Forced crossover (ensemble mean >80% of Preindustrial samples) and median no-analog crossover (ensemble member >100% of Preindustrial samples) in growing degree days from the Community Earth System Model 2 Large Ensemble (LENS2) for all points poleward of 50 °N.

A.2 Supplementary Videos for Chapter 2

Supplementary Videos B.1-B.4 are archived at the Open Science Framework: osf.io/2ncfv/. The captions for each video are below.

B.1 Video B.1. Left panel: Sea surface temperature anomalies in members from the Community Earth System Model 2 Large Ensemble (LENS2) corresponding to the average of the highest 20% of growing degree days in each decade 1850-2100 for the Brooks Range of Alaska (gray dot). Right panel: corresponding timeseries of growing degree days in LENS2 for

same location; gray thin lines show all members, with pink thin lines denoting members with SSTs averaged in left panel.

B.2 Video B.2 Left panel: Sea surface temperature anomalies in members from the Community Earth System Model 2 Large Ensemble (LENS2) corresponding to the average of the lowest 20% of growing degree days in each decade 1850-2100 for the Brooks Range of Alaska (gray dot). Right panel: corresponding timeseries of growing degree days in LENS2 for same location; gray thin lines show all members, with pink thin lines denoting members with SSTs averaged in left panel.

B.3 Video B.3 Trends in growing degree days in Global Historical Climatology Network (GHCN) stations 1873-2022 with daily data coverage greater than 97% over 30-year periods. Dots represent individual stations; dots outlined in a circle show where trends fall outside the distribution calculated at the closest grid point in the Community Earth System Model 2 Large Ensemble (LENS2).

B.4 Video B.4 Trends in growing degree days in Global Historical Climatology Network (GHCN) stations 1873-2022 with daily data coverage greater than 97% over 10-year periods. Dots represent individual stations; dots outlined in a circle show where trends fall outside the distribution calculated at the closest grid point in the Community Earth System Model 2 Large Ensemble (LENS2).

Appendix B

Supplementary Figures for Chapter 3

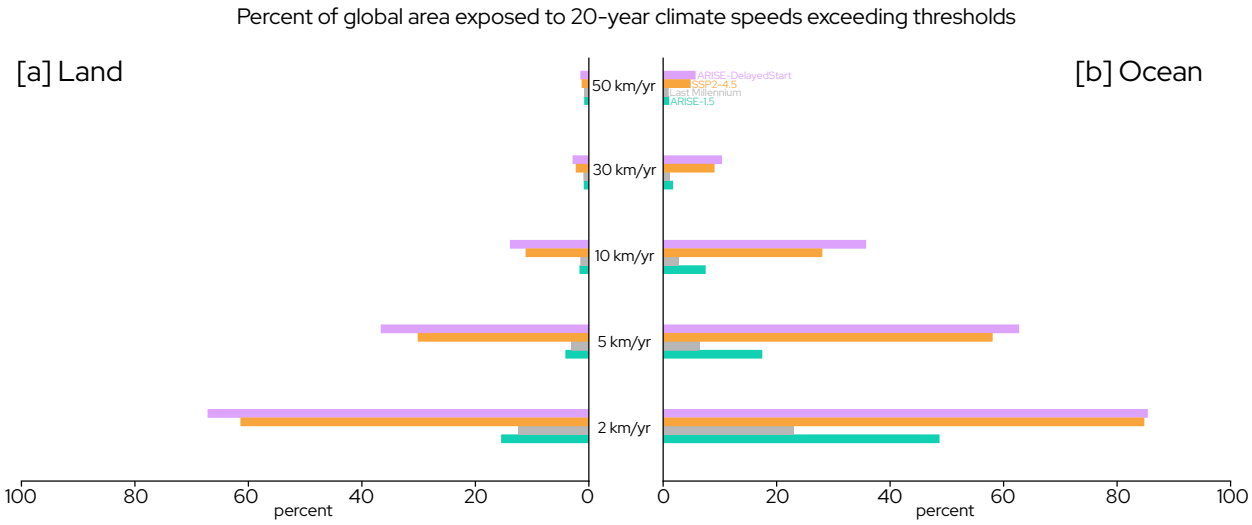

Figure B.1: Percent of global land [a] and ocean [b] area exposed to 20-year ensemble mean climate speeds beyond selected threshold values in Shared Socioeconomic Pathway 2-4.5 (SSP2-4.5), Last Millennium, and Assessing Responses and Impacts of Solar climate intervention on the Earth system (ARISE) 1.5 and DelayedStart simulations. Climate speeds are calculated over the ensemble mean of 2035-2054 (ARISE-1.5), 2045-2064 (ARISE-DelayedStart and SSP2-4.5), and the mean of ten 20-year periods (Last Millennium). Colors visually distinguish different datasets.

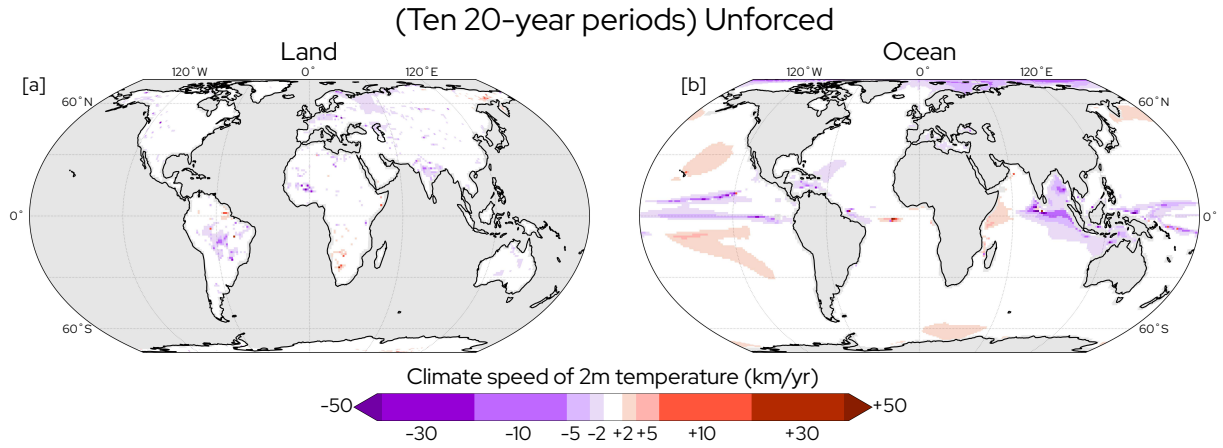

Figure B.2: Climate speeds in the mean of ten 20-year periods (to match ensemble size of other simulations, see Methods) in the Unforced simulation. The sign indicates whether the change in temperature associated with the climate speed is positive or negative. See Figure B.8 for maps for each interval. Masked area shown in gray (ocean for [a], land for [b]).

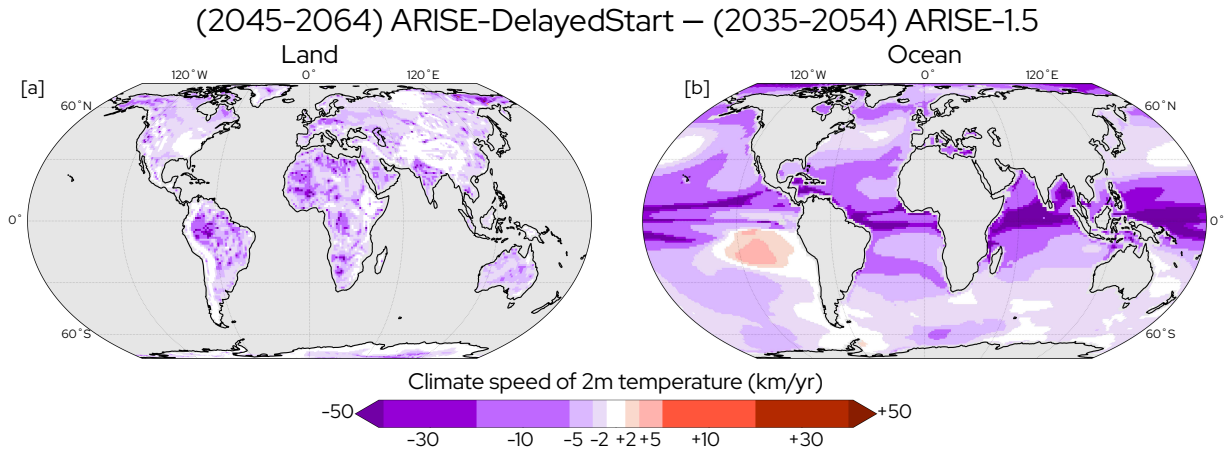

Figure B.3: Climate speeds during the 20-year period immediately following deployment of stratospheric aerosol injection (SAI) on land [a] and ocean [b] in the ensemble mean of Assessing Responses and Impacts of Solar climate intervention on the Earth system (ARISE) DelayedStart minus the ARISE-1.5 simulation. The sign indicates whether the change in temperature associated with the climate speed is positive or negative. Masked area shown in gray (ocean for [a], land for [b]).

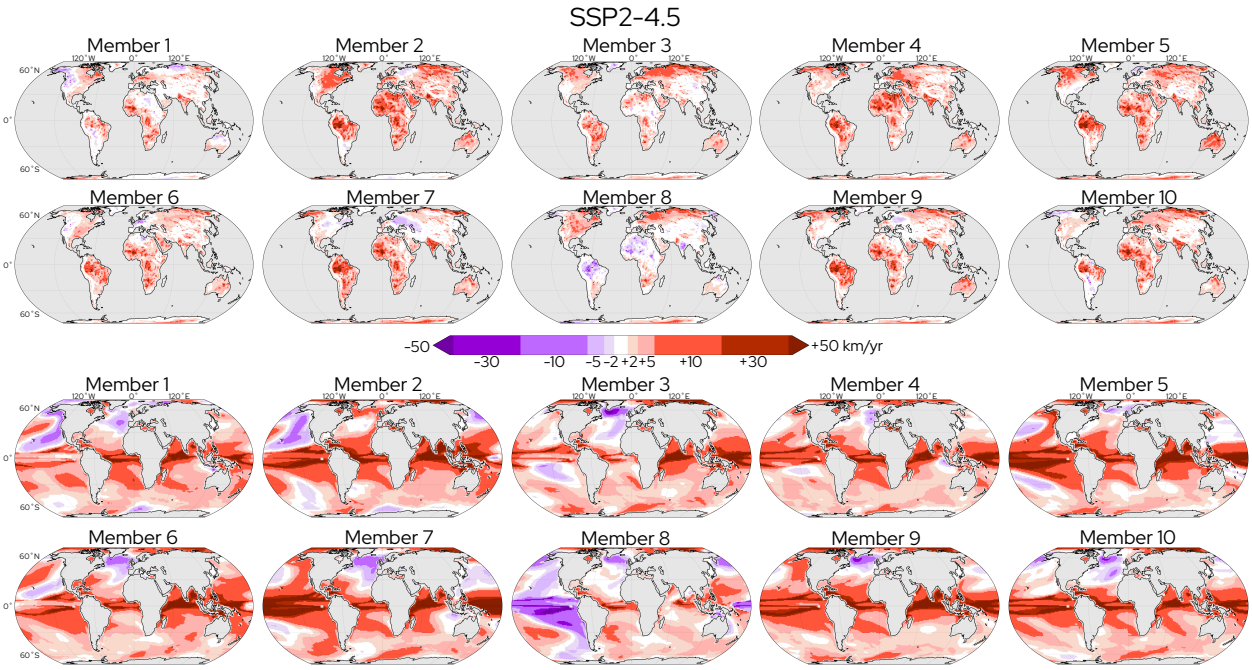

Figure B.4: 20-year climate speeds (2045-2064) for land (top half) and ocean (bottom half) in each of the ten ensemble members of Shared Socioeconomic Pathway 2-4.5 (SSP2-4.5). Masked area shown in gray (ocean for top half, land for bottom half).

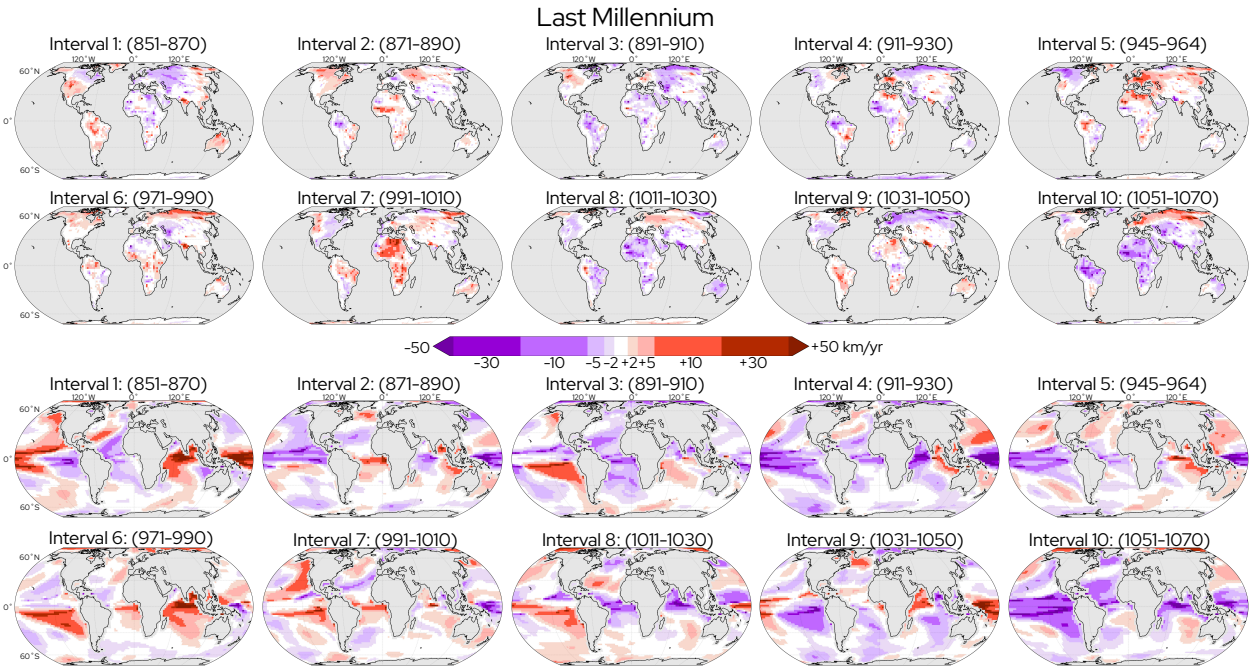

Figure B.5: 20-year climate speeds for land (top half) and ocean (bottom half) in each of the ten intervals treated as different ensemble members in the Last Millennium simulation for Figures 3.1, 3.3, and B.1 Masked area shown in gray (ocean for top half, land for bottom half).

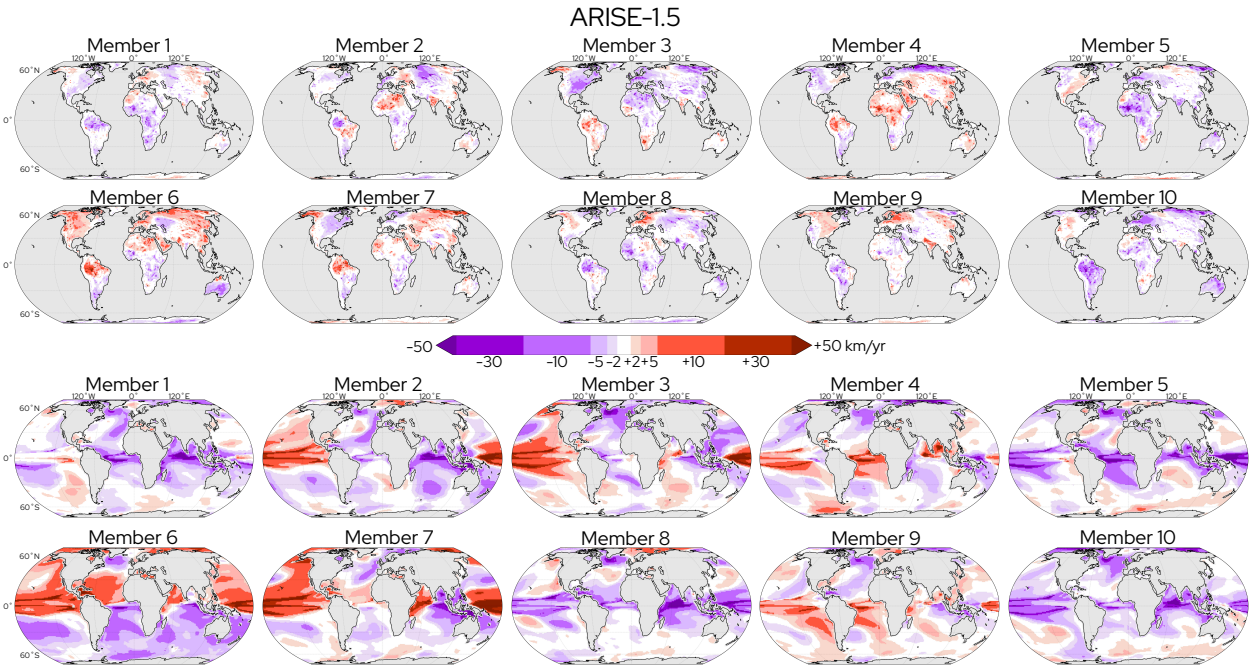

Figure B.6: 20-year climate speeds (2035-2054) for land (top half) and ocean (bottom half) in each of the ten ensemble members of the Assessing Responses and Impacts of Solar climate intervention on the Earth system-1.5 (ARISE-1.5) simulation. Masked area shown in gray (ocean for top half, land for bottom half).

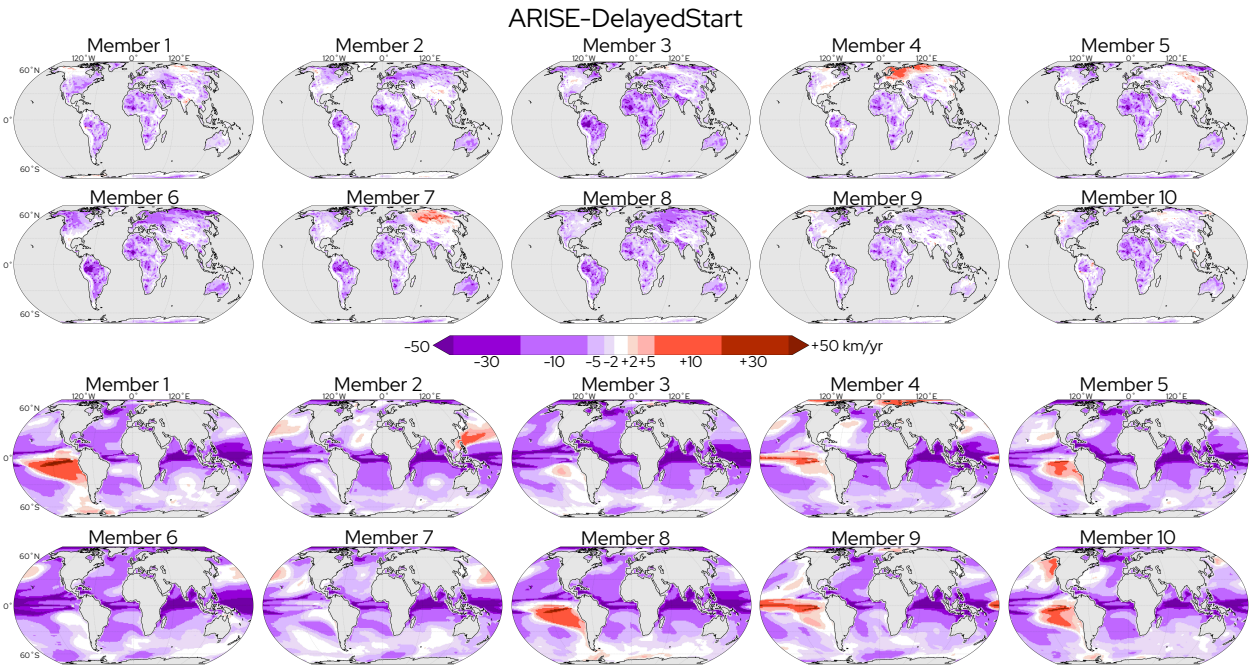

Figure B.7: 20-year climate speeds (2045-2064) for land (top half) and ocean (bottom half) in each of the ten ensemble members of Assessing Responses and Impacts of Solar climate intervention on the Earth system-DelayedStart (ARISE-DelayedStart) simulation. Masked area shown in gray (ocean for top half, land for bottom half).

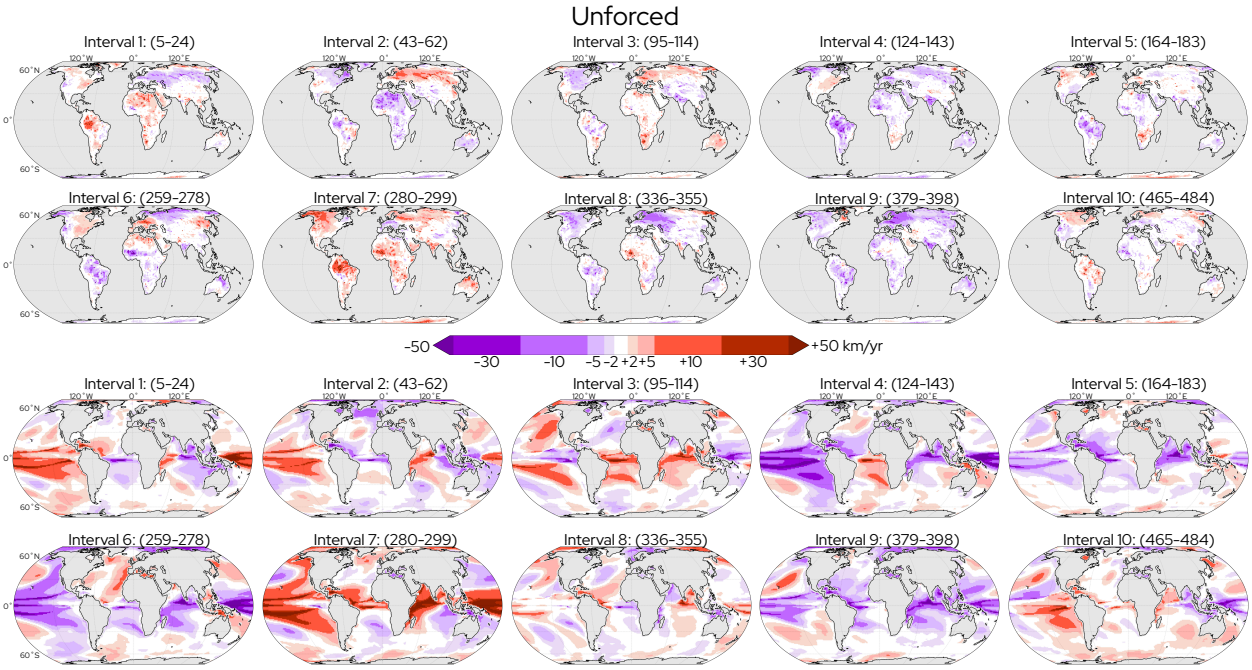

Figure B.8: 20-year climate speeds for land (top half) and ocean (bottom half) in each of the ten intervals treated as different ensemble members in the Unforced simulation for Figure B.2. Masked area shown in gray (ocean for top half, land for bottom half).

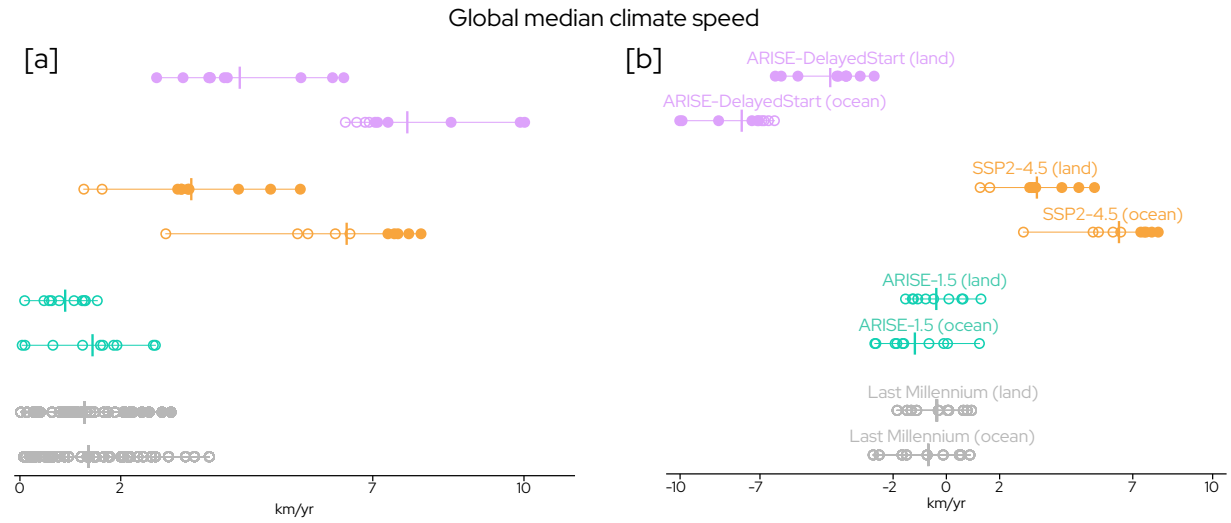

Figure B.9: Global median climate speeds of 2m temperature over land and ocean in Shared Socioeconomic Pathway 2-4.5 (SSP2-4.5), Last Millennium, and Assessing Responses and Impacts of Solar climate intervention on the Earth system (ARISE) 1.5 and DelayedStart simulations. Open circles denote climate speeds with magnitudes within the mean dispersal speed of terrestrial or ocean species, closed circles signify climate speeds with magnitude exceeding mean dispersal speeds, and vertical bars show the ensemble mean. In [a], climate speeds are calculated over 2035-2054 (ARISE-1.5), 2045-2064 (ARISE-DelayedStart and SSP2-4.5), and every non-overlapping 20-year period avoiding large volcanic eruptions (Last Millennium). In [b], climate speeds are calculated over 2035-2054 (ARISE-1.5), 2045-2064 (ARISE-DelayedStart and SSP2-4.5), and ten 20-year periods avoiding large volcanic eruptions (Last Millennium) and illustrate both the sign and magnitude of the responses. Colors visually distinguish different datasets.

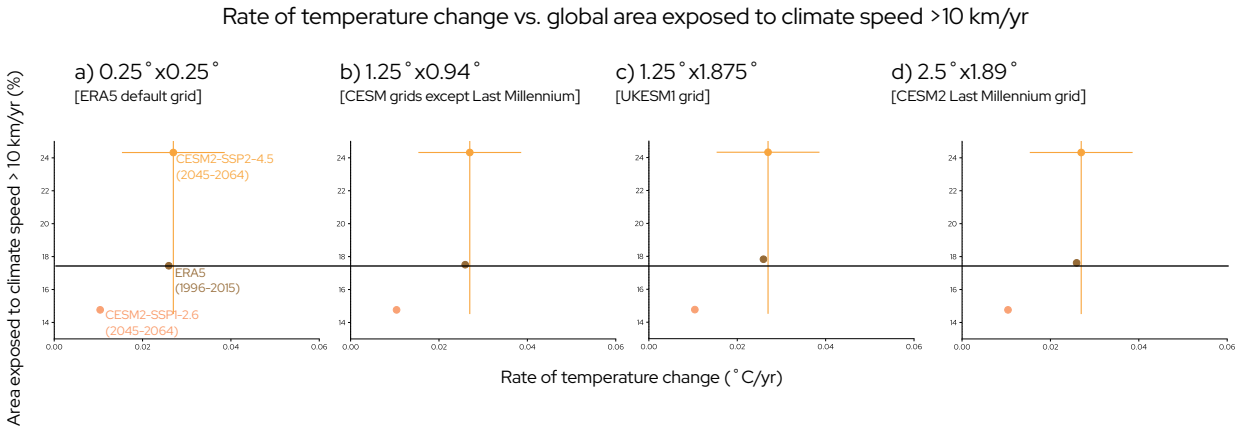

Figure B.10: 20-year rate of temperature change per year vs. percent of area exposed to a climate speed with magnitude greater than 10 km/yr, demonstrating the influence of grid resolution on the calculated climate speed in European Reanalysis 5 (ERA5). Horizontal black bar provides reference line of constant area exposed to provide greater clarity of the subtle difference between the three figures. Community Earth System Model 2-Shared Socioeconomic Pathway 1-2.6 (CESM2-SSP1-2.6) and CESM2-SSP2-4.5 shown for visual context. See Table 1 and Methods for detailed descriptions of each dataset. Colors visually distinguish different datasets.

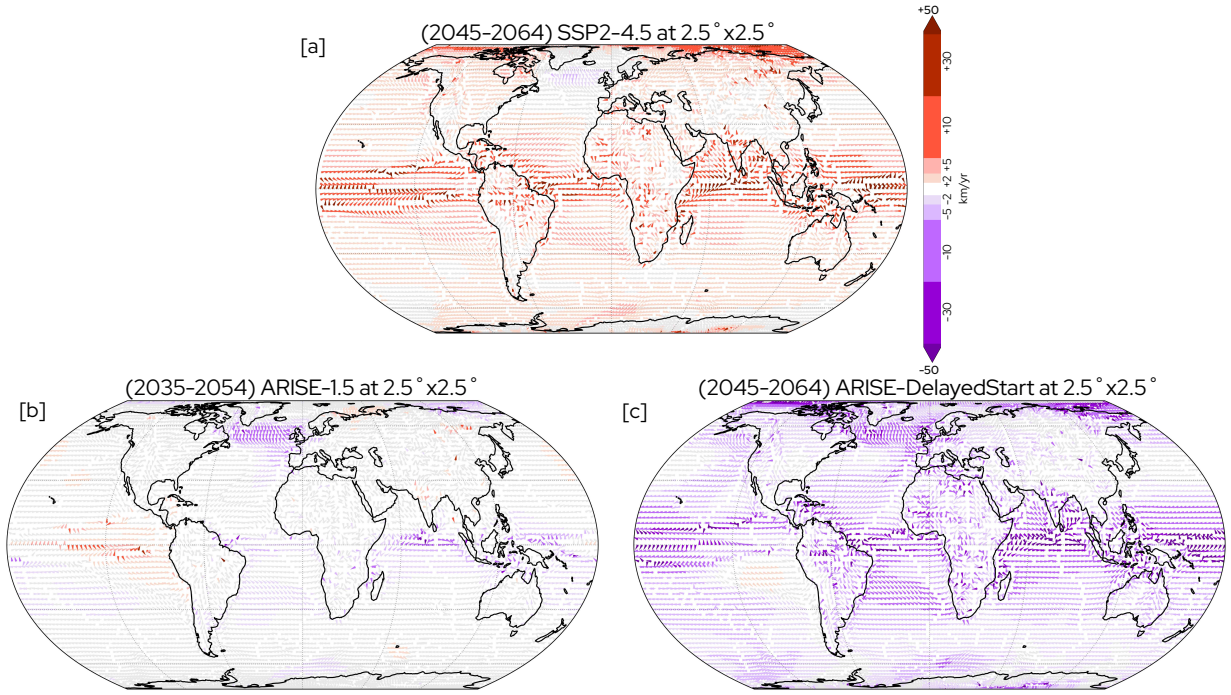

Figure B.11: 20-year climate velocities in the ensemble mean for Shared Socioeconomic Pathway 2-4.5 (SSP2-4.5) [a], Assessing Responses and Impacts of Solar climate intervention on the Earth system 1.5 (ARISE-1.5) [b], and ARISE-DelayedStart [c] simulations. The sign indicates whether the change in temperature associated with the climate velocity is positive or negative. Data regridded to 2.5°x2.5° for visual clarity.

Appendix C

Supplementary Figures for Chapter 4

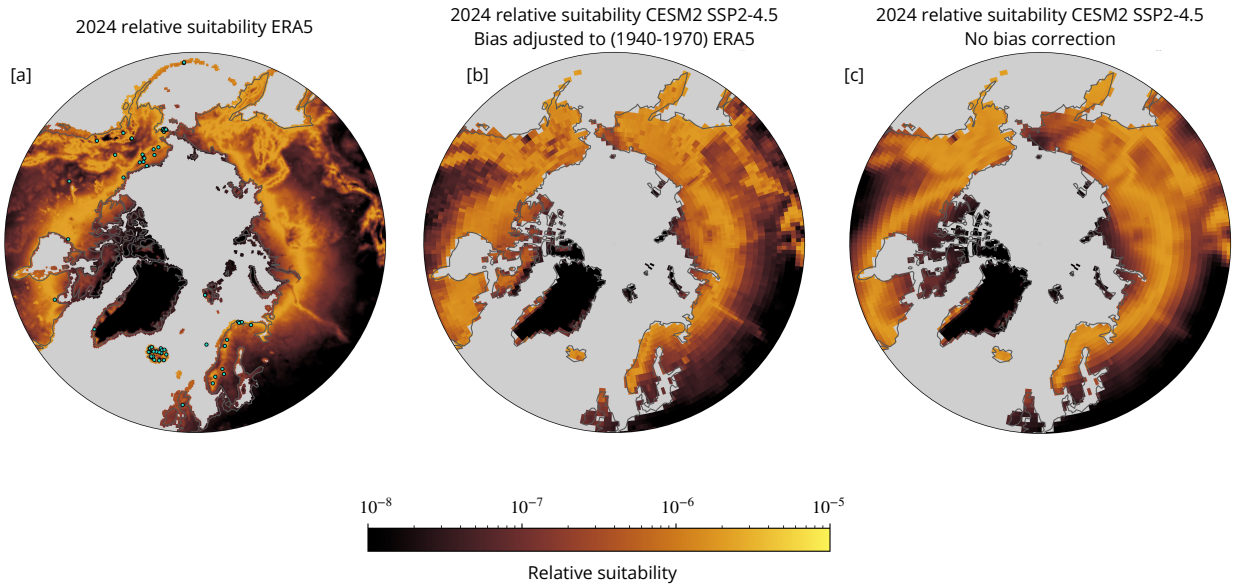

Figure C.1: Relative suitability from Maxent model for the year 2024 in ERA5 (a), projected to the ensemble mean of 2024 in SSP2-4.5 with bias adjustment to the 1940-1970 period in ERA5 (b), and projected to the ensemble mean of 2024 in SSP2-4.5 with no bias adjustment. Dots in [a] represent locations of eBird checklists with Gyrfalcon detections in 2024 (n=127).

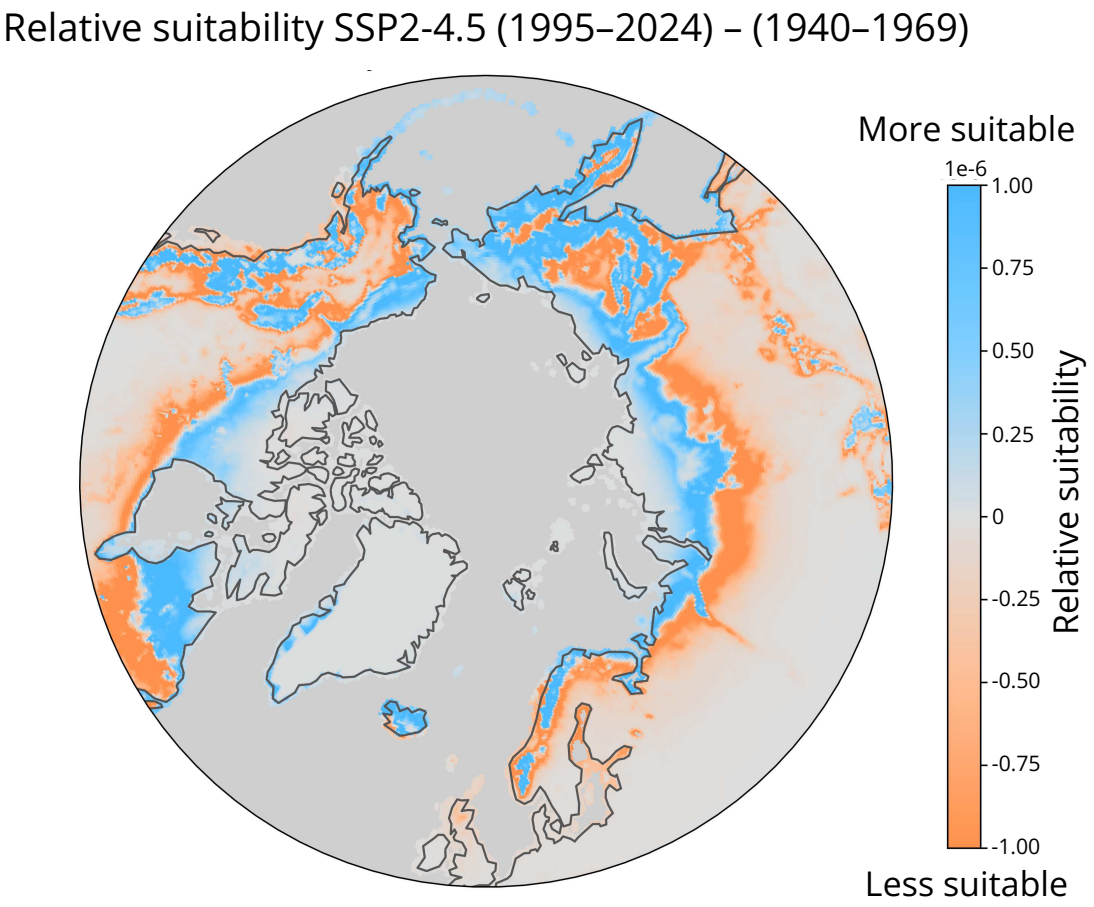

Figure C.2: Difference in relative suitability from Maxent model between 1995-2024 average and 1940-1969 average in ERA5.